

# **Monitoring regulation of cAMP dynamics in CD4<sup>+</sup> T cells considering inflammation and autoimmunity**

Doctoral thesis submitted

by Roberta Kurelić

University of Hamburg

Faculty of Mathematics, Informatics and Natural Sciences

Department of Chemistry

Hamburg, October 2022

1. Reviewer:

Prof. Dr. Elke Oetjen

2. Reviewer:

Prof. Dr. Manuel A. Frieze

Disputation Committee Members:

Prof. Dr. Chris Meier, Chair

Prof. Dr. Viacheslav O. Nikolaev, Deputy Chair

Prof. Dr. Christian Lohr, Member

Date of disputation: March 3, 2023

Date of print release: March 7, 2023

Die vorliegende Arbeit „Monitoring regulation of cAMP dynamics in CD4<sup>+</sup> T cells considering inflammation and autoimmunity“ wurde am Institut für Experimentelle Herz-Kreislaufforschung des Universitätsklinikums Hamburg-Eppendorf im Zeitraum 1. Januar 2019 - 31. Juli 2022 angefertigt.

## List of Publications

Krieg PF, Sonner JK, **Kurelic R**, Engler JB, Scharenberg MF, Bauer S, Nikolaev VO, Friese MA. GPR52 regulates cAMP in T cells but is dispensable for encephalitogenic responses. *Front Immunol.* 2023 Jan 24;13:1113348. doi: 10.3389/fimmu.2022.1113348. PMID: 36761164; PMCID: PMC9902724.

**Kurelić R**, Nikolaev VO. Generation of Transgenic Mice Expressing Cytosolic and Targeted FRET Biosensors for cAMP and cGMP. *Methods Mol Biol.* 2022;2483:241-254. doi:10.1007/978-1-0716-2245-2\_15

Bertović I, **Kurelić R**, Mahmutefendić Lučin H, Jurak Begonja A. Early Endosomal GTPase Rab5 (Ras-Related Protein in Brain 5) Regulates GPIIb $\beta$  (Glycoprotein Ib Subunit  $\beta$ ) Trafficking and Platelet Production In Vitro. *Arterioscler Thromb Vasc Biol.* 2022;42(1):e10-e26. doi:10.1161/ATVBAHA.121.316552

**Kurelic R**, Krieg PF, Sonner JK, et al. Upregulation of Phosphodiesterase 2A Augments T Cell Activation by Changing cGMP/cAMP Cross-Talk. *Front Pharmacol.* 2021;12:748798. Published 2021 Oct 5. doi:10.3389/fphar.2021.748798

Bertović I, **Kurelić R**, Milošević I, et al. Vps34 derived phosphatidylinositol 3-monophosphate modulates megakaryocyte maturation and proplatelet production through late endosomes/lysosomes. *J Thromb Haemost.* 2020;18(7):1756-1772. doi:10.1111/jth.14764

# Table of Content

1	Introduction .....	1
1.1	T cell development: long road from precursor cells to mature T cell soldiers and spies.....	1
1.1.1	T cell development and activation process.....	1
1.1.2	T cell subsets: conventional and regulatory T cells .....	3
1.1.2.1	Conventional T cells.....	4
1.1.2.2	Regulatory T cells .....	5
1.1.3	How regulatory T cells mediate immunosuppression and autoimmunity?.....	6
1.2	Dissecting cAMP pathway in CD4+ T cells.....	7
1.2.1	G protein-coupled receptors and their function in T cells.....	8
1.2.1.1	Adenosine receptors .....	9
1.2.1.2	$\beta$ -adrenergic receptors.....	10
1.2.2	Adenylyl cyclases and their role in modulating cAMP levels in T cells.....	11
1.2.3	Phosphodiesterase as crucial regulators of cAMP signaling in T cells .....	11
1.2.3.1	Cyclic nucleotide cross-talk.....	14
1.2.4	Mechanisms of cAMP-driven Treg-mediated immunosuppression .....	16
1.2.5	Gap junctions and their impact on T cell function .....	17
1.3	Live-cell imaging of cAMP and its dynamics via FRET .....	19
1.4	Objectives of the PhD thesis .....	22
2	Materials and methods.....	23
2.1	Materials .....	23
2.1.1	Animals.....	23
2.1.2	Antibodies.....	23
2.1.2.1	Primary antibodies for Fluorescence-activated cell sorting (FACS) analysis	23
2.1.2.2	Primary antibodies for immunoblotting .....	24

2.1.2.3	Secondary antibodies for immunoblotting .....	24
2.1.2.4	Primary antibodies for immunofluorescence .....	25
2.1.2.5	Secondary antibodies for immunofluorescence.....	25
2.1.3	Buffers and Solutions.....	26
2.1.3.1	FACS sorting .....	26
2.1.3.2	Immunoblotting .....	26
2.1.3.3	Immunofluorescence.....	29
2.1.3.4	Cell culture – eukaryotic cells lines .....	29
2.1.3.5	Cloning .....	29
2.1.3.6	Isolation and culture of primary murine T cells .....	31
2.1.3.7	Live-cell imaging.....	32
2.1.3.8	NanoString.....	33
2.1.4	Cells .....	33
2.1.4.1	Competent cells .....	33
2.1.4.2	Eucaryotic cell lines .....	33
2.1.5	Chemicals.....	33
2.1.5.1	Chemicals – non-sterile work .....	33
2.1.5.2	Chemicals – sterile work .....	36
2.1.6	Consumables.....	36
2.1.7	Devices.....	38
2.1.7.1	Live-cell imaging via FRET .....	38
2.1.7.2	Microscopes .....	38
2.1.7.3	Other devices and instruments .....	38
2.1.8	Kits .....	40
2.1.9	Oligonucleotides .....	40
2.1.9.1	Oligonucleotides for genetic engineering (mutagenesis, PCR amplification and sequencing).....	40
2.1.9.2	Oligonucleotide probes for NanoString .....	41
2.1.9.3	Oligonucleotides for qRT-PCR.....	42

2.1.10	Plasmids .....	43
2.1.11	Software .....	43
2.2	Methods.....	44
2.2.1	Animals.....	44
2.2.2	cAMP immunoassay .....	44
2.2.3	Cell culture and transient transfection .....	44
2.2.4	FACS sorting .....	45
2.2.5	Immunofluorescence.....	45
2.2.6	Live-cell imaging via FRET .....	46
2.2.7	Molecular cloning.....	47
2.2.8	NanoString.....	52
2.2.9	RNA isolation, cDNA synthesis and qRT-PCR .....	53
2.2.10	Sample preparation and Immunoblotting.....	54
2.2.11	T cells isolation and culture.....	55
2.2.12	Statistical analysis .....	57
3	Results.....	58
3.1	Validation of cytosolic FRET-based sensor Epac1-camps in CD4+ T cells .....	58
3.2	Probing cAMP levels and cAMP-relevant gene expression in CD4+ T cells .....	60
3.2.1	cAMP immunoassay .....	60
3.2.2	NanoString analysis .....	61
3.3	Orphan GPCRs – GPR52 .....	61
3.3.1	Testing specificity of GPR52 agonist drug - FTBMT .....	62
3.3.2	Impact of GPR52 stimulation on cAMP levels in CD4+ T cells .....	64
3.4	PDE regulation during T cell activation in T cell subsets .....	66
3.4.1	Provoking adenosine receptor activity in CD4+ T cells.....	66
3.4.2	Differences in PDE inhibition in activated vs. non-activated T cell subsets.....	68
3.4.2.1	Pan-PDE inhibition with IBMX in real-time .....	68
3.4.2.2	PDE4 in T cells .....	70
3.4.2.3	PDE3 in T cells .....	71

3.4.2.4	PDE2 in T cells .....	75
3.4.2.5	Regulation of cyclic nucleotide cross-talk in CD4+ T cells.....	79
3.4.3	Visualization of cAMP transfer between T cell subsets via live-cell imaging...	82
4	Discussion .....	86
4.1	Establishing live-cell imaging in T cells .....	86
4.2	Relevance of GPR52 in the context of T cell biology.....	87
4.3	cAMP immunoassay analysis of murine T cell subsets .....	89
4.4	Real-time dynamics of cAMP in T cells .....	90
4.5	Regulation of cyclic nucleotide cross-talk in T cell subsets.....	92
4.6	Connection between Connexin 43 and cAMP transfer .....	94
4.7	Summary and Conclusion .....	96
5	Bibliography .....	98
6	Appendix.....	122
7	Acknowledgments.....	127



## List of Tables

<b>Table 1.1.</b> List of mouse lines .....	23
<b>Table 2. 1.</b> List of antibodies for FACS-sorting.....	23
<b>Table 2. 2.</b> List of primary antibodies for immunoblotting .....	24
<b>Table 2.3.</b> List of horseradish peroxidase-conjugated (HRP) secondary antibodies for immunoblotting .....	24
<b>Table 2. 4.</b> List of primary antibodies for immunofluorescence staining .....	25
<b>Table 2. 5.</b> List of secondary antibodies for immunofluorescence staining.....	25
<b>Table 3. 1.</b> 10x FACS buffer .....	26
<b>Table 3. 2.</b> RIPA buffer .....	26
<b>Table 3. 3.</b> 4x Laemmli buffer .....	26
<b>Table 3. 4.</b> 4x Tris/SDS.....	27
<b>Table 3. 5.</b> 4x Tris/SDS.....	27
<b>Table 3. 6.</b> Ammonium persulfat (APS) solution.....	27
<b>Table 3. 7.</b> 10x SDS Running buffer .....	27
<b>Table 3. 8.</b> 1x SDS Running buffer .....	27
<b>Table 3. 9.</b> 10x Transfer buffer.....	27
<b>Table 3. 10.</b> 1x Transfer buffer.....	28
<b>Table 3. 11.</b> 10x Tris-buffered saline (TBS) buffer .....	28
<b>Table 3. 12.</b> 1x TBS-Tween 20 (TBS-T) buffer.....	28
<b>Table 3. 13.</b> Blocking buffer. ....	28
<b>Table 3. 14.</b> Separating gel.....	28
<b>Table 3. 15.</b> Stacking gel .....	29
<b>Table 3. 16.</b> Blocking buffer .....	29
<b>Table 3. 17.</b> Culturing medium for HEK293A cells .....	29
<b>Table 3. 18.</b> Agarose gel, 1%.....	29
<b>Table 3. 19.</b> Ampicilin (AMP) stock solution .....	30

<b>Table 3. 20.</b> 5x KCM buffer .....	30
<b>Table 3. 21.</b> LB Agar plates .....	30
<b>Table 3. 22.</b> LB Medium.....	30
<b>Table 3. 23.</b> Transformation storage buffer (TSB) .....	30
<b>Table 3. 24.</b> 50x Tris-acetate-EDTA (TAE) buffer .....	31
<b>Table 3. 25.</b> MACS buffer .....	31
<b>Table 3. 26.</b> RBC (Red blood cells) lysis buffer.....	31
<b>Table 3. 27.</b> T cell culturing medium .....	31
<b>Table 3. 28.</b> Supplement 1.....	32
<b>Table 3. 29.</b> Supplement 2.....	32
<b>Table 3. 30.</b> FRET buffer .....	32
<b>Table 3. 31.</b> 10x PDL (Poly-D-Lysin) stock solution .....	32
<b>Table 3. 32.</b> 1x PDL solution.....	32
<b>Table 3. 33.</b> TE buffer .....	33
<b>Table 4. 1.</b> List of competent cells.....	33
<b>Table 4. 2.</b> List of eukaryotic cell lines .....	33
<b>Table 5. 1.</b> List of chemicals used for non-sterile work (wet laboratory, live-cell imaging) ...	33
<b>Table 5. 2.</b> List of chemicals used for sterile work (cell culture).....	36
<b>Table 6. 1.</b> List of consumables (sterile and non-sterile work).....	36
<b>Table 7. 1.</b> List of equipment used to build up live-cell imaging setup via FRET .....	38
<b>Table 7. 2.</b> List of additional microscopes .....	38
<b>Table 7. 3.</b> List of devices and instruments .....	38
<b>Table 8. 1.</b> List of commercially available kits .....	40
<b>Table 9. 1.</b> List of oligonucleotides for genetic engineering.....	40
<b>Table 9. 2.</b> List of oligonucleotides for NanoString .....	41
<b>Table 9. 3.</b> List of oligonucleotides for qRT-PCR .....	42
<b>Table 10. 1.</b> List of plasmids .....	43
<b>Table 11. 1.</b> List of softwares .....	43

<b>Table 12. 1.</b> Sample reaction mix for site-directed mutagenesis by PCR .....	47
<b>Table 12. 2.</b> Cycling conditions for the site-directed mutagenesis by PCR.....	48
<b>Table 12. 3.</b> Components for chemicals transformation into competent <i>E. coli</i> cells .....	49
<b>Table 12. 4.</b> Sample reaction mix for PCR.....	50
<b>Table 12. 5.</b> Cycling conditions for PCR amplification of insert .....	50
<b>Table 12. 6.</b> Restriction digestion components.....	51
<b>Table 12. 7.</b> Ligation reaction mix .....	51
<b>Table 13. 1.</b> cDNA synthesis reaction mix.....	53
<b>Table 13. 2.</b> Cycling steps for cDNA sythesis .....	53
<b>Table 13. 3.</b> Reaction mix for qRT-PCR.....	54
<b>Table 13. 4.</b> Cycling conditions for qRT-PCR.....	54
<b>Table 14. 1.</b> List of hazardous substances according to Globally Harmonized System (GHS) of classification and labeling of chemicals .....	122

## List of Figures

<b>Figure 1.</b> Development of CD4+ and CD8+ T cells in the thymus .....	2
<b>Figure 2.</b> Cyclic nucleotide cross-talk .....	15
<b>Figure 3.</b> cAMP as crucial player in Treg-mediated immunosuppression.....	17
<b>Figure 4.</b> Principles of the FRET technique .....	21
<b>Figure 5.</b> T cells expressing Epac1-camps sensor .....	59
<b>Figure 6.</b> Regulatory T cells have higher basal intracellular cAMP levels compared to conventional T cells. ....	60
<b>Figure 7.</b> Expression of cAMP-relevant genes in Tcon and Treg .....	61
<b>Figure 8.</b> <i>Gpr52</i> expression is increased in non-activated regulatory T cells versus Tcon. .	62
<b>Figure 9.</b> FTBMT specifically activates GPR52 receptor to produce cAMP .....	63
<b>Figure 10.</b> Stimulation of non-activated Treg with GPR52 agonist results in a higher FRET change compared to Tcon .....	65
<b>Figure 11.</b> Real-time measurements of FRET response in T cells upon adenosine stimulation.....	67
<b>Figure 12.</b> Pan-PDE inhibitor IBMX differentially affects cAMP levels T cells subsets in activated vs. non-activated state .....	69
<b>Figure 13.</b> Conventional T cells highly express PDE4B and PDE4D .....	70
<b>Figure 14.</b> Live-cell imaging of T cell subsets expressing Epac1-camps sensor upon PDE4 inhibition.....	71
<b>Figure 15.</b> PDE3B expression is elevated in conventional T cells vs regulatory T cells .....	72
<b>Figure 16.</b> Real-time measurements of PDE3 inhibitor effects in the cytosol of CD4+ T cells via FRET .....	73
<b>Figure 17.</b> Live-cell imaging of T cell subsets expressing Epac1-camps sensor upon PDE3 inhibition.....	74

<b>Figure 18.</b> Activation of conventional T cells in vitro results in upregulation of PDE2A on a protein level .....	75
<b>Figure 19.</b> Real-time measurements of PDE2 inhibitor effects in the cytosol of CD4+ T cells via FRET.....	77
<b>Figure 20.</b> Live-cell imaging of T cell subsets expressing Epac1-camps sensor upon PDE2 inhibition.....	78
<b>Figure 21.</b> Expression of <i>Npr1</i> and <i>Npr2</i> in CD4+ T cells .....	79
<b>Figure 22.</b> Stimulation of T cells subsets with atrial and C-type natriuretic peptides changes cAMP levels measured via FRET .....	81
<b>Figure 23.</b> Gene expression levels of Connexin 43 in non-activated and activated CD4+ T cells .....	82
<b>Figure 24.</b> Cell contact between regulatory and conventional T cells increases cAMP level in Tcon.....	84
<b>Figure 25.</b> Localization of Connexin 43 in T cells subsets .....	85
<b>Figure 26.</b> GHS hazardous pictograms .....	122

## List of Abbreviations

A	Activated cells
AC	Adenylyl cyclase
ADO	Adenosine
A <sub>2A</sub> R	Adenosine 2A receptor
ADP	Adenosine diphosphate
AKAP	A-kinase anchoring protein
AMP	Adenosine monophosphate
ANP	Atrial natriuretic peptide
APC	Antigen presenting cells
ATP	Adenosine triphosphate
BAY	BAY 60-7550
BNP	Brain natriuretic peptide
cAMP	3', 5' - cyclic adenosine monophosphate
CD	Cluster of differentiation
CFP	Cyan fluorescent protein
cGMP	3', 5' - cyclic guanosine monophosphate
CiLO	Cilostamide
CNG	Cyclic nucleotide-gated ion channel
CNBD	Cyclic nucleotide-binding domain
CNP	C-type natriuretic peptide
CREB	cAMP responsive element binding protein
CTLA-4	Cytotoxic T lymphocyte antigen 4
Cx	Connexin
CxHC	Connexin hemichannels
DN	Double negative

DP	Double positive
EAE	Experimental autoimmune encephalomyelitis
Epac	Exchange protein directly activated by cAMP
Foxp3	Forkhead transcription factor family
FRET	Förster resonance energy transfer
FSK	Forskolin
GDP	Guanosine diphosphate
GEF	Guanine nucleotide exchange factors
GJIC	Gap junction intracellular communication
GPCR	G protein-coupled receptor
GPR52	G protein-coupled receptor 52
GTP	Guanosine triphosphate
h	Hour
HEK293A	Human embryonic kidney 293A
IBMX	3-Isobutyl-1-Methylxanthine
IFN- $\gamma$	Interferon-gamma
IL	Interleukin
IS	Immune synapse
ISO	Isoproterenol
KO	Knockout
$K_m$	Michaelis constant
MHC	Major histocompatibility complex
min	Minute
NA	Non-activated cells
NE	Norepinephrine
NK	Natural killer cells
norm	Normalized

on	Overnight
PDE	Phosphodiesterase
pGC	Particulate guanylyl cyclase
PKA	Protein kinase A
ROLI	Rolipram
RT	Room temperature
s	Second
S <sub>0</sub>	Ground state
S <sub>1</sub>	Excited state
SMAC	Supramolecular activation cluster
Tcon	Conventional T cells
TCR	T cell receptor
TG	Transgenic
TGF-β	Transforming growth factor-beta
Th	Helper T cells
TNF-α	Tumor necrosis factor-alpha
TNT	Tunneling nanotubes
Treg	Regulatory T cells
WT	Wild-type
YFP	Yellow fluorescent protein
β-AR	Beta-adrenergic receptor
5'-AMP	Adenosine 5'-monophosphate



## Zusammenfassung

Der *Second-Messenger* cAMP ist ein entscheidendes Element für die Regulierung von angeborenen und adaptiven Immunreaktionen. Die basalen intrazellulären cAMP-Spiegel in murinen T-Zell-Subtypen wurden mittels eines cAMP-*Immunoassays* gemessen. So wurden höhere cAMP-Werte in regulatorischen T-Zellen (Treg) gegenüber konventionellen T-Zellen (Tcon) beobachtet. Unterschiedliche cAMP-Konzentrationen in T-Zell-Untergruppen sind entscheidend für die Treg-vermittelte Immunsuppression gegenüber Tcon und die Kontrolle der Tcon-Aktivierung, -Proliferation, -Differenzierung und Zytokinproduktion. Im Laufe der Jahre wurden verschiedene Strategien im Rahmen der T-Zellforschung entwickelt, um die Ursachen der unterschiedlichen cAMP-Spiegel in den T-Zellsubtypen zu erforschen. Angriffspunkt für therapeutische Ansätze gegen verschiedene Neuro- und Autoimmunerkrankungen sind G Protein-gekoppelte Rezeptoren (GPCRs), insbesondere diejenigen, die an stimulierende G Proteine (Gs) gekoppelt sind. Diese aktivieren Adenylylzyklasen (ACs) entweder durch extrazelluläre Liganden oder durch ihre konstitutive Aktivität. Für den G Protein gekoppelten Rezeptor GPR52 wurde beim *Immune-Datenscreening* eine unterschiedliche Expression in Treg und Tcon Zellen festgestellt, weshalb dieser Rezeptor als erster vielversprechender Kandidat genauer untersucht wurde. GPR52 wurde bereits früher im Zusammenhang mit Neurodegeneration untersucht, doch die Auswirkungen dieses Proteins auf das Immunsystem waren bisher unbekannt. Deshalb wurde im Folgenden die Wirkung des GPR52-Agonisten FTBMT auf die Modulation der cAMP-Spiegel in primären murinen T-Zellen untersucht, die den hochsensitiven FRET-basierten Sensor Epac1-camps exprimieren. Durch die erfolgreiche Durchführung von *Live-Cell-Imaging* in intakten T-Zellen konnte eine höhere intrazelluläre cAMP-Produktion in nicht aktivierten Treg- im Vergleich zu Tcon-Zellen gemessen werden. Bei der Aktivierung von T-Zell-Untergruppen wurden vergleichbare cAMP-Spiegel als Reaktion auf die FTBMT-Behandlung festgestellt. Zusammenfassend konnte in Kooperation mit unseren SFB1328 A06-Projektpartnern (Forschungsgruppe von Prof. Dr. Frieze), die weitergehende Untersuchungen an T-Zellen durchgeführt haben, gezeigt werden, dass GPR52 weder *in vitro* noch *in vivo* einen Einfluss auf die T-Zell-Funktion hat. Um die cAMP-Erzeugung und -Regulierung durch ACs und Phosphodiesterasen (PDEs) in beiden T-Zell-Untergruppen weiter zu untersuchen, wurde ein *NanoString-Panel* mit relevanten cAMP-Genen entwickelt, mit dessen Hilfe weitere potenziell beteiligte Gene identifiziert werden können. Unter anderem wurden so Unterschiede in der Genexpression von *Pde2a* und *Pde3b* in Treg und Tcon festgestellt, worauf unser zweiter Ansatz basierte. Die Analyse der Proteinlevel mittels *Immunoblotting* bestätigte höhere PDE3B-Proteinkonzentrationen sowohl in nicht aktivierten als auch in aktivierten Tcon im Vergleich zu einer geringen Expression von PDE3B in

regulatorischen T-Zellen. Erstmals wurde eine Hochregulierung von PDE2A auf Proteinebene in aktivierten gegenüber nicht aktivierten Tcon nachgewiesen. Zusätzlich zu einer stärkeren FRET-Antwort, die nach der PDE2A-Hemmung in aktivierten Tcon beobachtet wurde, wurden auch FRET-Veränderungen nach der PDE3B-Hemmung gemessen. So konnte eine höhere cAMP-Produktion sowohl in nicht-aktivierten als auch in aktivierten Tcon im Vergleich zu Treg gezeigt werden. Darüber hinaus führte die Stimulation von T-Zellen mit natriuretischen Peptiden zu erhöhten cAMP-Spiegeln in nicht-aktivierten Tcon im Gegensatz zur beobachteten Reaktion der aktivierten T-Zellen, was auf eine Umwandlung von PDE3B-abhängigem positivem zu PDE2A-abhängigem negativem cGMP/cAMP-*Cross-Talk* hindeutet. Schließlich führte uns unsere Vorarbeit in die Richtung der Visualisierung des cAMP-Transfers in T-Zellen. Erste FRET-Daten zeigten einen signifikanten Anstieg des cAMP-Spiegels beim Zellkontakt zwischen aktivierten Tcon und nicht aktivierten Treg (aber nicht Tcon) während der Echtzeitmessungen, was jedoch noch weiter untersucht werden muss.

## Abstract

Intracellular second messenger, cAMP, is a crucial element for regulation of innate and adaptive immune responses. Basal intracellular cAMP levels in murine T cell subsets were measured via cAMP immunoassay and demonstrated higher basal cAMP levels in regulatory T cells (Treg) in comparison to conventional T cell (Tcon) subset. This difference in cAMP between T cell subsets is the key step for conducting Treg-mediated immunosuppression towards Tcon and control of Tcon activation, differentiation, proliferation, and cytokine production. The interest in addressing the mechanisms behind differences in cAMP levels between T cell subsets resulted in multiple research strategies performed in T cells over the years. G protein-coupled receptors (GPCRs), especially those coupled to stimulatory G proteins (Gs), activate adenylyl cyclases (ACs) either by extracellular ligands or through their constitutive activity, which puts them forward as interesting targets and therapeutic solutions in various neuro- and autoimmune diseases. Upon Immgene data screening, differential expression of GPR52 was observed and further investigated as a first promising candidate. GPR52 was previously exploited in the context of neurodegeneration, and the impact of this protein on the immune system has not been examined until now. Briefly, the impact of GPR52 agonist drug, FTBMT, was probed in modulating cAMP levels in primary murine T cells expressing a sensitive FRET-based sensor, Epac1-camps. By conducting successful live-cell imaging of intact cells, higher intracellular cAMP production in non-activated Treg in comparison to Tcon cells were measured. Upon activation of T cell subsets, comparable cAMP levels in response to FTBMT treatment were detected. In collaboration with our CRC1328 A06 project partners (Research group of Prof. Dr. Friesen), who have performed multiple T cell assays, it has also been shown that GPR52 has no impact on T cell function *in vitro* nor *in vivo*. To further explore the cAMP generation and regulation by ACs and phosphodiesterases (PDEs) in both T cell subsets, NanoString panel was designed with relevant cAMP genes to identify additional interesting candidate genes. Among others, differential gene expression of *Pde2a*, and *Pde3b* in Treg and Tcon was detected and it orchestrated direction of our second approach. Immunoblotting confirmed higher PDE3B protein levels in non-activated and activated Tcon in comparison to low expression in Treg. As a novel finding, upregulation of PDE2A was demonstrated at the protein level in activated vs. non-activated Tcon. In addition to the stronger FRET response observed consequent to PDE2A inhibition in activated Tcon, FRET changes were measured upon PDE3B inhibition as well, which revealed higher cAMP production in non-activated and activated Tcon compared to Treg. Furthermore, stimulation of T cells with natriuretic peptides resulted in augmented cAMP levels in non-activated Tcon opposite to the activated T cell response measured, which suggested the conversion in cyclic nucleotide cross-talk from PDE3B-dependent positive to negative cross-talk dependent of

PDE2A. Lastly, our groundwork guided us in the direction of cAMP transfer visualization in T cells. Preliminary FRET data could identify a significant increase in cAMP levels upon establishing cell contact between activated Tcon and non-activated Treg (but not Tcon) during real-time measurements which need to be further elucidated.

# 1 Introduction

## 1.1 T cell development: long road from precursor cells to mature T cell soldiers and spies

### 1.1.1 T cell development and activation process

T cells are known to be critical players during inflammatory responses, either to trigger inflammation or encourage its termination (Ghani et al. 2009). To highlight the impact of T cell actions during inflammation, the development of T cells will be first introduced as shown in the schematics (**Figure 1**).

Development of T cells is a complex process that evolves in the bone marrow starting from hematopoietic stem cells. Hematopoietic stem cells give rise to multiple cell types such as lymphoid progenitors, which are precursor cells of mature T lymphocytes, members of the white blood cell lineage (Doulatov et al. 2010). Daily migration of lymphoid progenitor cells via blood, from bone marrow to the thymus, results in low cell numbers reaching the destination. Consequently, upon entry of lymphoid progenitors at cortical-medullary junction in the thymus, prompt expansion of cells is observed alongside transcriptional re-programing specific for T cell lineage, including gradual elimination of the potential for development of B cells and natural killer (NK) cell (Rothenberg, Moore, and Yui 2008). As a result of absence of both T cell co-receptors, cluster of differentiation (CD)4 and CD8, on immature T-cell precursor cells, they are referred to as double negative (DN) cells. DN cells differentiate into either  $\gamma\delta$  or  $\alpha\beta$  T cell subsets, and ratio of their presence in the circulation is 1:20.  $\gamma\delta$  T cell subsets will not be furthermore mentioned here. Next, various differentiation stages of DN (DN1-4) are identified by expression of diverse phenotypic markers on the surface of the cell, like CD44 and CD25 (Godfrey et al. 1993). In early developmental stage, cells are named pro-T cells (DN1 and 2) and this step is located in the thymus cortex, functioning independently of the T cell receptor (TCR). Stage 3 of differentiation of DN (DN3)  $\alpha\beta$  T cells exhibits an expression of non-rearranged pre-TCR- $\alpha$ , as well as the termination of the extensive thymocyte proliferation. In addition, assembly of  $\alpha\beta$ -TCR during differentiation stage of DN4 is conducted by pairing the rearranged TCR- $\alpha$  chain with TCR- $\beta$  chain, and  $\beta$  chain is a product of DNA rearrangements dependent on the expression of recombination-activation gene 1 (RAG1 and RAG2) (Q. Yang, Bell, and Bhandoola 2010). Furthermore, successful  $\beta$ -selection influences increased proliferation and the expression of co-receptor proteins, CD8 and CD4, resulting in the next maturation stage of T cells referred to as  $\alpha\beta$ -TCR double positive (DP) cells. After inadequate

## Introduction

$\beta$ -selection, cells experience apoptosis (Germain 2002). Abundant number of DP cells is further screened by negative and positive selection. Positive selection step for DP cells involves interplay of TCR with the major histocompatibility complex (MHC) in thymus cortex. T cells recognizing antigens represented by MHC with adequate affinity survive and experience negative selection process. Alternatively, DP T cells with weakened engagement of TCR and antigen-MHC complex will be eliminated by cell death. Due to two different types of MHC molecules, class I and II, depending on their specific interaction with TCR antigen recognition site, DP cells differentiate into CD8+ (class I MHC) or CD4+ (class II MHC) single-positive cells upon antigen presentation. Negative selection step promotes elimination of T cells which react to self-antigens in thymus medulla. T cells with the receptor that favors strong interaction with complex of self-peptides and MHC undergo apoptosis. By finishing the last step of initial developmental process, single positive naïve T cells are ready to enter the blood circulation and populate peripheral lymphoid tissue (**Figure 1**) (Sompayrac 2019; Murphy 2014).

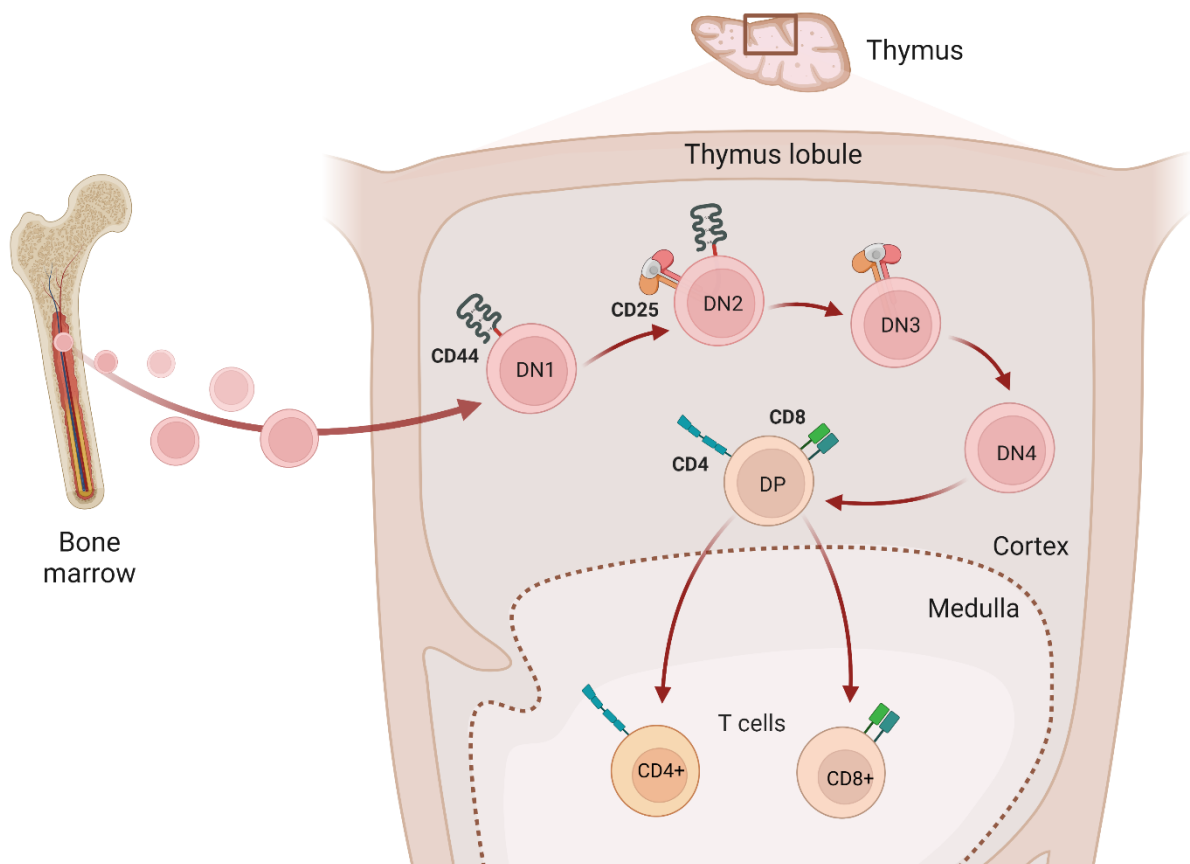


**Figure 1. Development of CD4+ and CD8+ T cells in the thymus.** Lymphoid progenitors are precursors of T cells. Precursor cells migrate from bone marrow to thymus where multiple T differentiation stages are completed. Double negative (DN) cells represent cells lacking both co-receptors, CD8 and CD4. Stage of differentiation for DN (DN1-4) is determined by expression pattern of specific phenotypic markers, CD44 and CD25. Functional T cell receptor (TCR) upon  $\beta$ -selection

## Introduction

(late DN3 and DN4) facilitates rise of double positive (DP) cells, expressing co-receptor proteins, CD8 and CD4. Final step of differentiation involves a positive and negative selection of TCR selectivity and results in single positive cells expressing either CD8 or CD4 on the T cell surface, ready to populate secondary lymphatic organs. This schematic was prepared using BioRender.com in reference to previously published schematics (Rothenberg, Moore, and Yui 2008; Germain 2002).

Naïve T cells that did not communicate yet with their specific antigen are programmed to enter secondary lymphatic organs via blood and re-enter blood via lymphatic fluid after antigen screening. Antigen screening by naïve T cells is facilitated via circulating near already activated antigen-presenting cells (APC), like macrophages and dendritic cells (DCs), previously activated by surrounding antigens. Antigen recognition by naïve T cells will initiate T cell activation process after they have encountered activated APC with expressed MHC molecules during body circulation (Gowans and Knight 1964; Hall 2015). To achieve proper T cell activation, Signal 1 and 2 are needed to subsequently initiate gene expression in T cells, and for stimulating proliferation of T cells as well. Signal 1 is accomplished upon assembly of immune synapses (IS) around TCR-MHC complex formed. Formation of IS is crucial step and expression of following molecules on surface of T cells is acquired: CD2, CD3, CD4/CD8, CD45, lymphocyte function-associated antigen-1 (LFA1), and TCR. CD2 expressed in T cells binds LFA3 expressed in APCs. Also, CD3 is expressed together with TCR. LFA1 serves as the first connection between T cells and APCs and binds to intracellular adhesion molecule 1 (ICAM1) on APCs (Dustin 2014). Signal 2 is generated after binding of CD28, expressed on cell surface of naïve T cells, and B7.1/2 (CD80/86) expressed on APCs (Harding et al. 1992).

### 1.1.2 T cell subsets: conventional and regulatory T cells

Specific T cell subsets are derived upon differentiation of naïve T cells after encountering specific antigens presented by APCs to achieve the most suitable adaptive immune reaction. Different T cell subsets have diverse expression of cytokine receptors and cytokines orchestrating their activation status and function. T cells expressing co-receptors CD4 or CD8 and  $\alpha\beta$ -TCR are introduced as conventional T cells (Tcon) which comprise 95% of T cell population. On the other hand, naturally occurring regulatory T cells (Treg) define 5% of total T cells, and on the side of expressing CD4 and  $\alpha\beta$ -TCR, their vital Treg lineage-specific marker is Forkhead box protein 3 (*Foxp3*) (Josefowicz and Rudensky 2009).

## Introduction

### 1.1.2.1 *Conventional T cells*

CD4<sup>+</sup> conventional T cells (Tcon), also called helper T (Th) cells, mediate immune response and immune protection through different actions such as cytokine and chemokine production, recruitment of granulocyte to inflamed tissue and infection site, helping B cell activation and subsequent antibody secretion. In the context of autoimmunity, relevant subsets of Th cells are Th1, Th2, and Th17. In the late 1980s, cytokine profiles were identified to discriminate Th cells (Th1 and Th2) with differential immunological actions (Coffman and Carty 1986; Mosmann et al. 1986; Zhu and Paul 2008, 4).

CD4<sup>+</sup> Th1 cells respond to intracellular infections, bacteria, and viruses. However, they are capable to induce autoimmunity and allograft rejections as well (Wan and Flavell 2009). Viral or tumor antigens presented by APCs in combination with pro-inflammatory cytokine interferon- $\gamma$  (IFN- $\gamma$ ) and interleukin-12 (IL-12) drive Th0 polarization towards Th1. The lineage-specific transcriptional master regulator is T-bet, upregulated during development of Th1 cells. T-bet is under control of activated signal transducer and activator of transcription (STAT) 1 and IFN- $\gamma$  (Lighvani et al. 2001; Kaplan and Grusby 1998). Th1 cells mainly produce cytokine IFN- $\gamma$ , but IFN- $\gamma$  also inhibits Th2 differentiation (Gajewski and Fitch 1988).

CD4<sup>+</sup> Th2 cells engage against parasites, allergens, and asthma. Polarization of Th2 cells is achieved by differentiation of Th0 cells under stimuli of IL-4. Binding of IL-4 to its receptor IL-4 $\alpha$  will promote activation of STAT6 resulting in Th2 differentiation (Shimoda et al. 1996). Key transcriptional factor regulating this particular differentiation process is GATA-3 which acts by binding to the locus of IL-4 (Zheng et al. 2007). Th2 cells secrete IL-4, IL-5 and IL-13. One of the effects of IL-4 secretion by Th2 is the blockage of Th1 cell differentiation and IFN- $\gamma$  secretion (Swain et al. 1990).

More recently identified Th subset, CD4<sup>+</sup> Th17 cells fight against extracellular infections, bacteria, and fungi, besides this, they have an important role in mediating autoimmunity (Aranami and Yamamura 2008). Differentiation of Th0 cells into Th17 subset is induced by transforming growth factor (TGF)- $\beta$  and IL-6. Also, for Th17 differentiation, a crucial segment on transcriptional level is retinoic acid-related orphan receptor (ROR)- $\gamma$ t together with ROR- $\alpha$  (Martinez et al. 2008). Th17 cells generate cytokines like IL-17A, IL-17E, IL-21, and IL-22. IL-17 suppresses differentiation of Th1 cells, while both IFN- $\gamma$  and IL-4 inhibit development of Th17 cells (Park et al. 2005).



## Introduction

### 1.1.2.2 Regulatory T cells

Regulatory T cells (Treg) are subset of CD4<sup>+</sup> T cells characteristic for their suppressive potential necessary to actively control immune responses and protect against autoimmunity. Balance of Treg number is crucial for immune homeostasis since an insufficient cell number can influence severe autoimmunity while an increase in Treg triggers immune suppression (Liston and Gray 2014). Treg cells were identified in a ground-breaking study where authors showed that suppressor CD4<sup>+</sup>CD25<sup>+</sup> cells can be obtained from periphery of nonimmunized mice (Sakaguchi et al. 1995).

Lineage-specific marker is transcription factor *Foxp3*, a key element for proper Treg development and function (Fontenot et al. 2005). For example, *Foxp3*-defective mice, also called *scurfy* mice, are lacking Treg cells which results in severe lymphoproliferative autoimmune syndrome with fatal consequences (Brunkow et al. 2001). In humans, mutations in *Foxp3* gene will trigger development of genetic disorder immunodysregulation, polyendocrinopathy, enteropathy X-linked (IPEX) syndrome, accountable for disease development in boys presented through aggressive autoimmunity (Wildin et al. 2001).

Surface markers of naïve Treg cells are CD25, CD127, cytotoxic T lymphocyte antigen 4 (CTLA-4), and glucocorticoid-induced tumor necrosis factor receptor family-related gene (GITR) (Becker et al. 2006). CD25, the  $\alpha$ -chain of the IL-2 receptor, is indeed present on plasma membrane of all activated T cells with a contrast of low and transient expression in Tcon compared to constitutive activity observed in Treg (Sakaguchi et al. 1995). Negative regulator of T cell activation is CTLA-4 thus playing important role in Treg-mediated immunosuppression (Takahashi et al. 2000). In fact, Treg surface markers are also detected on the surface of activated conventional T cells implying that activation of T cells is important for T cell-mediated immunosuppression. Treg cells produce immunosuppressive cytokines: IL-10, IL-35, and TGF- $\beta$  (Schmidt, Oberle, and Krammer 2012). Overall, TGF- $\beta$  produced by Treg mediates immunosuppression in the gut (Powrie et al. 1996), while IL-35 inhibits proliferation of Tcon (Collison et al. 2007, 35).

Depending on their developmental origin, Treg can be subdivided into subsets, naturally-occurring Treg (nTreg) and induced Treg (iTreg). nTreg are thymus-derived from CD4<sup>+</sup> T cell precursors while iTreg differentiate from naïve CD4<sup>+</sup> Tcon in the periphery. In humans, *Foxp3* and CD25 are not as specific markers to distinguish between two T cell subsets (Getnet et al. 2010), so both nTreg and iTreg are together called Treg cells. In mice, peripheral Tcon can differentiate into iTreg by stimulating cells with retinoic acid and TGF- $\beta$  (Coombes et al. 2007).

Presence of Treg includes a broad spectrum of actions in the immune system. Suppressing allergic inflammatory disorders, antitumor immunity, and T cell activation induced by weak

## Introduction

antigen stimulation but also maintaining maternal tolerance to the fetus, immune self-tolerance, and homeostasis by controlling Tcon are just some of them (Togashi, Shitara, and Nishikawa 2019).

### 1.1.3 How regulatory T cells mediate immunosuppression and autoimmunity?

Immunosuppression is a condition caused by reduced immune system function in terms of activation and efficiency. There are multiple humoral and cellular mechanisms of how Treg implement their suppressive actions toward responder cells, including B cells, Tcon (both CD4+ and CD8+), APCs (dendritic cells), NK cells, etc., further described in this paragraph (Schmidt, Oberle, and Krammer 2012). The first mechanism is focused on IL-2 consumption. Treg express IL-2R $\alpha$  receptor (CD25) which has a high affinity for IL-2, therefore, restricting accessibility of this particular cytokine to Tcon cells (Thornton and Shevach 1998). The second mechanism involves secretion of perforins and granzymes by Treg which can induce apoptosis of Tcon (Gondek et al. 2005). The third mechanism aims at reduction of APCs and Tcon activity with production of immunosuppressive cytokines as IL-10, TGF- $\beta$ , and IL-35 by Treg (Powrie et al. 1996; Collison et al. 2007, 35). CTLA-4 is in the center of the fourth mechanism and it is expressed on Treg surface. Binding of CTLA-4 to B7.1/2 (CD80/86) on APCs with higher affinity than CD28 will directly suppress activation of these cells and consequently, block activation of Tcon due to inhibition of signal 2 required for T cell activation (Qureshi et al. 2011). Lastly, the fifth mechanism introduces adenosine (ADO) and 3',5'-cyclic adenosine monophosphate (cAMP). Treg express ectoenzymes (CD39 and CD73) on their surface which convert ATP to ADO, and ADO further activates adenosine 2A receptors (A<sub>2A</sub>R) on Tcon and APCs resulting in cAMP production (Ernst, Garrison, and Thompson 2010). Also, direct transfer of cAMP from Treg to Tcon is achieved through gap junction intracellular communication (Bopp et al. 2007).

Autoimmunity is induced by an immune response directed towards self-antigens manifesting in vast prospect of autoimmune disorders (Khan and Ghazanfar 2018). Substantial imbalance in number and activity of Tcon and Treg will result in an autoimmune disorder. Sufficient number of Treg cells exhibiting proper inhibitory functions is capable of maintaining immune homeostasis (Bluestone and Tang 2005). In autoimmunity, increased ratio between Tcon to Treg with a decreased suppressive function of Treg is observed due to inflammation. Opposed, in a healthy state, balance between Tcon and Treg is preserved in a low ratio with an appropriate Treg-suppressive capacity (Gouirand, Habrylo, and Rosenblum 2022).

## Introduction

### 1.2 Dissecting cAMP pathway in CD4+ T cells

cAMP was first identified in the late 1950s by Sutherland as part of the mechanistic study of hormone actions (Sutherland and Rall 1958), and up to date, this intracellular second messenger was found in numerous cells and tissues.

cAMP synthesis, as well as the production of other second messengers, 3', 5' - cyclic guanosine monophosphate (cGMP), and calcium ( $\text{Ca}^{2+}$ ), is initiated by extracellular stimuli from drugs, hormones, and neurotransmitters. Ligand binds to G protein-coupled receptors (GPCRs) at the plasma membrane and induces conformational change after dissociation of  $\alpha$  subunit ( $G_\alpha$ ) of the guanine nucleotide-binding protein (G protein) from  $\beta\gamma$  subunit complex (Kamenetsky et al. 2006). Generation of cAMP upon  $G_\alpha$  subunit binding to AC will subsequently activate effector molecules: cyclic nucleotide-gated ion (CNG) channels, exchange protein directly activated by cAMP (EPAC), and protein kinase A (PKA). A predominantly investigated cAMP effector molecule is PKA, assembled of two symmetric catalytic and regulatory subunits. Binding of cAMP to regulatory subunits activate PKA and execute dissociation of active catalytic subunit monomers which further phosphorylate threonine (*Thr*) and serine (*Ser*) residues on numerous protein substrates (Taylor et al. 1992; Shabb 2001). cAMP-response element binding protein (CREB), cAMP-response element modulator/inducible cAMP early repressor (CREM/ICER), activating transcription factor-1 (ATF-1), and nuclear factor- $\kappa$ B (NF- $\kappa$ B) are only some of numerous PKA targets (Scott 1991). EPAC is a guanine-nucleotide-exchange factor (GEF) provoking activation of small guanosine triphosphate (GTP)ses of Ras superfamily, e.g. Rap1 and Rap2, by promoting guanosine diphosphate (GDP) to GTP exchange (de Rooij et al. 1998, 1). Balance in intracellular cAMP levels within the cell is restored by different families of ACs, cyclic nucleotide phosphodiesterase (PDEs), and guidance of PKA towards explicit substrates with A-kinase anchoring proteins (AKAPs) (Kjetil Taskén and Aandahl 2004). Role of ACs is to catalyze cyclization of ATP to cAMP, while PDEs are in control of cAMP degradation to 5'-AMP (Kanda and Watanabe 2001). AKAPs associate with regulatory subunit of PKA inside the cell and interact with ACs, GPCRs, G proteins, PDEs, and others (Wehbi and Taskén 2016).

cAMP function is largely diverse and it has a great impact on regulating multiple physiological processes in brain (Kandel 2012), heart (Nikolaev et al. 2010), lungs (Billington et al. 2013), immune system (Raker, Becker, and Steinbrink 2016), etc. In this particular PhD thesis, the goal was to uncover the role of cAMP in T cell biology.

Next, cAMP is also described as a second messenger with potent immunomodulatory functions. In the immune system, cAMP is orchestrating anti-inflammatory and pro-

## Introduction

inflammatory activities. It has been previously shown that cAMP-elevating drugs inhibit T cell proliferation, activation, and production of pro-inflammatory cytokines, such as IFN- $\gamma$  and TNF- $\alpha$  (T. Vang et al. 2001).

In 2007, cAMP levels have been compared between T cell subsets via cAMP ELISA. Naïve Treg showed elevated cAMP levels as compared to Tcon. Upon *in vitro* activation of T cells, intracellular cAMP levels were further increased in Treg and unchanged in Tcon. Co-culture of T cell subsets resulted in a substantial increase in cAMP levels in Tcon after 16 hours (Bopp et al. 2007). The same group also suggested that a rise in cAMP in Treg acts as a mechanism of cAMP-mediated suppressive potency of Treg. Moreover, differences in cAMP metabolism between T cell subsets will be further elaborated in the following paragraphs.

### 1.2.1 G protein-coupled receptors and their function in T cells

GPCRs are widely expressed in the human body, with over 800 membrane receptors identified (Fredriksson et al. 2003). This major class of membrane-bound receptors regulates multiple cellular processes by intracellular signal transduction and second messengers, e.g. cAMP and  $\text{Ca}^{2+}$ , after extracellular stimuli. Extracellular signal is achieved by first messengers, such as chemokines, drugs, hormones, lipid mediators, and neurotransmitters (Calebiro and Koszegi 2019). GPCR structure is characterized by seven transmembrane  $\alpha$ -helices (H1-7), containing three intracellular (IC1-3) and extracellular (EC1-3) loops, disulfide bond, and intracellular C-terminus in addition to extracellular N-terminus (Weis and Kobilka 2018). GPCRs interact with three families:  $\beta$ -arrestins, G protein-coupled receptor kinases (GRKs), and heterotrimeric G proteins. Heterotrimeric G protein complex consists of  $\alpha\beta\gamma$  subunit. External stimuli and binding of the ligand to GPCRs trigger exchange of GDP to GTP on  $G_\alpha$  subunit resulting in active GPCR. Moreover, binding of GTP to  $G_\alpha$  subunit consequence disengagement from its  $G_{\beta\gamma}$  subunit and activates downstream signaling actions.  $G_\alpha$  subunit binds to AC and further stimulates ( $G_{\alpha s}$ ) or inhibits ( $G_{\alpha i}$ ) cAMP synthesis (Hilger, Masureel, and Kobilka 2018). In murine T cells, localization of  $G_{\alpha s}$  subunit was reported in lipid rafts upon T cell activation with anti-CD3/CD28 followed by cAMP increase measured in fraction from the lipid raft (Abrahamsen et al. 2004). Moreover, there are two more members of  $G_\alpha$  subunit family,  $G_{\alpha q}$  which stimulates signaling pathway mediated by phospholipase  $\text{C}\beta$  ( $\text{PLC}\beta$ ) and  $G_{\alpha 12/13}$  known for activating Rho small GTPases (Hilger, Masureel, and Kobilka 2018). Downstream signaling of GPCRs is discontinued by receptor desensitization after GTPase activity inductions followed by receptor internalization. Some of the ligands that activate  $G_{\alpha s}$  are  $\beta$ -adrenoreceptor drugs, histamine, serotonin, adenosine, and prostaglandins ( $\text{E}_2$  and  $\text{I}_2$ ) while ligands possessing inhibitory properties are chemokines and leukotrienes (Neves, Ram, and

## Introduction

Iyengar 2002). GPCRs are classified into distinct families due to structure and sequence: class A (rhodopsin-like), class B1 (secretin receptor-like) and B2 (adhesion receptors), class C (glutamate receptor-like), and class F (frizzled-like) proteins (Foord et al. 2005; Wada et al. 2021). Class A is the largest family of GPCRs, which includes some of the receptors explored within this PhD thesis in the context of modulating cAMP levels in T cell subsets, including adenosine  $A_{2A}$  receptor ( $A_{2A}R$ ),  $\beta$ -adrenergic receptor ( $\beta$ -AR), and G protein-coupled receptor 52 (GPR52).

Many GPCRs have no specific ligand or it has not yet been identified. These GPCRs are named orphan and they are constitutively active. Role of some orphan GPCRs, like GPR3, GPR6, GPR12, GPR21, GPR52, and GPR65, has been investigated in different cell types. In brief, expression of GPR3, GPR6, and GPR12 was detected at high levels in the central nervous system (CNS) and their overexpression led to increase in cAMP production detected in neurons (Tanaka et al. 2007). Next, GPR52 is highly expressed in the murine striatum and nucleus accumbens. Upon treatment of murine striatal neurons with receptor agonist drug, FTBMT, an increase in cAMP level was detected in a dose-dependent manner (Nishiyama, Suzuki, Harasawa, et al. 2017; Nishiyama, Suzuki, Maruyama, et al. 2017). Furthermore, diverse GPCRs have been explored in connection with immunity and T cell functions. For example, GPR83 expression was reported high in Treg cells. Afterward, GPR83-deficient mice were generated and further characterized in line with T cell biology. Authors concluded that GPR83 is unnecessary in thymic development and Treg-mediated suppression (Lu et al. 2007), leaving the position available for another GPCR to show its significance in preserving high cAMP levels in Treg subsets.

### *1.2.1.1 Adenosine receptors*

Adenosine binds and activates adenosine receptors expressed in multiple cell types including immune cells. These GPCRs are grouped into 4 subtypes:  $A_1$ ,  $A_{2A}$ ,  $A_{2B}$ , and  $A_3$  (Borea et al. 2018). Resting and activated Tcon and Treg predominately express  $A_{2A}R$  (Deaglio et al. 2007). ADO is an endogenous mediator of physiological processes and its level increases due to ATP consumption. High extracellular ATP levels are a hallmark of inflammation but also arise during extreme physical activity, metabolic stress, or cell death. Production of ADO is facilitated through several pathways, and particularly engaging is metabolism of extracellular ATP via ectonucleoside triphosphate diphosphohydrolase (CD39) and ecto-5'-nucleotidases (CD73). In T cells, extracellular ATP or ADP are rapidly dephosphorylated to 5'-AMP by CD39, and AMP by CD73 further to ADO (Ernst, Garrison, and Thompson 2010). ADO binds  $A_{2A}R$ , coupled to stimulatory G protein, activates ACs, and triggers intracellular pathway driven by

## Introduction

cAMP as described in section 1.2.4. Activation of A<sub>2A</sub>R by ADO or another agonist drug resulted in obstructed proliferation of T cells and affected production of IL-2, IFN- $\gamma$ , and TNF- $\alpha$  (S. Huang et al. 1997, 2; Lappas, Rieger, and Linden 2005). Next, murine model of asthma was performed on wild-type (WT) and A<sub>2A</sub>R-deficient mice, where A<sub>2A</sub>R-deficient mice developed airway inflammation and hyperresponsiveness (Nadeem et al. 2007). Additionally, A<sub>2A</sub>R-deficient mice were subject to experimental autoimmune encephalomyelitis (EAE), which resulted in increased inflammation in the early stages of disease, as well as aggravated disease manifestation (Ingwersen et al. 2016).

### 1.2.1.2 *$\beta$ -adrenergic receptors*

$\beta$ -adrenergic receptors ( $\beta$ -AR) are members of the GPCR family. Three subtypes of  $\beta$ -AR have been identified up to date:  $\beta_1$ -AR,  $\beta_2$ -AR, and  $\beta_3$ -AR (Lohse, Engelhardt, and Eschenhagen 2003).  $\beta_1$ -AR and  $\beta_2$ -AR are G<sub>s</sub>-coupled receptors and signaling transduction is conducted as mentioned in section 1.2.1.  $\beta$ -ARs have a vital role in mediating cardiac function. Also, stimulation of  $\beta$ -AR mimics a checkpoint for controlling heart rate and myocardial contractility.  $\beta$ -blockers are in clinical use for multiple decades to treat human diseases as arrhythmia, heart failure, angina pectoris, and others (Wachter and Gilbert 2012).  $\beta_2$ -AR expression is predominant in naïve CD4<sup>+</sup> T and Treg cells, and a superior subtype of adrenoceptors in T cells (Sanders et al. 1997; Guerreschi et al. 2013). The functional relevance of  $\beta_2$ -AR in T cells was previously confirmed by using  $\beta_2$ -AR agonist drug, fenoterol hydrobromide, which led to inhibited proliferation of naïve T cells, together with reduced production of IL-2. Same group established Treg suppression assay in mouse T cell subsets and showed that  $\beta_2$ -AR stimulation boosts Treg suppressive function (Guerreschi et al. 2013). Moreover, differential effects were reported after stimulation of T cells in particular differentiation stage with cAMP-inducing agents. In naïve T cells, stimulation with norepinephrine (NE) elevated secretion of IFN- $\gamma$  (Swanson, Lee, and Sanders 2001). Co-culture with NE or specific  $\beta_2$ -AR agonist drug in addition to anti-CD3 induced differentiation of naïve CD4<sup>+</sup> T cells into iTreg (Guerreschi et al. 2013). Some autoimmune diseases have already been linked with  $\beta_2$ -AR dysregulation, such as multiple sclerosis (Axelrod and Bielory 2007) and rheumatoid arthritis (Lubahn et al. 2014). Also, it has been reported earlier that the immune system is in direct relationship with the sympathetic nervous system (SNS), which induces or abolishes inflammation via triggering  $\alpha$ -AR or  $\beta$ -AR (Lorton and Bellinger 2015).

## Introduction

### 1.2.2 Adenylyl cyclases and their role in modulating cAMP levels in T cells

ACs are enzymes that catalyze the formation of cAMP from ATP. In general, ACs comprise ten families, nine of them are membrane-bound (AC1-9), and one soluble isoenzyme (AC10) (Sunahara and Taussig 2002). Transmembrane AC isoforms are regulated by G proteins, while soluble AC is activated with  $\text{Ca}^{2+}$  or bicarbonate. Complex structure of membrane-bound ACs consists of two six-transmembrane ( $M_1$  and  $M_2$ ) regions, along with two cytoplasmic regions ( $C_1$  and  $C_2$ ) retaining variable cytosolic N-terminus (Krupinski et al. 1989). Activity of ACs is tightly regulated by GPCRs, as mentioned in section 1.2.1. Synthesis of cAMP after AC activation in T cells is conducted by many different agents such as adenosine,  $\beta$ -adrenergic receptor agonist drugs, or prostaglandins (Arumugham and Baldari 2017). In T cells, only transmembrane AC isoforms are expressed, including AC3, 6, 7, and 9 which are reported so far (Duan et al. 2010; B. Huang et al. 2009). Most relevant AC for T cell function is AC9. It has been shown earlier that in murine Tcon AC9 expression is downregulated at gene level by microRNA, miR-142-3p. On the contrary, Treg-specific transcriptional regulator, *Foxp3*, inhibits miR-142-3p expression, thus maintaining AC9 activity high and cAMP pathway effective (B. Huang et al. 2009). Abundant expression of AC7 was reported in both T and B cells. AC7-deficient chimeric mice exhibited a defect in production and conducting cAMP response in immune cells together with diminished generation of memory T cells (Duan et al. 2010; Jiang et al. 2008).

### 1.2.3 Phosphodiesterase as crucial regulators of cAMP signaling in T cells

PDEs are enzymes controlling cyclic nucleotide diffusion by degrading cAMP/cGMP to 5'-AMP/GMP. Cyclic nucleotide PDEs include a total of 11 enzyme families (PDE1-11) encoded by 21 gene and further branching into 100 diverse subtypes and isoforms discovered in different cells and tissues (Marco Conti and Beavo 2007). PDEs are built of functional domains including regulatory domain on N- and C-terminus and a catalytic domain. Catalytic domain is highly conserved among PDE families. N-terminus defines allosteric regulation such as phosphorylation sites and binding of cyclic nucleotides, metal ions, and calmodulin (Essayan 2001). Various isoforms of PDE families are mainly determined by the complexity of regulatory domain on N-terminus, while classification into families is based on homology of catalytic domain on C-terminus (Baillie, Tejeda, and Kelly 2019). Next, PDEs can be subdivided into categories depending on substrate affinity toward cyclic nucleotides. cAMP-specific PDEs are PDE4, 7, and 8 while cGMP-specific PDEs comprise PDE5, 6, and 9. PDE families that hydrolyze both cyclic nucleotides involve PDE1, 2, 3, 10, and 11 (M. Conti and Jin 1999). Expression of PDE1-5, PDE7, and PDE8 was previously confirmed in T cells (Essayan 2001; Bazhin et al. 2010).

## Introduction

PDE1 is a unique PDE due to activation by  $\text{Ca}^{2+}$  and calmodulin (CaM) so this PDE is described as  $\text{Ca}^{2+}$ /CaM-dependent family. Three subfamilies of PDE1 are PDE1A, PDE1B, and PDE1C. While PDE1C has a dual-substrate activity for hydrolyzing both cAMP and cGMP, PDE1A and PDE1B have significantly lower affinity for cAMP compared to PDE1C. Phosphorylation of PDE1 by PKA inhibits PDE1 activity (Bender and Beavo 2006). Expression of PDE1 was studied in human T cells. Resting T cells showed no expression of PDE1 on mRNA level while stimulation with phytohemagglutinin or anti-CD3/CD28 induce expression of PDE1B after 3 hours of stimulation and further increased over time (Kanda and Watanabe 2001).

PDE2 is a dual-substrate enzyme that is able to hydrolyze cyclic nucleotides with diverse Michaelis constant ( $K_m$ ) values, 10  $\mu\text{M}$  for cGMP and 30  $\mu\text{M}$  for cAMP (Martins, Mumby, and Beavo 1982). There are three reported PDE2A isoenzymes: PDEA1, PDEA2, and PDEA3. Different isoenzymes are a result of variable N-terminus, with a consequence of diverse localization within the cell. PDE2A1 is localized in the cytosol, PDE2A2 in mitochondria, and PDE2A3 is found on the plasma membrane, Golgi body, and sarcoplasmic reticulum. PDE2A contains the cGMP-specific PDEs, adenylyl cyclases and FhlA (GAF)-A and GAF-B regulatory domain (Juilfs et al. 1999). GAF-B is binding site of cyclic nucleotides. A low concentration of cGMP results in allosteric activation of PDE2A and conformational change in the catalytic domain of enzyme, leading to increased cAMP hydrolysis, so PDE2A can be named as cGMP-activated PDE (Bender and Beavo 2006). Role of PDE2A in T cells has not been fully investigated yet. The most relevant study was conducted almost two decades ago. It has been reported that an increase in intracellular cGMP levels in murine thymocytes increases PDE2 activity which can be diminished by EHNA, a selective PDE2A inhibitor (Michie et al. 1996).

PDE3 family binds both cyclic nucleotides with high affinity and reported  $K_m$  values are 0.08  $\mu\text{M}$  for cAMP and 0.02  $\mu\text{M}$  for cGMP. Due to the greater catalytic rate for cAMP over cGMP, in essence, PDE3 functions as a cGMP-inhibited enzyme for cAMP hydrolysis (Zaccolo and Movsesian 2007). PDE3 has two major subfamilies, PDE3A, further subdivided into three isoforms, and PDE3B. Activity of both PDE3A and PDE3B is increased by PKA phosphorylation (Marco Conti and Beavo 2007). In T cells, PDE3B is a predominant isoenzyme. Group of A. Rudensky showed in 2007 that *Foxp3*, as master regulator of Treg cells, directly suppresses *Pde3b* gene expression and therefore Treg are accumulating higher intracellular cAMP levels (Gavin et al. 2007). Differential expression of PDE3B was further confirmed in murine T cell subsets, where naïve T cells exhibited higher level of PDE3B, and as well in human T cell line, Jurkat cells (A. G. Vang et al. 2013; Dong et al. 2010). Next, inhibiting PDE3 in mouse and human CD4<sup>+</sup> T cells led to differentiation into a fully functional



## Introduction

T cells population with Treg characteristics able to prevent allograft rejection (Feng et al. 2011).

PDE4 is a predominant family of PDEs expressed in numerous cell types and tissues including T cells (Francis, Blount, and Corbin 2011; Erdogan and Houslay 1997). PDE4 is selective for cAMP with  $K_m$  values varying between 1-10  $\mu$ M. PDE4 is a complex family and contains four genes, PDE4A-D, encoding for different variants of this enzyme (Marco Conti and Beavo 2007). There are different PDE4 proteins exerting long, short or super-short forms depending on their upstream conserved regions (UCR) 1 and/or UCR2 in addition to unique regions on the N-terminus. In general, UCR1/2 and N-terminus are important for the control of PDE4 activity by phosphorylation actions together as well as for interplay with other proteins (Houslay, Baillie, and Maurice 2007). Highly expressed subtypes of PDE4 in T cells are PDE4A, PDE4B, and PDE4D (Landells et al. 2001). PDE4 and its different isoforms have been already well-explored in the context of T cell function and biology. Association of PDE4B2 and TCR/CD3 complex has been shown previously (Baroja et al. 1999). Same isoform has been detected as important during T cell activation since TCR signaling activates PDE4B and thus influences production of IL-2 (Arp et al. 2003).  $\beta$ -arrestins are intracellular scaffolding proteins, and they form a complex with PDE4. PDE4/ $\beta$ -arrestin complex has been introduced to the lipid rafts where affected cAMP decrease and increased T cell activation in primary T cells. For recruitment to occur, stimulation of CD28 alone is efficient (Abrahamsen et al. 2004). Moreover, PDE4 has been extensively studied also for treating inflammatory disorders. Multiple PDE4 inhibitors are being investigated as potential therapeutic solutions, while three PDE4 inhibitors have been approved in 2011, 2014, and 2016 for clinical use by European Medicines Agency (EMA) and Food and Drug Administration (FDA). Roflumilast is approved to treat chronic obstructive pulmonary disorder (COPD), Apremilast is used for psoriasis while Crisaborole is applied as therapy for moderate atopic dermatitis (Baillie, Tejeda, and Kelly 2019).

PDE7 family has universal affinity for cAMP as a substrate with  $K_m$  values for cAMP ranging between 0.03-0.2  $\mu$ M (Zaccolo and Movsesian 2007). PDE7 has two genes, PDE7A and PDE7B, each consisting of three splice variants. In the immune system, expression of Golgi-localized PDE7A isoenzymes has been reported (Szczypka 2020), particularly isoforms PDE7A1 and PDE7A3, in human CD4<sup>+</sup> T cells upon activation with anti-CD3/CD28 (Glavas et al. 2001). This was confirmed by another group showing that costimulation of resting human CD4<sup>+</sup> T cells with CD3/CD28 elevates PDE7 mRNA expression (Kanda and Watanabe 2001). For PDE7A1 was reported to be important in conducting proper IL-2 production and T cell proliferation upon CD3/CD28 costimulation (Li, Yee, and Beavo 1999, 7). In animal study performed on a mouse model of multiple sclerosis, EAE, use of a PDE7 inhibitor was reported

## Introduction

to exhibit a beneficial effect on inhibiting T cell proliferation but also weakened clinical symptoms during EAE (Redondo et al. 2012).

PDE8 family is comprised of two genes, PDE8A and PDE8B, with relatively high affinity for cAMP and reported  $K_m$  values from 0,04 to 0,15  $\mu\text{M}$  (Bender and Beavo 2006). Both isoforms have several splice variants involved in diverse biological processes. Protein expression of PDE8A has been reported in murine T cells, with increased expression in naïve Tcon subsets (A. G. Vang et al. 2013). In human T cells, costimulation with CD3/CD28 resulted in upregulation of PDE8A1 isoform in time-dependent manner (Glavas et al. 2001). S. Brocke with his group and collaborators performed extensive research over the years on the impact of PDE8 on T cell function (Epstein, Basole, and Brocke 2021). Some of the key findings implied that PDE8 could be an interesting target for suppressing function of Tcon since selective PDE inhibitor, PF-4957325, diminished adhesion of T cells to vascular endothelial cells (A. G. Vang et al. 2010, 8). Next, they could also show that T cell motility and not proliferation of T cell is under control of PDE8A due to interaction between PDE8 and V-Raf-1 murine leukemia viral oncogene homolog 1 (Raf-1) (Basole et al. 2017) and many more. In the EAE model, the treatment of mice with PDE8 inhibitor, PF-4957325, decreased inflation of Th1 and Th17 in the central nervous system (CNS). Also, a reduction in the clinical score for the EAE has been observed as well as the formation of an inflammatory lesion in CNS (Basole et al. 2022).

### 1.2.3.1 *Cyclic nucleotide cross-talk*

Generation of cAMP, as well as its degradation, has already been explained in detail in sections 1.2.1, 1.2.2, and 1.2.3. In brief, cAMP is produced by ACs upon binding of  $G_{\alpha s}$  subunit, and  $G_{\alpha s}$  subunit is detached from its  $G_{\beta\gamma}$  complex after GPCR (such as  $\beta$ -adrenoreceptors – e.g.  $\beta_2$ -AR or adenosine receptors – e.g.  $A_{2A}R$ ) activation by receptor agonists (**Figure 2**). ACs afterward catalyze the cyclization of ATP to cAMP (Beavo and Brunton 2002). One of the pathways how cGMP is generated within the cell is via membrane-bound particulate guanylyl cyclase (pGC). Activity of pGC is result of natriuretic peptide (NP) stimulation. Different NPs stimulate different receptors, meaning that atrial (ANP) and brain NP (BNP) activate pGC-A and C-type NP (CNP) activates pGC-B (Kuhn 2016). Although NPs have a vital role in cardiovascular function, especially through regulation of blood pressure and blood volume (Špiranec Spes et al. 2020), interest in their characterization in the immune system emerges after reported expression of ANP in lymphoid organs (Vollmar 1997). Cyclic nucleotide cross-talk is mediated with PDE2A and PDE3 activity (Zaccolo and Movsesian 2007). Generated cGMP in the cell cytosol binds to the GAF-B domain of PDE2A allosterically,

## Introduction

leading to conformational change within a catalytic domain and elevated cAMP hydrolysis. Even low concentrations of cGMP are sufficient for initiating negative cGMP/cAMP cross-talk. As a result, PDE2A is also called cGMP-activated PDE. Accordingly, PDE3, as cGMP-inhibited PDE, moderates positive cGMP/cAMP cross-talk. When cGMP binds to the catalytic domain of PDE3 it can block cAMP hydrolysis due to cGMP-mediated inhibitory effects resulting in cAMP augmentation (S. Weber et al. 2017, 2) (**Figure 2**). cGMP/cAMP crosstalk is well-studied in cardiomyocytes (Perera et al. 2015; Pavlaki and Nikolaev 2018), but the role of NP and cyclic nucleotide cross-talk in T cell biology has still not been established.

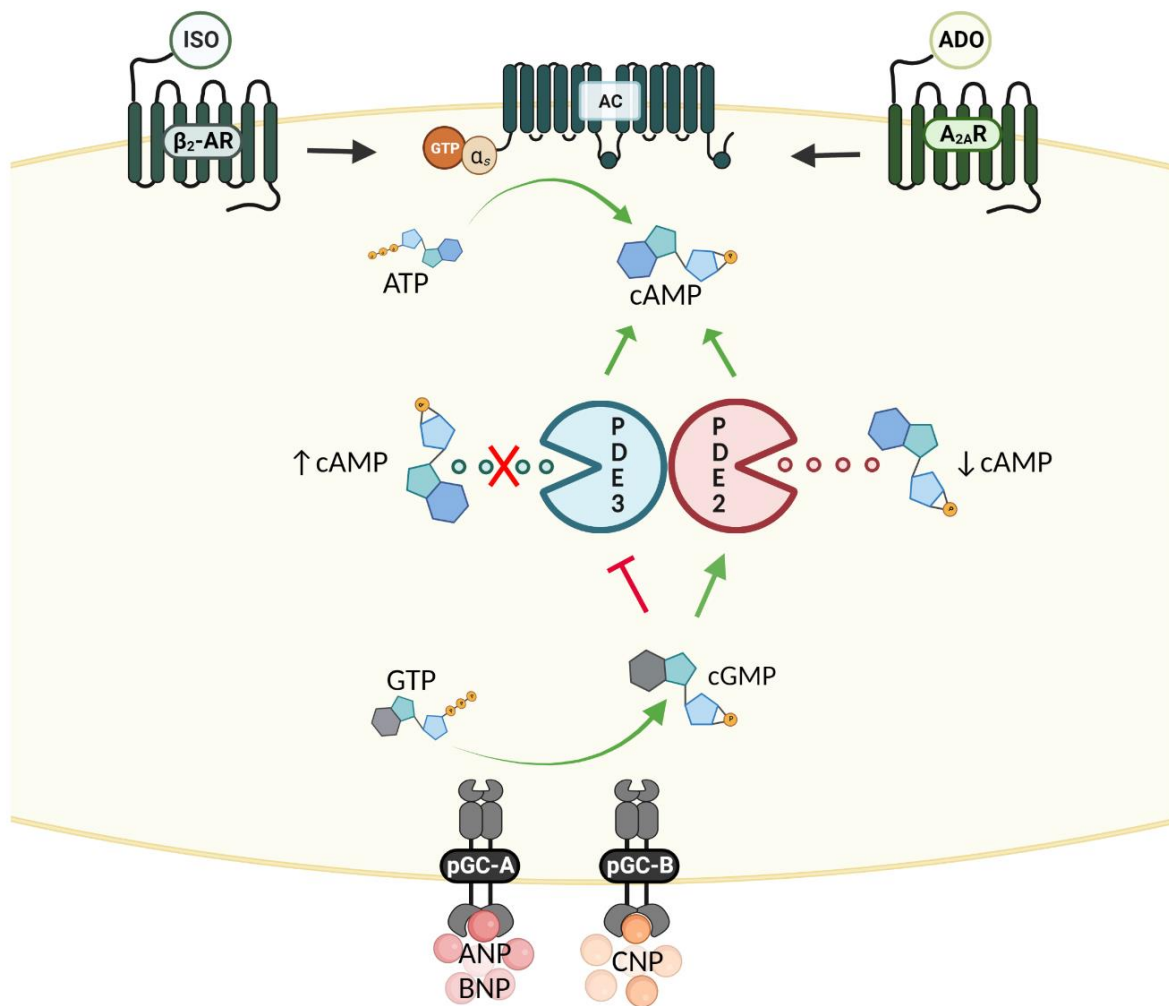


**Figure 2. Cyclic nucleotide cross-talk.** Cyclic nucleotides are produced by activated cyclases, ACs that generate cAMP, or by GCs that synthesize cGMP. PDE2A, as cGMP-activated PDE, mediates negative cGMP/cAMP cross-talk, and degradation of cAMP occurs at a higher rate. PDE3, as cGMP-inhibited PDE, upon cGMP binding, inhibits cAMP hydrolysis, thus preserving high cAMP levels. Schematics was prepared in BioRender.com in reference to previously published schematics (Sadek et al. 2020). ISO – isoproterenol, ADO- adenosine,  $\beta$ -adrenoreceptors – e.g.  $\beta_2$ -AR or adenosine receptors – e.g.  $A_{2A}R$ , AC -adenylyl cyclase,  $G_{\alpha s}$  – stimulatory  $G\alpha$  subunit, pGC – particulate guanylyl cyclase, NP- natriuretic peptides, ANP – Atrial NP, BNP – Brain NP, CNP – C-type NP.

## Introduction

### 1.2.4 Mechanisms of cAMP-driven Treg-mediated immunosuppression

Immunosuppression has been previously mentioned in section 1.1.3. Among the different described mechanisms of Treg-mediated immunosuppression, only two involve the interaction of Treg with cAMP (**Figure 3**). The first mechanism shows how extracellular nucleotides ATP and ADP are converted to ADO via ecto-5'-nucleotidases (CD39 and CD73) expressed on Treg plasma membrane. Degradation of ATP and ADP to AMP is facilitated by CD39, and AMP is further converted into ADO by CD73. Subsequently, generated ADO engages A<sub>2A</sub>R on the surface of target cells (e.g. Tcon), which activates AC and induces cAMP generation within the cell (Klein and Bopp 2016). The second mechanism depends on gap junction intracellular communication (GJIC). Treg cells produce and accumulate higher cAMP levels. Expression of miR-142-3p is downregulated in Treg by *Foxp3*, which in turn elevates AC9 activity and phosphorylation of ATP to cAMP. Similarly, *Foxp3* also inhibits PDE3B expression and activity by acting as a transcriptional repressor of *Pde3b* gene. On the contrary, miR-142-3p inhibits transcription of *Adcy9* gene and the production of cAMP is reduced (Rueda, Jackson, and Chougnet 2016). Increased cAMP generation in Treg enables direct transfer of cAMP from Treg to Tcon. This transfer is completed via gap junctions (GJ) through the coupling of hemichannels on the cell plasma membrane, thus directly connecting cytoplasms of interacting cells (Bopp et al. 2007). cAMP-mediated suppressive action in Tcon involve inhibitory effect on proinflammatory cytokine production, differentiation, and proliferation of Tcon cells by hindering TGF- $\beta$  and IL-2 production. Next, elevated cAMP levels upregulate CTLA-4 in Tcon which inhibits binding of CD28 mandatory for T cell activation as Signal 2 (Lorton and Bellinger 2015).

## Introduction

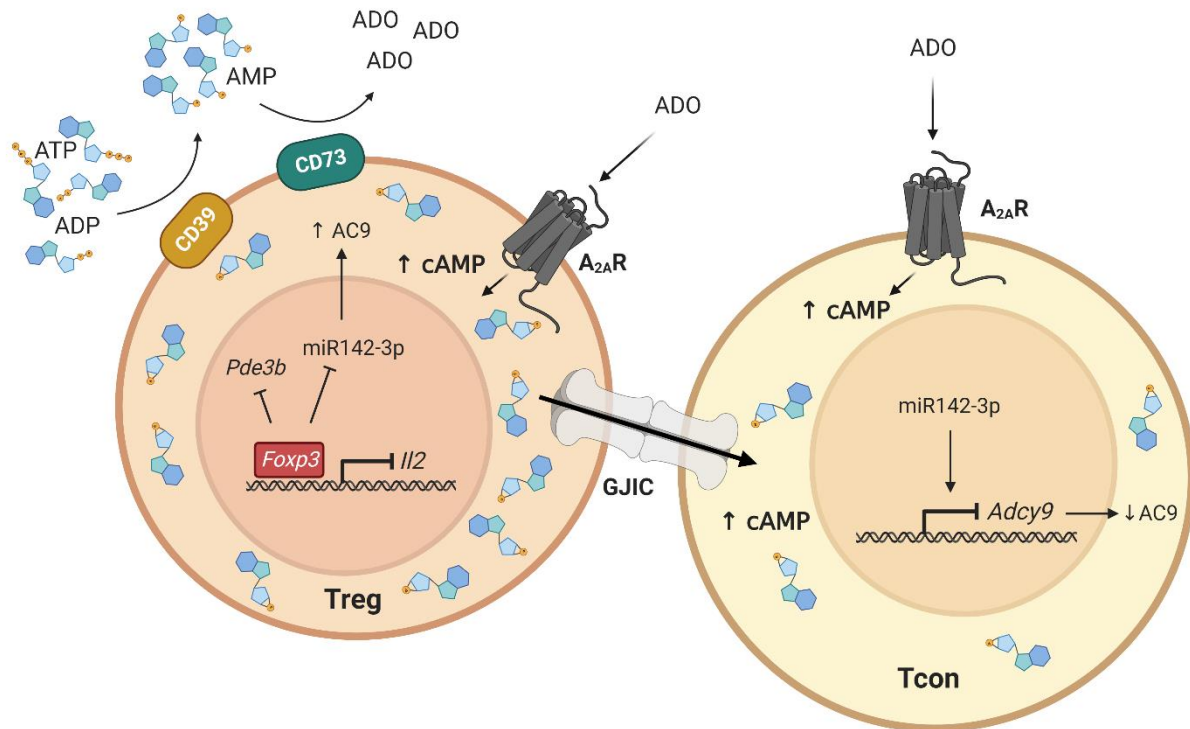


**Figure 3. cAMP as crucial player in Treg-mediated immunosuppression.** Various mechanisms have been suggested for how Treg control immunosuppression and two have cAMP as the main player. The first mechanism is focused on the degradation of extracellular ATP to adenosine via ectonucleotidases (CD39 and CD73) on Treg surface, engagement of adenosine A<sub>2A</sub> receptor (A<sub>2A</sub>R) on Tcon surface, and subsequent cAMP generation. The second mechanism describes a direct transfer of cAMP from Treg to Tcon via intracellular communication through gap junctions (GJIC). Schematic was prepared in BioRender.com in reference to previously published schematics (Klein and Bopp 2016). AC9, *Adcy9* – adenylyl cyclase 9, *Foxp3* - forkhead box protein 3, *IL2* – interleukin-2, *Pde3b* – phosphodiesterase 3b.

### 1.2.5 Gap junctions and their impact on T cell function

Gap junctions are essential for intercellular communication of ions, metabolites, and other small molecules through the coupling of hemichannels on the cell plasma membrane (Nielsen et al. 2012; Söhl and Willecke 2004). Hemichannels are combined of two connexons which contain a hexameric assembly of proteins called connexins (Goodenough, Goliger, and Paul 1996). Connexins (Cx) are transmembrane proteins with conserved structures among families. Cx structure consists of cytoplasmic (CL) and extracellular loop (E1 and E2), and N- and C-terminus in the cell cytoplasm (Sáez et al. 2003). Cx hemichannels are already expressed on the plasma membrane before forming GJ with a half-life of approximately 1 to 2,5 hours, although its expression does not ultimately imply the formation of GJ (Laird and Lampe 2018). Dominantly expressed GJ protein in both human and mouse immune systems is Connexin 43 (Cx43) (E. Oviedo-Orta, Hoy, and Evans 2000; Bermudez-Fajardo et al. 2007; Ernesto Oviedo-Orta and Howard Evans 2004), although it was reported that both T cell

## Introduction

subsets also express Cx31.1, Cx32, Cx45, Cx46 (Bopp et al. 2007). In T cells, GJIC is essential for normal T cell function, such as regulation of T cell activation, differentiation, and expansion but also for maintaining a balance between self-tolerance and response of T cells to different surrounding antigens (Uhl and Gérard 2020). In addition, one study also revealed that Treg in non-obese diabetic mice are losing their suppressive capacity in an age-dependent manner which is directly connected to reduced GJIC due to decreased expression of Cx43 (Kuczma et al. 2015). When Cx43 was overexpressed in Treg of these mice, the suppressive capacity of the cell was restored. One of the first confirmations that formation of GJ is occurring during cAMP transfer between Treg and Tcon emerges from an experimental setup performed by T. Bopp in 2007 (Bopp et al. 2007). In summary, co-culture of murine Tcon and calcein-loaded Treg for 20 hours resulted in an accumulation of calcein in Tcon afterward. Presence of GAP27, Cx43 inhibitory peptide, decreased calcein levels substantially.

Although gap junctions, immune synapses, and tunneling nanotubes are often mentioned when intracellular communication of the immune system is in question, they are not synonyms and they do not manifest identical structures, expression patterns, and function within cells. Immune synapses (IS) are characterized as contact sites of adjacent cells, and at least one is mandatory to be an immune cell (Onnis and Baldari 2019). Formation and function are not yet fully uncovered but it is considered to be entangled in the priming and activation of NK cells and T cells, both CD4+ and CD8+, as well as T cell proliferation and downstream signaling events (Tittarelli et al. 2020). IS are formed from supramolecular activation clusters (SMAC): central (cSMAC), distal (dSMAC), and peripheral (pSMAC). Localization of GJ and Cx43 within IS is reported in the pSMAC region (Mendoza-Naranjo et al. 2011). IS are known for being involved in conducting signal 1 which is vital for APC-mediated activation of T cells. Tunneling nanotubes (TNTs), serve as a long-distance communication network between cells and exchange of small molecules, organelles, and vesicles mostly in the diseased environment. TNTs usually exist as long cytoplasmic or open-ended protrusions. Cx and GJ formation have been also observed in TNTs but their function is not well understood yet. It has been reported that the communication process via TNTs is rapid since 30-60 seconds is sufficient for the transfer of cargo (Ariazi et al. 2017).

## Introduction

### 1.3 Live-cell imaging of cAMP and its dynamics via FRET

Levels of total cAMP in cells are widely measured with traditional immunoassays such as radioactive immunoassay (RIA) or cAMP enzyme immunoassay (EIA), however, these types of assays do not give information about spatio-temporal cAMP dynamics in real-time (Brooker, Terasaki, and Price 1976). An additional disadvantage of these particular assays is extremely large cell numbers needed to obtain enough material to conduct such measurement, which is not always possible due to limited cell number. Interest in analyzing cyclic nucleotide spatio-temporal dynamics at the single-cell level has risen at the beginning of the 1990s, with the development of the first fluorescent biosensors and has revolutionized the cyclic nucleotide live-cell imaging field (Willoughby and Cooper 2008). FRET-based biosensors currently in use to measure cyclic nucleotides are primarily based on downstream signaling targets. To measure intracellular cAMP levels, single-molecule probes have been developed such as PKA (Nikolaev et al. 2004; Zaccolo et al. 2000), EPAC (Nikolaev et al. 2004; Klarenbeek et al. 2015; Massengill et al. 2021), and cyclic nucleotide-gated channel probes (Nikolaev et al. 2006). A plethora of the currently used cAMP sensors are designed for bioluminescence (BRET) or Förster resonance energy transfer (FRET)-based approaches (Sprenger and Nikolaev 2013; Nikolaev and Lohse 2006).

In this particular thesis, imaging of living cells was performed by using FRET. FRET is quantum-mechanical mechanism where energy is transferred among two fluorophores in a non-radiative manner (Förster 1948). FRET happens between the adjacent donor and acceptor molecules with distance ranging from 2 to 10 nm due to dipole-dipole interactions (Pietraszewska-Bogiel and Gadella 2011). Transfer of molecular energy between donor and acceptor is defined through the Jablonski diagram (**Figure 4A**). The donor molecule is excited with its specific wavelength and after it absorbs the energy its electron rise from the ground state ( $S_0$ ) to the first excited state ( $S_1$ ) (timescale: attoseconds). Next, the electron encounters vibrational relaxation and achieves the lowest levels of energy in  $S_1$  (timescale: picoseconds). Afterward, electron can either return to the ground state ( $S_0$ ) after emitting the photon, a process called fluorescence, or transfer its energy to a nearby acceptor molecule, a phenomenon known as FRET (timescale: pico-/nanoseconds). Transfer of donor electron energy to acceptor results in a decrease of donor and increase of acceptor fluorescent intensity (Shrestha et al. 2015). FRET happens when the following requirements are completed: distance between donor and acceptor molecule up to 10 nm, fluorophore dipole orientation (parallel orientations of dipole exert higher FRET efficiency), and spectral overlap of the donor emission spectrum and acceptor excitation spectrum (**Figure 4B**).

To achieve expression of a particular target fluorescent protein or biosensors in cells, genetic manipulations are required; transient expression by using conventional transfection protocols

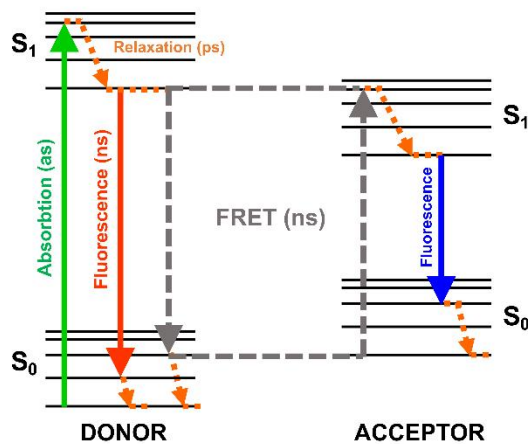
## Introduction

with liposomes/electroporation or maintained expression by transduction with diverse viral vectors (Fus-Kujawa et al. 2021). This can be avoided by generating a transgenic animal model expressing FRET biosensor which brings multiple advantages in performing real-time measurements. Expression of FRET biosensors in transgenic animals is either cell-specific or ubiquitous in all tissues and organs and provides an opportunity to isolate fresh and intact cells that can be directly used to perform real-time measurement (Börner et al. 2011; Sprenger et al. 2015). In order to measure FRET in T cells, cytosolic Epac1-camps biosensor has been used (Nikolaev et al. 2004; Calebiro et al. 2009). Epac1-camps biosensor contains cyclic nucleotide-binding domain (CNBD) derived from human Epac1 protein (amino acids: E157-E316). Single binding domain is flanked by fluorescent proteins, cyan (CFP) and yellow (YFP). In absence of cAMP, fluorophores are close in distance and FRET happens. Once when cAMP is bound to CNBD induces conformational change and the distance between two fluorophores increases leading to a decrease in FRET (**Figure 4C,D**; (Börner et al. 2011)). This type of FRET biosensor is suitable for spectral FRET imaging since CFP is excited with light emitting diode (LED) at 436 nm and emission spectral profiles of CFP and YFP are measured at 480 and 535 nm (Sprenger et al. 2012). FRET signal is calculated based on ratiometry, representing CFP/YFP or YFP/CFP ratio, obtained as raw data and further analyzed as mentioned in Section 2.2.6.

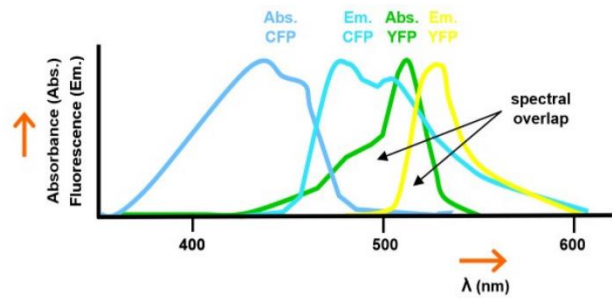


## Introduction

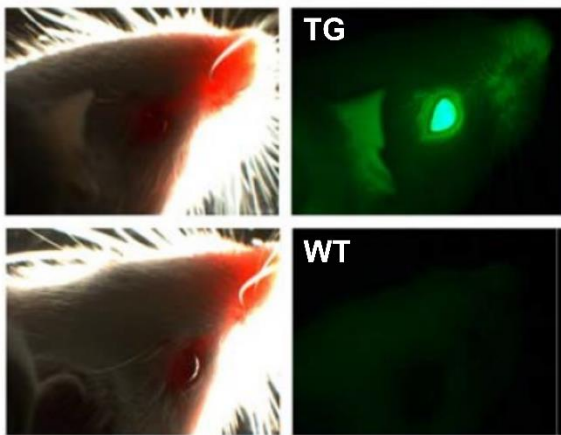
### A Jablonski diagram



### B Spectral overlap: CFP and YFP



### C Transgenic animal model



### D FRET biosensor: Epac1-camps

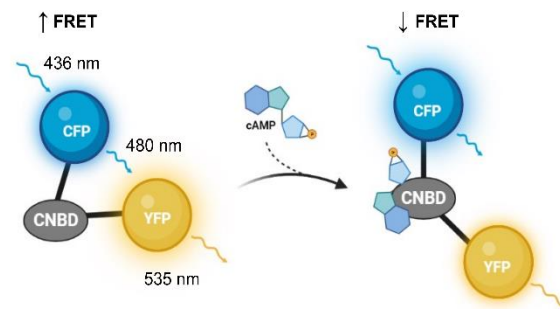


**Figure 4. Principles of the FRET technique.** **A)** Jablonski diagram depicting molecular energy of donor and acceptor fluorescent molecules (as-attoseconds, ps-picooseconds, ns-nanoseconds,  $S_0$ -ground state,  $S_1$ -excited state). **B)** Spectral overlap of widely used FRET pair, cyan (CFP) and yellow (YFP) fluorescent proteins. **C)** Example of ubiquitous expression of cytosolic Epac1-camps sensor in transgenic animal model (TG) compared to wild-type (WT) mouse. **D)** Schematics of the FRET biosensor, Epac1-camps (CNBD-cyclic nucleotide-binding domain). Schematics prepared in Power Point and BioRender.com in reference to previously published sources (Calebiro et al. 2009; Lakowicz 1999).

## Introduction

### 1.4 Objectives of the PhD thesis

cAMP is recognized as an important factor in innate and adaptive immune cell processes. As has been shown earlier, the rise of cAMP in Tcon or DC is a vital mechanism through which Treg mediate their suppressive action. Crucial step in Treg-mediated immunosuppression via utilizing cAMP is to influence Tcon responses such as proliferation and cytokine production. Formation of cAMP by ACs and degradation by PDEs select both as key targets for therapeutic intervention which results in great interest in understanding the underlying mechanisms of cAMP production and regulation of cAMP transfer in T cell biology more engaging to study.

Aims of the presented PhD study are summarised below.

Aim 1: Determine variance in cAMP production and regulation in T cell subsets

- design NanoString panel for the analysis of RNA expression cAMP-relevant genes such as ACs, PDEs, and GPCRs in non-activated T cell subsets
- implement measurements of basal cAMP level via cAMP immunoassay in murine T cell subsets
- enforce immunoblotting and qRT-PCR analysis of selected candidates in murine T cell subsets (non-activated and *in vitro* activated T cells)
- establish real-time cAMP imaging in T cell subsets expressing highly-sensitive Förster resonance energy transfer (FRET) based biosensor, Epac1-camps
- perform FRET measurements by applying different receptor ligands and PDE inhibitors in non-activated and activated T cell subsets isolated from transgenic mouse model expressing Epac1-camps sensor

Aim 2: Visualize cAMP transfer between T cell subsets via FRET

To investigate the real-time dynamics of cAMP with high temporal and spatial resolution, murine T cell subset will be measured in close contact to allow gap junction formation and potential cAMP exchange shown by live-cell imaging technique.

## 2 Materials and methods

### 2.1 Materials

#### 2.1.1 Animals

**Table 1.1.** List of mouse lines.

Mouse line	Background	Originator
CAG-Epac1-camps	FVB/N1	Prof. Dr. Viacheslav Nikolaev (Calebiro et al. 2009)
B6-DEREG (C:B6-Tg(Foxp3-DTR/EGFP)23.2SPAR/Mmjax)	C57/BL6	The Jackson Laboratory (Lahl et al. 2007)
<i>Gpr52</i> -deficient mice ( <i>Gpr52</i> <sup>tm1Kohi</sup> )	C57/BL6	Masaaki Mori (Komatsu et al. 2014)
<i>Adcy6</i> -deficient mice	C57/BL6	Prof. Dr. Kurt Krobert (Tang et al. 2008)

#### 2.1.2 Antibodies

##### 2.1.2.1 Primary antibodies for Fluorescence-activated cell sorting (FACS) analysis

**Table 2. 1.** List of antibodies for FACS-sorting. Antibodies prepared and used as follows.

Antigen	Fluorochrome	Clone	Dilution	Manufacturer (catalog number)
CD3ε	PerCP-Cy5.5	145-2C11	1:50	BioLegend (#100328)
CD4	Pacific Blue	RM4-5	1:100	BioLegend (#100531)
CD8a	APC	53-6.7	1:100	BioLegend (#100712)
CD16/32 (Fc receptor blocking)	/	93	1:100	BioLegend (#101319)

## Materials and methods

### 2.1.2.2 Primary antibodies for immunoblotting

**Table 2. 2.** List of primary antibodies for immunoblotting. Antibodies prepared and used as follows.

Primary antibody	Dilution	Blocking buffer	Species	Incubation conditions	Manufacturer (catalog number)
Anti-GAPDH	1:160000	5% non-fat milk	mouse	20 min, RT	HyTest (#5G4)
Anti-PDE2A	1:750	3% non-fat milk	rabbit	on, +4°C	Fabgennix (#PDE2A-101AP)
Anti-PDE3B	1:2000	5% non-fat milk	rabbit	on, +4°C	kind gift from Dr. Sergei Rybalkin
Anti-PDE4B	1:2500	5% non-fat milk	rabbit	on, +4°C	abcam (#ab170939)
Anti-PDE4D	1:2500	5% non-fat milk	rabbit	on, +4°C	abcam (#ab171750)

### 2.1.2.3 Secondary antibodies for immunoblotting

**Table 2. 3.** List of horseradish peroxidase-conjugated (HRP) secondary antibodies for immunoblotting. Antibodies prepared and used as follows, diluted in identical blocking buffer as primary antibody.

Secondary antibody	Dilution	Blocking buffer	Incubation conditions	Manufacturer (catalog number)
Goat anti-mouse	1:5000	3-5% non-fat milk	1 h, RT	Biorad (#170-5047)
Goat anti-rabbit	1:5000	3-5% non-fat milk	1 h, RT	Biorad (#170-5046)

## Materials and methods

### 2.1.2.4 Primary antibodies for immunofluorescence

**Table 2. 4.** List of primary antibodies for immunofluorescence staining. Antibodies prepared and used as follows.

Primary antibody	Dilution	Blocking buffer	Species	Incubation conditions	Manufacturer (catalog number)
Anti-Connexin 43	1:500	10% FBS	rabbit	1,30 h, RT	Sigma Aldrich (#C6219-100UL)
CD4, clone GK1.5	1:200	10% FBS	rat	1,30 h, RT	eBioscience (#14-0041-82)

### 2.1.2.5 Secondary antibodies for immunofluorescence

**Table 2. 5.** List of secondary antibodies for immunofluorescence staining. Antibodies prepared and used as follows.

Secondary antibody	Dilution	Blocking buffer	Incubation conditions	Manufacturer (catalog number)
Goat anti-Rabbit IgG (H+L) Highly Cross Adsorbed Secondary Antibody, Alexa Fluor 633	1:500	10% FBS	1 h, RT, dark	Invitrogen (#A-21071)
Goat anti-Rat IgG (H+L) Cross Adsorbed Secondary Antibody, Alexa Fluor 488	1:500	10% FBS	1h, RT, dark	Invitrogen (#A-11006)

## Materials and methods

### 2.1.3 Buffers and Solutions

All buffers and solutions were made in double-distilled (dd) water, Ampuwa water, or DPBS, as listed below.

#### 2.1.3.1 FACS sorting

**Table 3. 1.** 10x FACS buffer. Stored at +4°C.

Chemical	Work concentration ( $C_{final}$ )
Albumin Fraction V	0,05 g/mL
DPBS	10x
NaN <sub>3</sub>	0,002 g/mL

#### 2.1.3.2 Immunoblotting

**Table 3. 2.** RIPA buffer. Prepared in Ampuwa water. Aliquoted and stored at -20°C. Before use, RIPA buffer was supplemented with Halt protease inhibitor (100x).

Chemical	Stock concentration ( $C_{stock}$ )	Work concentration ( $C_{final}$ )
EDTA, pH 8,0	0,5 M	1 mM
NaCl	3 M	150 mM
SDS	20% (v/v)	0,1% (v/v)
NaDOC	10% (w/v)	1% (v/v)
Tris, pH 7,5	1 M	20 mM
Triton X-100	10% (v/v)	1% (v/v)

**Table 3. 3.** 4x Laemmli buffer. Prepared in 100 mL dd water. Stored at RT.

Chemical	Mass (g) / Volume (mL)
Tris, 1M (pH 6,8)	2,4 g
Glycerol, 100%	40 mL
SDS Solution, 20%	40 mL
Bromophenol blue sodium salt	0,2 g

## Materials and methods

**Table 3. 4.** 4x Tris/SDS, pH 6,8. Prepared in 100 mL dd water. Stored at RT.

Chemical	Work concentration ( $c_{final}$ )
SDS Solution, 20%	0,4% (v/v)
Tris (pH 6,8)	500 mM

**Table 3. 5.** 4x Tris/SDS, pH 8,8. Prepared in 250 mL dd water. Stored at RT.

Chemical	Work concentration ( $c_{final}$ )
SDS Solution, 20%	0,4% (v/v)
Tris (pH 8,8)	1,5 M

**Table 3. 6.** Ammonium persulfat (APS) solution. Prepared in 10 mL dd water. Aliquoted and stored at -20°C.

Chemical	Work concentration ( $c_{final}$ )
APS	10% (w/v)

**Table 3. 7.** 10x SDS Runing buffer, pH 8,3. Prepared in 2 L dd water. Stored at RT.

Chemical	Work concentration ( $c_{final}$ )
Glycin	1,9 M
SDS solution, 20%	1% (v/v)
Tris	250 mM

**Table 3. 8.** 1x SDS Runing buffer. Prepared in 1 L dd water. Stored at RT.

Chemical	Work concentration ( $c_{final}$ )
10x SDS Running buffer	1x

**Table 3. 9.** 10x Transfer buffer. Prepared in 2 L dd water. Stored at RT.

Chemical	Work concentration ( $c_{final}$ )
Glycin	1,9 M
Tris	325 mM

## Materials and methods

**Table 3. 10.** 1x Transfer buffer. Prepared in 1 L dd water. Stored at RT.

Chemical	Work concentration ( $c_{\text{final}}$ )
Methanol	20% (v/v)
10x Transfer buffer	1x

**Table 3. 11.** 10x Tris-buffered saline (TBS) buffer, pH 7,4. Prepared in 2 L dd water. Stored at RT.

Chemical	Work concentration ( $c_{\text{final}}$ )
NaCl	1,5 M
Tris	100 mM

**Table 3. 12.** 1x TBS-Tween 20 (TBS-T) buffer. Prepared in 1 L dd water. Stored at RT.

Chemical	Work concentration ( $c_{\text{final}}$ )
Tween 20	0,1% (v/v)
10x TBS buffer	1x

**Table 3. 13.** Blocking buffer. Prepared in 50 mL 1x TBST buffer. Stored at +4°C and used up to 3 days.

Chemical	Work concentration ( $c_{\text{final}}$ )
Powdered non-fat milk	3-5% (w/v)

**Table 3. 14.** Separating gel. Recipe for 2x 10% gels (with 1,0 mm gel tickness).

Chemical	Volume (mL)
Acrylamide	4
dd H <sub>2</sub> O	5
4xTris/SDS, pH 8,8	3
APS, 10%	0,048



## Materials and methods

**Table 3. 15.** Stacking gel. Recipe for 2x gels (with 1,0 mm gel thickness).

Chemical	Volume (mL)
Acrylamide	0,5
dd H <sub>2</sub> O	2,31
4xTris/SDS, pH 8,8	0,94
APS, 10%	0,0188
TEMED	0,0075

### 2.1.3.3 Immunofluorescence

**Table 3. 16.** Blocking buffer. Prepared in 10 mL DPBS and stored at +4°C.

Chemical	Work concentration (c <sub>final</sub> )
FBS	10% (v/v)

### 2.1.3.4 Cell culture – eukaryotic cells lines

**Table 3. 17.** Culturing medium for HEK293A cells. Stored at +4°C.

Chemical	Stock concentration (c <sub>stock</sub> )	Volume (mL)
DMEM	/	440
FBS	/	50
L-Glutamine solution	200 mM	5
Penicillin/Streptomycin	10000 U/mL, 10000 µg/mL	5

### 2.1.3.5 Cloning

**Table 3. 18.** Agarose gel, 1%. Prepared in 100 mL 1x TAE buffer. Agarose is dissolved by heating the solution in the microwave. Next, dissolved agarose solution is cooled down and used as follows in Section 2.2.7.

Chemical	Work concentration (c <sub>final</sub> )
Powdered agarose	1% (w/v)

## Materials and methods

**Table 3. 19.** Ampicilin (AMP) stock solution. Stock solution prepared in 10 mL dd water. Aliquoted and stored at -20°C.

Chemical	Stock concentration ( $c_{stock}$ )	Work concentration ( $c_{final}$ )
AMP	100 mg/mL	100 µg/mL

**Table 3. 20.** 5x KCM buffer. Stock solutions and KCM buffer prepared in 50 mL dd water. Stored at +4°C.

Chemical	Stock concentration ( $c_{stock}$ )	Work concentration ( $c_{final}$ )
KCl	1 M	500 mM
CaCl <sub>2</sub>	1 M	150 mM
MgCl <sub>2</sub>	1 M	250 mM

**Table 3. 21.** LB Agar plates. LB Agar prepared in 400 mL dd water. Mixed well, autoclaved and cooled down to approx. 50-55°C. Afterward, supplemented with AMP ( $c_{final}=100$  µg/mL) and poured into Petri dishes for cultivating microorganisms. Stored protected from light at +4°C.

Chemical	Mass (g)
LB Agar	16

**Table 3. 22.** LB Medium. Prepared in 400 mL dd water. Mixed well, autoclaved and stored at RT.

Chemical	Mass (g)
LB Medium	10

**Table 3. 23.** Transformation storage buffer (TSB). Mixed well, aliquoted and stored at -20°C.

Chemical	Volume (mL)
DMSO	5
LB Medium (without antibiotics)	73
MgCl <sub>2</sub> , 1M	2
PEG 3000 solution	20

## Materials and methods

**Table 3. 24.** 50x Tris-acetate-EDTA (TAE) buffer. Prepared in 1 L dd water and stored at RT.

Chemical	Work concentration ( $c_{\text{final}}$ )
Glacial acetic acid	1 M
EDTA, pH 8.0	50 mM
TRIS	2 M

### 2.1.3.6 Isolation and culture of primary murine T cells

**Table 3. 25.** MACS buffer. Freshly prepared in sterile DPBS (without  $\text{Ca}^{2+}/\text{Mg}^{2+}$ ) on the day of isolation. Filtered (0,22  $\mu\text{m}$ ) after dissolving and stored at +4°C.

Chemical	Work concentration ( $c_{\text{final}}$ )
BSA	0,5% (w/v)

**Table 3. 26.** RBC (Red blood cells) lysis buffer, pH 7.4. Prepared in Ampuwa water. Filtered (0,22  $\mu\text{m}$ ) after dissolving. Stored at +4°C, used up to one month.

Chemical	Work concentration ( $c_{\text{final}}$ )
EDTA, pH 8.0	0,1 mM
$\text{NaHCO}_3$	10 mM
$\text{NH}_4\text{Cl}$	150 mM

**Table 3. 27.** T cell culturing medium. Stored at +4°C, used up to two weeks.

Chemical	Volumes (mL)
RPMI 1640	40
Supplement 1	4,23
Supplement 2	2,3

## Materials and methods

**Table 3. 28.** Supplement 1. Aliquoted and stored at -20°C.

Chemical	Stock concentration ( $c_{stock}$ )	Work concentration ( $c_{final}$ )
L-Glutamine solution	200 mM	2 mM
MEM non-essential amino acids	100x	1x
Na-Pyruvate	100 mM	1 mM
Penicillin/Streptomycin	10000 U/mL, 10000 µg/mL	100 U/mL, 100 µg/mL
β-mercaptoethanol	50 mM	30 µM
FCS, heat-inactivated	/	5% (v/v)

**Table 3. 29.** Supplement 2. Aliquoted and stored at -20°C.

Chemical	Work concentration ( $c_{final}$ )
FCS, heat-inactivated	5% (v/v)

### 2.1.3.7 Live-cell imaging

**Table 3. 30.** FRET buffer, pH 7.4. Preped in 2 L Ampuwa water. Stored at RT.

Chemical	Work concentration ( $c_{final}$ )
CaCl <sub>2</sub>	1 mM
HEPES	10 mM
KCl	5,4 mM
MgCl <sub>2</sub> x 6H <sub>2</sub> O	1 mM
NaCl	144 mM

**Table 3. 31.** 10x PDL (Poly-D-Lysin) stock solution. Preped in 10 mL Ampuwa water. Aliquoted and stored at -20°C.

Chemical	Stock concentration ( $c_{stock}$ )
PDL	1 mg/mL

**Table 3. 32.** 1x PDL solution. Preped in 10 mL Ampuwa water. Diluted and stored at +4°C, used up to one week.

Chemical	Work concentration ( $c_{final}$ )
PDL, 10x	0.1 mg/mL

## Materials and methods

### 2.1.3.8 NanoString

**Table 3. 33.** TE buffer. Prepared in 5 mL Diethyl pyrocarbonate (DEPC) water. Stored at RT.

Chemical	Work concentration ( $c_{\text{final}}$ )
EDTA, pH 8,0	1 mM
TRIS, pH 8,0	10 mM
Tween-20	0,1% (v/v)

### 2.1.4 Cells

#### 2.1.4.1 Competent cells

**Table 4. 1.** List of competent cells.

Cells	Manufacturer (catalog number)
<i>E. Coli</i> cells – Top 10	Invitrogen (#C4040-10)

#### 2.1.4.2 Eucaryotic cell lines

**Table 4. 2.** List of eukaryotic cell lines.

Cell line	Manufacturer (catalog number)
Human embryonic kidney (HEK) 293A	Invitrogen (#R705-07)

### 2.1.5 Chemicals

#### 2.1.5.1 Chemicals – non-sterile work

**Table 5. 1.** List of chemicals used for non-sterile work (wet laboratory, live-cell imaging).

Chemical	Manufacturer (catalog number)
Adenosine	Merck (#PHR1138-1G)
Agarose universal peqGold	VWR (#35-1010)
Albumin Fraction V	Carl Roth (#8076.3)
Ammonium chloride ( $\text{NH}_4\text{Cl}$ )	Sigma Aldrich (#254134-5G)
Ammonium persulfate (APS)	Sigma Aldrich (A3678-25G)
Ampicillin sodium salts	Sigma Aldrich (#9518-5G)
Ampuwa water	Fresenius Kabi (40676.00.00)
Atrial natriuretic peptide (4-18, ANP), mouse	Bachem (#H-3134.0500)
BAY 60-7550	Santa Cruz (#sc396772)
Bovine serum albumin (BSA)	Sigma Aldrich (#A6003-25MG)

## Materials and methods

Bromophenol blue sodium salt	Carl Roth (#A512.1)
Calcium chloride (CaCl <sub>2</sub> )	Sigma Aldrich (#C8106)
Cilostamide	Santa Cruz (#sc201180A)
Cilostazol	Sigma Aldrich (#C0737-10MG)
C-type natriuretic peptide (1-53; CNP), human	Bachem (#01-H-7766)
DAPI	Sigma Aldrich (#D9542-1MG)
Deoxyribonucleotide triphosphate (dNTP) mix	Promega (#U1511)
Diethyl pyrocarbonate (DEPC)	Roth (K028.1-25ML)
Dimethyl sulfoxide (DMSO)	AppliChem (#A3672,0250)
DNA ladder, 1 kb	New England BioLabs (#N3232S)
Dulbecco's Phosphate buffered saline (DPBS)	PAN-Biotech (#P04-53500)
Ethanol, Rotipuran, >99,8% p.a.	Carl Roth (#9065.2)
Ethanol, 70%	Th.Geyer (#2202-5L)
Ethylenediaminetetraacetic acid (EDTA) disodium salt 2-hydrate	Applichem (#A1104, 0500)
E7	Analyticon Discovery (#NP-012321)
Forskolin	Hello Bio (#HB1348-10MG)
Gel Loading Dye Purple, 6x	New England BioLabs (#B7025S)
Glycerol	Millipore (#356350-500ML)
Glycine	Carl Roth (#3908.3)
Halt protease inhibitor cocktail, 100x	Thermo Scientific (#87786)
Hydrochloric acid (HCl), 37%	Carl Roth (#9277.1)
LB Medium (Luria/Miller)	Carl Roth (#X968.2)
LB Agar (Luria/Miller)	Carl Roth (#969.2)
Lipofectamine 2000	Thermo Scientific (#11668027)
L-Ascorbic acid	Sigma Aldrich (#A0278)
Isoflurane (Forane)	AbbVie (#B506)
Magnesium chloride hexahydrate (MgCl <sub>2</sub> x 6H <sub>2</sub> O)	Sigma Aldrich (#M2670)
Methanol, 99%	Thermo Scientific (#L13255.0F)
Midori Green Advance	Nippon Genetics (#MG04)
N,N,N',N'-Tetramethylethylenediamine (TEMED)	Sigma Aldrich (T9281-100ML)

## Materials and methods

<i>Pfu</i> DNA Polymerase, 100U	Promega (#M7741)
PF-04957325	MedChem (#HY-15426)
PF-05180999	Sigma Aldrich (#PZ0251-5MG)
Poly-D-lysine hydrobromide	Sigma Aldrich (#P1149-10MG)
Ponceau S	Sigma Aldrich (#P3504-10G)
Potassium chloride (KCl)	Sigma Aldrich (#P9541-500G)
Potassium hydrogencarbonate (KHCO <sub>3</sub> )	Merck (#1.04854.0500)
Powdered milk	Carl Roth (#T145.2)
Protein Ladder (10-250 kDa)	Thermo Scientific (#26619)
Rolipram	Sigma Aldrich (#6520-10MG)
Rotiphorese Gel 30 (37,5:1; Acrylamide)	Carl Roth (#3029.1)
Sodium azide (NaN <sub>3</sub> )	Sigma Aldrich (#S2002-25G)
Sodium chloride (NaCl)	Carl Roth (#9265.1)
Sodium deoxycholate (SOD)	Sigma Aldrich (#D6750-10G)
Sodium dodecyl sulfate (SDS)	Sigma Aldrich (#05030)
SDS-Solution, 20%	AppliChem (#A0675-1L)
Sodium hydroxide (NaOH)	Carl Roth (#6771.1)
Tris-acetate-EDTA (TAE) buffer, 50x	AppliChem (#A1691,1000)
Tris-(hydroxymethyl)-aminomethane (TRIS)	Carl Roth (#4855.2)
Triton X-100 Solution, 10%	AppliChem (#A1287,0100)
Type F Immersion liquid	Leica (#11513859)
Tween 20	Sigma Aldrich (#P1379-500ML)
T4 DNA Polymerase, 100U	Promega (#M421A)
β-Mercaptoethanol	Sigma Aldrich (#M6250-100ML)
(-)-Isoproterenol hydrochloride	Sigma Aldrich (#I6504-100MG)
2-Propanol	ChemSolute (#1136.1000)
3-Isobutyl-1-Methylxanthine (IBMX)	Applichem (#A0695-0001)
4-(2-hydroxyethyl)-1-piperazineethanesulfonic acid (HEPES)	Sigma Aldrich (#H4034-500G)
4-(3-(3-fluoro-5-(trifluoromethyl)benzyl)-5-methyl-1H-1,2,4-triazol-1-yl)-2-methylbenzamide (FTBMT)	MedChemExpress (#HY-101787)

## Materials and methods

### 2.1.5.2 Chemicals – sterile work

**Table 5. 2.** List of chemicals used for sterile work (cell culture).

Chemical	Manufacturer (catalog number)
Anti-Biotin MicroBeads	Miltenyi Biotec (#130-090-485)
Bovine serum albumin (BSA)	Sigma Aldrich (#A6003-25MG)
CD25 Antibody, Biotin, mouse	Miltenyi Biotec (#130-123-860)
Dulbecco's Modified Eagle's Medium (DMEM)	Sigma Aldrich (#D6546)
Dulbecco's Phosphate buffered saline (DPBS)	Sigma Aldrich (#D8537)
Dynabeads Mouse T-Activator CD3/CD28	Gibco (#11452D)
Fetal Bovine Serum (FBS), heat-inactivated	Sigma Aldrich (#F4135-500ML)
L-Glutamine solution, 200 mM	Sigma Aldrich (#G7513-100ML)
MEM Non-Essential Amino Acids Solution, 100x	Gibco (#11140050)
Penicillin/Streptomycin, 10000 U/ml, 10000 µg/ml	Sigma Aldrich (#P0781-100ML)
Recombinant Murine IL-2	Preprotech (#212-12)
Roswell Park Memorial Institute (RPMI)-1640	Gibco (#42401018)
Sodium pyruvate, 100 mM	Gibco (#11360070)
Trypan blue	Biochem (#L6323)
Trypsin/EDTA, 0,25%/0,02% in PBS	PAN-Biotech (#P10-020100)
2-Mercaptoethanol, 50 mM	Gibco (#31350010)

### 2.1.6 Consumables

**Table 6. 1.** List of consumables (sterile and non-sterile work).

Consumable	Manufacturer (catalog number)
Amersham Protran 0,45 NC nitrocellulose	Cytiva (#10600002)
Bacillol 30 Foam	Hartmann (#ANY8.1)
Falcon tube, 15 mL	Sarstedt (#62.554.016)
Falcon tube, 50 mL	Sarstedt (#62.559.004)
Filter paper, Type 598	Hahnemühle (#5984657)
Filtropur S 0,2 Syringe Filter	Sarstedt (#83.1826.001)



## Materials and methods

Gloves M (nitrile, powder free)	Medimex (#700103)
Kimtech	Kimberly Clark (#P502.1)
Laboratory film	Parafilm (#PM-996)
LD Column	Miltenyi Biotec (#130-042-901)
LS Column	Miltenyi Biotec (#130-042-401)
Luer-Lok syringe, 50 mL	BD Plastipak (#300865)
Microcentrifuge tube 1,5 mL	Sarstedt (#72.690.001)
Microcentrifuge tube 2 mL	Sarstedt (#72.691)
MS Column	Miltenyi Biotec (#130-042-201)
Nalgene Cryogenic vials	Thermo Scientific (#5000.0012)
PCR 0,1 mL 4-tube and 4-cap strips	Biozym (#711200)
Pipette tips 10 µL	Sarstedt (70.1130.600)
Pipette tips 200 µL	Sarstedt (70.760.502)
Pipette tips 1000 µL	Sarstedt (70.3050.100)
PluriStrainer, 30 µm	pluriSelect (#43-50030-03)
Polyethylene glycol (PEG) 3000	Sigma Aldrich (#81269)
Round glass coverslips, 25 mm	VWR (#631-0171)
Safe Seal reaction tubes 1,5 mL	Sarstedt (#72.706.400)
Safe Seal reaction tubes 2 mL	Sarstedt (#72.695.500)
Serological pipette 2 mL	Sarstedt (#86.1252.001)
Serological pipette 5 mL	Sarstedt (#86.1253.001)
Serological pipette 10 mL	Sarstedt (#86.1254.001)
Serological pipette 25 mL	Sarstedt (#86.1685.001)
Serological pipette 50 mL	Sarstedt (#86.1256.001)
Softa-Man acute	Braun (#19114)
Steriflip-GP Sterile Filter Unit	Millipore (#SCGP00525)
Sterilin 90mm-Standard Petri dishes	Thermo Scientific (#101R20)
Syringe, 2 mL	BD Discardit (#300928)
TC culture dish (100x200mm), Cell+	Sarstedt (#83.3902.300)
UVette, 220-1600 nm	Eppendorf (#0030106.300)
X-ray films (Super RX)	Fujifilm (#741019230)
µ-slide 18 Well Glass Bottom	Ibidi (#81817)
6-well plates	Sarstedt (#83.3920)
24-well plates	Sarstedt (#83.3922.500)
96-well plates, U bottom	Sarstedt (#83.3926.500)

## Materials and methods

### 2.1.7 Devices

#### 2.1.7.1 Live-cell imaging via FRET

**Table 7. 1.** List of equipment used to build up live-cell imaging setup for FRET.

Equipment	Manufacturer
Arduino board	Arduino
CMOS camera (OptiMOS)	QImaging
DV2 CUBE 05-EM, 505 dcxr, D480/30nm, D535/40nm	Photometrics
HP EliteDesk 800nG1 TWR	HP
HP Elite Display E241i	HP
LED pE-100, 440 nm	CoolLED
Leica DMI 3000B microscope	Leica

#### 2.1.7.2 Microscopes

**Table 7. 2.** List of additional microscopes.

Microscope	Manufacturer
Leica DMI1 microscope	Leica
Zeiss LSM 800	Zeiss

#### 2.1.7.3 Other devices and instruments

**Table 7. 3.** List of devices and instruments.

Devices/Instruments	Manufacturer
Accu-jet pro Pipette Controller	Brand
BD FACS LSR II analyzer	BD Bioscience
Centrifuge Fresco 17	Thermo Scientific
Centrifuge Megafuge 8R	Thermo Scientific
Centrifuge Pico 17	Thermo Scientific
Centrifuge 5810 R	Eppendorf
CO <sub>2</sub> -incubator MCO-5AC	Sanyo
E-box Gel documentation	Vilber
Film Proccesor SRX-101A	Konica
FlexStation3 Multi-Mode	Molecular devices
Microplate Reader	
Freezer	Liebherr

## Materials and methods

Fridge	Liebherr
Gene Touch (PCR machine)	Bioer
Glacier Ultralow temperature freezer	Nuaire
HERAcell vios 160i CO <sub>2</sub> -Incubator	Thermo Scientific
Laboclav	HSP
Laboratory balance	Precisa
Labgard, Biological safety cabinet (Class II)	ibs   tecnomara
MACS MultiStand	Miltenyi Biotec
Magnetic stirrer	IKA
MaxQ4450 Benchtop Orbital Shaker	Thermo Scientific
Microcentrifuge	VWR
Microwave	Panasonic
MidiMACS Separator	Miltenyi Biotec
MiniMACS Separator	Miltenyi Biotec
Mixing Block MB-102	Bioer
Mupid-ONE Electrophoresis System	Nippon Genetics
Neubauer improved (cell count chamber)	Marienfeld Superior
pH meter, Level 1	inoLab
Precision Scale	KERN PCB
Reserach Plus (10-1000 µL)	Eppendorf
Rotor Gene-Q Cycler	Qiagen
Scanner LiDE 220	Canon
Shaker DRS-12	ELMI
Shaker SSL4	Stuart
Sonoplus GM mini20	Bandelin
Spectrophotometer, DS-11+	DeNovix
ThermoMixer C	Eppendorf
Tilt/roler mixer	Phoenix Instruments
UV-transilluminator	Whatman Biometra TI 1
Vortex-Genie 2	Scientific Industries
Water bath	GFL
Western blot equipment	BioRad

## Materials and methods

### 2.1.8 Kits

**Table 8. 1.** List of commercially available kits.

Kit	Manufacturer (catalog number)
cAMP Enzyme Immunoassay Kit, Direct	Sigma Aldrich (#CA200)
CD4+ T cell Isolation Kit, mouse	Miltenyi Biotec (#130-104-454)
CD4+CD25+ Regulatory T cell Isolation Kit, mouse	Miltenyi Biotec (#130-091-041)
iScript cDNA Synthesis Kit	BioRad (#170-8891)
MojoSort CD3+ T cell Isolation Kit, mouse	BioLegend (#480024)
PicoPure RNA Isolation Kit	Thermo Scientific (#KIT0202)
QIAquick Gel Extraction Kit	Qiagen (#28704)
QIAprep Spin Miniprep Kit	Qiagen (#27106)
QIAGEN Plasmid Plus Midi Kit	Qiagen (#12943)
QuickChange Site-Directed Mutagenesis Kit	Agilent (#200518)
RNeasy Plus Micro Kit	Qiagen (#74034)
SuperSignal West Pico PLUS	Thermo Scientific (#34580)
SyberGreen (Perfecta) for IQ	QuantaBio (#95053-500)

### 2.1.9 Oligonucleotides

#### 2.1.9.1 Oligonucleotides for genetic engineering (mutagenesis, PCR amplification and sequencing)

Oligonucleotides were synthesized by Eurofins Genomics and diluted in Ampuwa water at stock concentration 100 pmol/μL. The stock was stored at -20°C. To obtain work concentration, oligonucleotides were diluted in Ampuwa water (dilution – 1:10).

**Table 9. 1.** List of oligonucleotides for genetic engineering.

Name	Sequence
bGH poly(A)	5'-TAGAAGGCACAGTCGAGG-3'
signal_reverse	
Mutation_forward	5'-GCTAATTCTTGCTCCATTGGACTCGAGTCTAGAGGGCC-3'
Mutation_reverse	5'-GGCCCTCTAGACTCGAGTCCAATGGAGCAAGAATTAGC-3'
GFP_forward	5'-AAACTCGAGGTGAGCAAGGGCGAGG-3'
GFP_reverse	5'-AAAGGGCCCTTACTTGTACAGCTCGTCCATG-3'

## Materials and methods

### 2.1.9.2 Oligonucleotide probes for NanoString

Oligonucleotide probes were designed and custom Gene Expression CodeSet was purchased from NanoString Technologies. Master Stock for Probe A and B were reconstituted in TE buffer (Table 3.33.) in concentration 5 nM and 25 nM, respectively, and stored at -80°C.

**Table 9. 2.** List of oligonucleotides for NanoString.

Gene name	Sequence
<i>Actb</i>	AGTTCGCCATGGATGACGATATCGCTGCGCTGGTCGTCGACAACGGCTCC GGCATGTGCAAAGCC GGCTTCGCGGGCGACGATGCTCCCCGGGCTGTATT
<i>Gapdh</i>	GGCACAGTCAAGGCCGAGAATGGGAAGCTTGTCATCAACGGGAAGCCCAT CACCATCTTCCAGGAGCGAGACCCCACTAACATCAAATGGGGTGAGGCCG
<i>Gusb</i>	AATACGTGGTCGGAGAGCTCATCTGGAATTCGCCGACTTCATGACGAAC CA GTCACCGCTGA GAGTAATCGGAAACAAGAAGGGGATCTTCACTCGCCA
<i>Hprt</i>	TGCTGAGGCGGCGAGGGAGAGCGTTGGGCTTACCTCACTGCTTTCCGGAG CGGTAGCACCTCCTCCGCCGGCTTCCTCCTCAGACCGCTTTTGGCCGGA
<i>Rpl19</i>	GAAGAGGCTTGCCTCTAGTGCTCCTCCGCTGCGGGAAAAAGAAGGTCTGGT TGGATCCCAATGAGACCAATGAAATCGCCAATGCCAACTCCCGTCAGCAG
<i>Tbp</i>	GTGGCGGGTATCTGCTGGCGGTTTGGCTAGGTTTCTGCGGTCGCGTCAT TTTCT CCGCAGTGCCCAGCATCACTATTTTCATGGTGTGTGAAGATAACCCA
<i>Crem</i>	AGGGGAAGAGGTTAGAGGTTAGCCTTTGTGCTGTACTAGGCTTCTTGCTG ATCGTCTGGAGAGTTTCTGCTGATGACCCTCCATTGTGAATTCCTGCAAC
<i>Gpr52</i>	ATGGCATACGCTGACCTCCTCGTTGGAGTTACCTGCTTGGTTCTACTC TGTCCC TTCTTCATTACTCTACAGGTGTCCATGAGTCATTGACTTGCCAGG
<i>Adrb1</i>	ACTAATTCCGAGTACTGGTGTCTCCTGTTCTTAAAGCAAAGGGAAAAAGAA GGATGCGAAA CAGACAAATCTGGTTTCGAGAACTATGTGTGGAGCACG
<i>Adrb2</i>	GATTGTATCTGGCCTTACCTCCTTTTGCCTATCCAGATGCACTGGTACC GTGCCACCCA CAAGAAAGCTATCGATTGTTACACCGAGGAGACTTGCTGT
<i>Adcy3</i>	CAACAACGGCGGCATCGAGTGTCTACGCTTCTCAATGAGATCATCTCTG ATTTTGACTCTCTCCTGGACAATCCCAAATTCCGGGTCATACCAAGATC
<i>Adcy4</i>	GTTTCCTCTCCTGCTCCCTTTTCTGCACATGAGCTTCGAAGTGAAGCT GCTCCTAC TTCTGCTGTGGCTGGTGGCATCTTGTCCCTATTTCTGCATTC
<i>Adcy5</i>	CTCTGGACTCTAATTCGTAGCTACTTCTCACCTCGGGGCTGCGCTGTCTCC CCGCTAG CCTTCCCGTTGTCTCCACCGCTCAGGACGGGGGTGCCACGA
<i>Adcy6</i>	TTGCACAGGAGGTTGGGTGGTGTGGTAGTAAATGATAACGGTCTGGG GAGAGGAG TCCTTTTTTGTGCCAAATCCCTAAGTGCCATTTGGGGGCCAC
<i>Adcy7</i>	ATCCGTCCGGACTTCAAAGTGTCTACACTGAGTGTGATGTCAACAAAG AAGGACTGGAGTGCCTTCGACTGCTGAATGAGATAATTGCTGATTTTGAC
<i>Adcy9</i>	CTGGTGTGGAGTGCCGTATCCAGGTGAGCGAAGAGAGCTACCGTGTGCTG AGCAAGATGGGTATGACTTTGACTACCGAGGGACCGTGAATGTCAAGGG
<i>Akap7</i>	CTTAATTAATGAAGCTTTGCACCGAGAAAGGATGGAGCTGAAATCCAAAGT GAAACAGATAAAAGAACTTTTGTAAAGCCTGAGACTCAGGCCAAGATT
<i>Akap9</i>	AAACCAACACTCAGCTTGAACATGCGAAAGTTACACAGACAGAGTTGATG CGTGAG TCCTTTAGACAAAAACAAGAGGCAACAGAGTCATTTCATTGCCT
<i>Akap13</i>	TTGATATTTTCTGGCTCTACCCTCTATCACTGCACAAGTACCCGAAAGT CAGTTCT GATACGTTGGAGACAATTGCTCCTGGTCACGACTGCTGTGAGA
<i>Pde1a</i>	GGTCGGACGTTGCTATTCTGTACAACGACCGCTCAGTGCTTGAGAAATCA CCACGTCAG CGCAGCCTACAGACTTATGCAAGAGGAGGAAATGAATATTTT

## Materials and methods

<i>Pde1b</i>	CTTTTCCTTGAACCGGGCAGCCGATGACCACGCTCTGAGGACCATTGTTT
<i>Pde1c</i>	TTGAGTTGCTGACTCGGCATAGCCTCATCAGCCGCTTAAAGATTCCCACA
<i>Pde2a</i>	GCTGTAATCGATGCATTGAAGGATGTGGATACGTGGTCCTTCGATGTCTT
<i>Pde3a</i>	TTCCCTCAATGAGGCCAGTGAGATCATGCACTGAAGTTCATTTTCTATG
<i>Pde3b</i>	CCACTAGCTTCTCTTCTGTTTTGTTCCCTATGTGTCGTGGGTGGGGGAGG
<i>Pde4a</i>	GGGCCA CCTGCCTTACCTACTCTGAGTTGCCTTTAGAGAGATGCATTTTT
<i>Pde4b</i>	ATATAGGAAGAAAATGTGGCCGTATTCTGAGCCAGGTATCATACAGACTG
<i>Pde4d</i>	TTTGAA GACATGGGGCTCTTTGAAGCCTTTAAAAATCCCGTTAGGGAGTT
<i>Pde7a</i>	TCCTGGATTTTATCCCTGCTCTGAAGTAGAAGATCCAGTTGAGAAAGGAG
<i>Pde7b</i>	ATCGAAAACCTTACAAGGGATTGAGTGGCAGAACCAGTTTCCCAACTCCA
<i>Pde8a</i>	GAAGCTTGAACATCAATGTCCACGATTTGGAGTCAAGACAGATCAGGAG
<i>Pde8b</i>	GACCTCTTAGCACAAGAACTGGAGAACTTGAGCAAATGGGGCCTGAACAT
<i>Pde11a</i>	CAGCAGTTAAGGACAGGAATGGTCATTGTTCCAAGGTCTGCCCTTTCTCT
	TGTCTTGAGTCCCTAGTTCTGCCCAACCCTTTGATGAGCTGGTTTTGCAA
	TGTGAATTTATGGCTTAGTTCACAGGGTTAACTTGCTGATACCAGTCAGC
	CTCGTGCAGCATGTGTCTAGCCTAGACCTTAGTTGTCTTCTTGGTGAAG
	TTTGCACTCTACCTTACCCTCAGTCCTTTGGAAGTGACATGCTGGATTCT
	TTAGGTGATCAGTTAGCTGCTGCCTCTCCCGTTGAGTCTGGGTATTTTG
	TTCTGACCCGCTTAAAGCTCACCTCCACAATAAAGATTGAGACTGGAG
	AATGTACAGGACAGACACTTTATGCTTCAGATCGCCTTGAAGTGTGCTGA
	CACACTTCCGAAAACCGAACGTTTAGCCACAGCGACGGCGAGGACGAGGA
	CGTGGACGTGGACGTCCCGGGCCCCGCGCCGAGATCTATTACGCGATGGT
	AGTTCAGCTCAACTGTTACCAGAAAATAACGACGGAGGCTTTCCTCAGT
	GGCAAAAGGATGAAGGATTCTTAAACATCTTCTGAGCAAATGGATGTG
	CAACGTGTGCCAACTGATGTTGCCATGCTAACTACTGCTGGGTCCAAG
	AGATTCTGACCGAGGTGGAATTTTAGCGGTGATTGTGGGATGCCTGTGT

### 2.1.9.3 Oligonucleotides for qRT-PCR

Oligonucleotides were synthesized by Eurofins Genomics and diluted in Ampuwa water at stock concentration 100 pmol/μL. The stock solution was stored at -20°C. To obtain work concentration, oligonucleotides were diluted in Ampuwa water (dilution – 1:20).

**Table 9. 3.** List of oligonucleotides for qRT-PCR.

Gene name	Sequence
Gja1_forward	5'-CATTGGGGGAAAGGCGTGA-3'
Gja1_reverse	5'-CCATGTCTGGGCACCTCTCTTT-3'
Gpr52_forward	5'-TTGTCTTGCTGACATTTCTGATCA-3'
Gpr52_reverse	5'-GGAGCACAGTGAAAGACAAAGATG-3'
Npr1_forward	5'-TGGAGACACAGTCAACACAGC-3'
Npr1_reverse	5'-CCGAAGACAAGTGGATCCTG-3'
Npr2_forward	5'-TGTTTGGTGTTCAGTTTCC-3'
Npr2_reverse	5'-AGTTCTTCCCAGCGAATGC-3'
Tbp_forward	5'-GTAGCGGTGGCGGGTATC-3'

## Materials and methods

Tbp\_reverse

5'-CATGAAATAGTGATGCTGGGA-3'

### 2.1.10 Plasmids

**Table 10. 1.** List of plasmids.

Plasmids	Vector backbone	Originator/Manufacturer
AKAP79-GFP	pcDNA3	kind gift from Dr. John Scott
Epac1-camps	pcDNA3	Prof. Dr. Viacheslav Nikolaev
pcDNA3.1	pcDNA3.1	Clontech
GPR52	pcDNA3.1	Addgene
GPR52-GFP	pcDNA3.1	Roberta Kurelić

### 2.1.11 Software

**Table 11. 1.** List of software.

Software	Version	Manufacturer
Excel	Office Professional 2019	Microsoft
FlowJo	10	BD Bioscience
GraphPad Prism	6.01	GraphPad
ImageJ	1.48v	National Institutes of Health
Inkscape	1.1	Inkscape Developers
Micro-Manager	1.4.22	Open Source Microscopy Software
nSolver analysis software	4.0	NanoString Technologies
PowerPoint	Office Professional 2019	Microsoft
Rotor Gene-Q analysis software	2.3.1	Qiagen
SnapGene	1.1.3	GSL Biotech
ZEN (Blue)	3.4	Carl Zeiss
Zotero	5.0.96	Corporation for Digital Scholarship
Word	Office Professional 2019	Microsoft

## Materials and methods

### 2.2 Methods

#### 2.2.1 Animals

Eight to twelve-week-old wild-type (WT) and transgenic mice (TG, Table 1.1), both males and females, were used in conducting this study. Animals were kept and bred in the central animal facility of the University Medical Center Hamburg-Eppendorf (UKE) under pathogen-free conditions. Animals had perpetual access to food and water and were handled following national and international animal welfare guidelines authorized by Behörde für Justiz und Verbraucherschutz Hamburg (N20/106 and ORG1010).

#### 2.2.2 cAMP immunoassay

CD4<sup>+</sup> T cells were isolated from spleen and lymph nodes (superficial cervical, axillary, brachial, and inguinal) collected from WT mice. To obtain both Treg and Tcon cells, CD4<sup>+</sup>CD25<sup>+</sup> Regulatory T Cell Kit was used as described in later section 2.2.11. Upon collecting Tcon and Treg, cells were washed with ice-cold PBS and centrifuged at 500 x g, 5 min at +4°C. Cells were counted with trypan blue and approx. 1 100 000 cells per sample were collected. Cells were lysed in 110 µL 0,1 M HCl for 10 min at RT. After 10 min, cell lysis was inspected with trypan blue. Samples were stored and kept at -20°C until the sample set was not completed. Shortly before performing cAMP immunoassay, samples were centrifuged at 600 x g, 10 min at RT and supernatants were directly used in the next steps of provided protocol. Furthermore, samples were acetylated to increase assay detection sensitivity following the manufacturer's instructions. Assay and data analysis was performed in accordance with the protocol provided by the manufacturer. The absorbance was measured at 405 nm with FlexStation3 Multi-Mode Microplate Reader. Acquired raw data were analyzed in Microsoft Excel and GraphPad Prism software.

#### 2.2.3 Cell culture and transient transfection

In this PhD thesis, HEK293A cells were used as a cell line that can be simply transfected with plasmid DNA of choice. HEK293A cells were cultured in DMEM medium supplemented as reported in Table 3.17. at 37°C and 5% CO<sub>2</sub>. Cells were passaged approx. every three days when cell confluency reached 80-90%. Passaging step included aspiration of old culture medium, washing the cells with PBS, trypsinization for 3-4 min to detach the cells from surface of the plate, and trypsin neutralization with complete DMEM medium. Cells were centrifuged at 800 rpm for 5 min. Cell pellet was resuspended in 1 mL of complete DMEM medium, split in ratio 1:4 or 1:5 and cells were seeded in 10 cm Petri dish at 37°C and 5%



## Materials and methods

CO<sub>2</sub>. For FRET measurements, cells were plated onto sterile glass coverslips (25 mm) in 6-well plates in ratio 1:40 per well and cultured overnight to assure proper cell attachment. Next day, cell confluency was around 50-60% and transient transfection step was performed with Lipofectamine 2000 reagent. Transfection mix for 6 well plate included 300  $\mu$ L of plain DMEM medium, 7  $\mu$ L of Lipofectamine 2000 reagent, and 3  $\mu$ g of each plasmid DNA (control: Epac1-camps and pcDNA3.1, test: Epac1-camps and GPR52). Transfection mix was well resuspended, incubated for 20 min at RT, and afterward, 50  $\mu$ L transfection mix per well was added. Before adding transfection mix to each well, detached cells were removed by adding fresh, complete DMEM medium. FRET measurements were performed after approx. 36-40 h long culture on cells with proper expression of plasmid DNA.

### 2.2.4 FACS sorting

Enriched CD3<sup>+</sup> T cells were stained with antibodies conjugated to specified fluorophores listed in Table 2.1. and incubated for 10 min at +4°C. Living cells were separated from dead cell fraction by staining with Alexa Fluor 750 NHS Ester for 20 min at 4°C. Single-cell suspensions were washed two times with MACS buffer and centrifuged at 400 x g, for 5 min at +4°C. Cell pellets were resuspended in 400  $\mu$ L PBS (+1 mM EDTA) and filtered through 30  $\mu$ m filter into new falcon tube. The filter was rinsed with PBS (+EDTA). Samples were sorted on a BD Aria III Cell Sorter. Tcon (CD3 $\epsilon$ <sup>+</sup> CD8 $\alpha$ <sup>-</sup> CD4<sup>+</sup> Foxp3-GFP<sup>-</sup>) and Treg (CD3 $\epsilon$ <sup>+</sup> CD8 $\alpha$ <sup>-</sup> CD4<sup>+</sup> Foxp3-GFP<sup>+</sup>) were collected in 500  $\mu$ L complete RPMI medium. 100 000-200 000 Treg and Tcon cells per sample were sorted and stored on ice followed by RNA isolation with PicoPure RNA Isolation Kit by pursuing manufacturer's protocol.

### 2.2.5 Immunofluorescence

CD4<sup>+</sup> T cells were isolated from splenocytes collected from WT mice and cultured as mentioned in Section 2.2.11. Activated Tcon were plated in  $\mu$ -Slide 18 well chambers coated with PDL (0.1 mg/mL) for 45 min and cells were left in the incubator at 37°C and 5% CO<sub>2</sub>. Cells that did not adhere were removed by washing with PBS and non-activated T cells (Tcon or Treg) were added to the well for additional 45 min incubation. After 45 min, cells were fixed and permeabilized with pre-cooled methanol for 20 min at -20°C. Cells were washed two times with PBS for 10 min. Next, cells were incubated with blocking buffer (Table 3.16.) for 1 h at RT. Furthermore, primary antibodies were diluted as reported in Table 2.4. and were incubated at RT for 90 min followed by two 10 min-long washing steps with PBS. Secondary antibodies, as listed in Table 2.5. were diluted, in blocking buffer and used at RT for 60 min in dark. Cells were washed two times with PBS for 10 min. The last step was incubation with DAPI (100

## Materials and methods

ng/mL, diluted in PBS) for 2 min at RT and immunofluorescent staining was finished by 10 min washing step.

### 2.2.6 Live-cell imaging via FRET

Tcon and Treg subsets were isolated from spleen of TG mice ubiquitously expressing Epac1-camps sensor and cultured as described in Section 2.2.11. After overnight culture, non-activated and activated T cells were further used for real-time measurements. Before start of the measurement on each day, 25 mm round glass coverslips were coated with Poly-D-Lysine (PDL, 0.1 mg/mL) for 45 min at RT. Upon 45 min, coverslips were washed with Ampuwa water for 5 min at RT, and were further used. T cells were plated on PDL-coated glass coverslips for short period (up to 30-45 min) to achieve proper cell attachment. To assemble FRET bath, Autofluor cell chamber was used for appropriate securing of glass coverslips. 400  $\mu$ L FRET buffer (Table 3.30.) was added to FRET bath upon assembly. T cells that did not adhere to glass surface were washed with FRET buffer. Next, all pharmacological modulators (antagonist and agonist drugs) tested in FRET experiments were diluted in FRET buffer and carefully pipetted in volume of 400  $\mu$ L by circular motion to the measuring bath, gently not to wash or move measuring cells. Stable baseline was achieved at the start of the measurement, and after any of the tested compound added to the measuring bath. FRET setup utilized in conducting this PhD thesis (Table 7.1.) included inverted fluorescent microscope equipped with oil-immersion 63x/1.40 objective, CooLED as a fluorescent light source at 440 nm (to excite CFP fluorophore), beam splitter named DV2 Dual View (Cube 05-EM, 505 dxcr, D480/30m, D535/40m) and CMOS camera chip. As vital part of the FRET setup, Arduino digital-to-analog input-output board was needed, since it controls LED performance. MicroManager 1.4 software was used to monitor imaging in real-time on computer screen. Only T cells with appropriate sensor expression were used for FRET measurements, and excluding criteria were too bright or too dim sensor expression. FRET was performed at RT, without an additional supply of O<sub>2</sub> or temperature control. Images of both YFP (acceptor molecule) and CFP (donor molecule) channels were recorded every 5 or 10 s. Raw data were analyzed offline by using ImageJ and Microsoft Excel for spectral bleedthrough factor (b) corrections and further data normalization. Due to overlapping spectrum of donor (CFP) and acceptor molecule (YFP), bleedthrough correction factor was calculated. In order to perform this, HEK293A cells were cultured and transfected by using Lipofectamine 2000 reagent with plasmid DNA encoding for CFP protein as described in Section 2.2.3. After 32-36 h culture, CFP fluorescent intensity in YFP channel was measured via FRET. To calculate corrected FRET ratio, equation is employed as follows: corrected FRET ratio=(YFP-b\*CFP)/CFP. Corrected FRET ratio values were further normalized to values obtained from the first baseline

## Materials and methods

(start of the measurement, before applying any drug) and normalized FRET ratio values were quantified and further used for statistical analysis.

### 2.2.7 Molecular cloning

Molecular cloning was performed for fluorescent labeling of C-terminus of plasmid DNA encoding for GPR52 protein.

#### Mutagenesis of GPR52 construct

*In vitro* site-directed mutagenesis was performed to introduce point mutation on the C-terminus of recombinant DNA of interest to remove STOP codon in the region encoding for protein on interest and further enable fluorescent labeling of GPR52 with GFP. Firstly, to amplify DNA, Polymerase Chain Reaction (PCR) was used. PCR reaction mix was prepared as shown in Table 12.1. As a double-stranded (ds) DNA template, GPR52 plasmid DNA was used. Both sample reaction mix (Table 12.1.), as well as cycling parameters (Table 12.2.) were assembled in accordance with QuickChange Site-Directed Mutagenesis Kit instructions. Extension time was altered concerning the length of dsDNA template (*Pfu* DNA polymerase replication: 1 kb / 2 min).

**Table 12. 1.** Sample reaction mix for site-directed mutagenesis by PCR.

Component	Volume (μL)
Ampuwa water	37,5
dNTP mix (200 μM)	1,0
dsDNA template (50 ng)	3,0
oligonucleotide primer – forward (125 ng)	1,25
oligonucleotide primer – reverse (125 ng)	1,25
Reaction buffer (10x)	5,0
<i>Pfu</i> DNA polymerase	1,0
Total volume	50,0

## Materials and methods

**Table 12. 2.** Cycling conditions for the site-directed mutagenesis by PCR.

Steps	Cycles	Temperature (°C)	Time (min)
Initial denaturation	1x	95	1,5
Denaturation	18x	95	0,5
Annealing		55	1
Extension		72	14

Upon finishing, PCR reaction tube was placed at RT for 20 min to cool down. We further proceeded with DpnI digestion of PCR amplicons. 1,5 µL of restriction enzyme DpnI was added to the PCR product, mixed well, and incubated at 37°C for 2 h. After mutagenesis step, sample reaction was further introduced into competent *E. coli* cells as specified in section below (Table 12.3.).

### Preparation of competent *E. coli* cells

Commercially available competent cells for chemical transformation were used to produce new and fresh stock of cells. Smear of competent *E. coli* cells was cultured overnight at 37°C on LB plates without selective antibiotic. Next days, colonies were inspected and one single colony was picked with sterile pipette tip and further cultured overnight in 4 mL of LB medium (Table 3.22.) without selective antibiotic at 37°C. Next day, 500 µL of overnight bacterial culture was transferred into 250 mL of LB medium without selective antibiotic and was further incubated at 37°C by shaking at 225 rpm for approx. 4 to 5 h with constant measuring of optical density (OD) value at wavelength of 600 nm. OD value was assessed by pipetting 0,5 mL of bacterial culture into 1 mm cuvettes and OD600 measured by spectrophotometer with optimal value range was between 0,3 and 0,6. As a blank reference, LB medium was used. Subsequently, bacterial culture was pelleted down at 4000 rpm, for 12 min. at +4°C. Cell pellet was resuspended in 25 mL of TSB buffer (Table 3.23.) at incubated on ice for 5 h. Afterward, aliquots of 400 µL chemically competent cells were prepared and frozen in liquid nitrogen. Aliquots were stored at -80°C.

## Materials and methods

### Transformation of competent *E. coli* cells

Chemical transformation was performed by using 5x KCM buffer (Table 3.20.) and reaction was set as shown in Table 12.3.

**Table 12. 3.** Components for chemicals transformation into competent *E. coli* cells.

Component	Volume (μL)
Ampuwa water	70
Sample reaction (after mutagenesis step)	10
10x KCM buffer	20
Total volume	100

Transformation mix was kept on ice for 5 min following the addition of 100 μL competent *E. coli* cells, thawed on ice, and further incubated for 20 min. Next, the transformation reaction mix tube was transferred from ice to room temperature for 10 min. 800 μL of pre-warmed LB medium (without antibiotics) was added to the transformation mix tube and further incubated at 37°C for 1 h with constant shaking at 250 rpm. Lastly, cells were centrifuged at 6000 rpm, for 2 min at RT. Pellet was resuspended in 200 μL LB medium (without antibiotics) and plated on selective LB agar plates (Table 3.21.) supplemented with ampicillin (AMP, Table 3.19.). Plates with recombinant bacteria were incubated at 37°C for 16-18 h (overnight) when single colonies were inspected.

### Plasmid isolation - Miniprep

Single colony was picked with the sterile, clean pipette tip and incubated in 3 mL selective LB medium (supplemented with AMP, Table 3.19.a) with constant shaking at 225 rpm for 16-18 h at 37°C. Plasmid DNA was isolated with QIAprep Spin Miniprep Kit by following detailed manufacturer's instructions. Final DNA was eluted from the column containing silica membrane in 30 μL of elution buffer (10 mM Tris, pH 8,5) and DNA concentration was determined with a spectrophotometer. As a blank reference, elution buffer was used. DNA purity was validated through  $A_{260}/A_{280}$  value, and good-quality DNA values are between 1,7-2,0.

### Sequencing

Plasmid DNA was sent to sequencing to Eurofins Genomics ( $c_{\text{plasmid DNA}}=50 \text{ ng}/\mu\text{L}$ ) to confirm mutagenesis of GPR52 plasmid was successful. As a primer for sequencing, bGH poly(A) signal promoter sequence was used (Table 9.1.).

## Materials and methods

### Restriction Cloning and Plasmid isolation – Midi prep

Restriction cloning is based on cutting both vector (backbone) and insert with identical set of restriction enzymes to generate compatible overhangs which result in direct binding of vector and DNA sequence of interest (insert). For DNA amplification of desired insert, PCR was used. PCR reaction mix was prepared as shown in Table 12.4. As a double-stranded (ds) DNA template, plasmid with GFP (Table 10.1.) was used. Also, cycling conditions for PCR amplification step of the insert are reported in Table 12.5. Extension time was altered concerning the length of dsDNA template (*Pfu* DNA polymerase replication: 1 kb / 2 min).

**Table 12. 4.** Sample reaction mix for PCR.

Component	Volume (µL)
Ampuwa water	19,0
dNTP mix (200 µM)	0,5
dsDNA template (1,5 µM)	0,5
primer – forward (0,4 µM)	1,0
primer – reverse (0,4 µM)	1,0
<i>Pfu</i> DNA polymerase	0,5
Reaction buffer (10x)	2,5
Total volume	25,0

**Table 12. 5.** Cycling conditions for PCR amplification of insert.

Steps	Cycles	Temperature (°C)	Time (min)
Initial denaturation	1x	95	1,5
Denaturation	30x	95	0,5
Annealing		56	0,5
Extension		72	1,5
Final Extension	1x	72	7
Soak	1x	4	∞

Furthermore, restriction digestion was set up for mutated GPR52 plasmid (backbone) and amplified insert (GFP fragment). Restriction digestion reaction components are shown in Table 12.6. Cutting with restriction enzymes (RE) is performed in correlation with the manufacturer's instructions; Apal at 25°C for 2 h following addition of XhoI and additional 2 h of cutting at 37°C.

## Materials and methods

**Table 12. 6.** Restriction digestion components.

Component	Volume (µL)
Ampuwa water	x
Backbone (1 µg) / Insert (2 µg)	x
CutSmart buffer (10x)	2
RE (ApaI/XhoI)	1 (each RE)
Total volume	20

DNA fragments of interest were separated from the rest of restriction digestion reaction mix over gel purification with agarose gel electrophoresis. Difference in voltage across the agarose gel allows negatively charged DNA fragments to migrate from cathode (negative) to anode (positive). For this purpose, agarose gel (Table 3.18.) was supplemented by in-gel-staining (Midori Green) of DNA. To detect right size of DNA fragments, pre-stained DNA ladder (1 kb) was run on the gel next to samples which were additionally mixed with 6x purple loading dye before loading. To visualize DNA fragments of interest UV transilluminator and clean scalpel were used to excise bands of the right size. For purification of DNA from gel, QIAquick Gel Extraction Kit by manufacturer's instructions was used. DNA was eluted from column containing silica membrane with elution buffer (10 mM Tris, pH=8,5) in the following volumes: 25 µL of EB for insert and 50 µL for backbone.

To ligate purified backbone and vectors T4 DNA ligase was used. Ligation reaction was established as shown in Table 12.7. and was performed in ThermoMixer at 16°C for approx. 16 h.

**Table 12. 7.** Ligation reaction mix.

Component	Volume (µL)
Ampuwa water	13,5
Backbone	4,0
Insert	12,0
T4 ligase buffer (10x)	3,5
T4 DNA ligase	2,0
Total volume	35,0

Chemical transformation of ligation mix into competent *E. coli* was used as described above (Table 12.3.). Cells were plated on selective LB Agar plates and incubated for approx. 18 h. Grown colonies were picked and plasmid DNA was isolated with QIAprep Spin Miniprep Kit

## Materials and methods

by following detailed manufacturer's instructions. Clones were tested by restriction digestion with pairs of restriction enzymes, Apal+EcoRI and XhoI+HindIII, using suggested conditions by manufacturer. Next, samples were run on 1% agarose gel to check DNA fragments size as mentioned earlier. Positive colony with DNA fragments of the right size was further grown for plasmid production on a larger scale. In this step, 50 mL selective LB medium (supplemented with AMP, Table 3.19.) was used and picked positive clone with clean, sterile tip from its -80°C glycerol stock. After approx. 16 h culture at 37°C in shaker at 225 rpm, bacterial culture was pelleted at 6000 rpm and 4°C for 10 min. Cells were further processed to isolate plasmid DNA with QIAGEN Plasmid Plus Midi Kit using protocol provided by the manufacturer. Final DNA was eluted from the silica membrane column in 100 µL of EB (10 mM Tris, pH 8,5) and DNA concentration was determined with a spectrophotometer as described above.

### 2.2.8 NanoString

NanoString nCounter analysis was performed on RNA samples isolated from T cell subsets (Section 2.2.9 and 2.2.11). The amount of total RNA was determined by using the Qubit RNA Assay Kit by following manufacturer's instructions, and approx. 35 ng of RNA was used per sample. CodeSet was custom-made and included 36 genes (30 genes of interest and 6 housekeeping genes, as shown in Table 9.2.). Oligonucleotide probes were diluted in TE buffer (Table 3.33.) in concentration, Master Stock Probe A 5 nM, and Probe B 25 nM and stored at -80°C. At the start of the experiment, Master Stock Probes were further diluted in TE buffer into Probe A and B Working Pool in final concentrations 0,6 nM and 3 nM. After bringing all components to RT (Probe A and B Working Pool and TagSet36), before proceeding with hybridization. Master mix was created by pipetting 7 µL of each Probe Working Pool dilution. Next, 8 µL of TagSet followed by pipetting 7 µL of total RNA. Tubes were mixed, spun down, and incubated at a pre-heated thermocycler at 67°C overnight (approx. 16 h). The following day, prepared samples were pipetted into nCounter SPRINT Cartridge and expression levels were measured by NanoString nCounter FLEX Analysis System. Raw expression data were analyzed in the nSolver Analysis Software 4.0 from NanoString. nSolver 4.0 User Manuel was employed for quality control of obtained raw data as well for data normalization to the housekeeping genes. Acquired normalized data were examined in GraphPad Prism software.



## Materials and methods

### 2.2.9 RNA isolation, cDNA synthesis and qRT-PCR

RNA isolated from CD4+ T cells was further used either for NanoString analysis or quantitative reverse transcriptase-polymerase chain reaction (qRT-PCR). Total RNA was collected with RNAeasy Plus Micro Kit according to manufacturer's protocol. RNA was eluted from silica membrane column in 14  $\mu$ L RNase-free water. RNA concentration was determined with spectrophotometer, and as a blank reference, RNase-free water was used. Complementary DNA (cDNA) was synthesized by using reverse transcriptase (RT), enzyme that transcribes RNA into cDNA. For this purpose, iScript cDNA Synthesis Kit was used following provided manufacturer's instructions. Reaction mix is reported in Table 13.1. 200 ng of RNA was used per sample. Also, cycling protocol was shown in Table 13.2.

**Table 13. 1.** cDNA synthesis reaction mix.

Component	Volume ( $\mu$ L)
iScript RT	1
Nuclease-free water	x
RNA template (200 ng)	x
5x iScript reaction mix	4
Total volume	20

**Table 13. 2.** Cycling steps for cDNA synthesis.

Steps	Temperature ( $^{\circ}$ C)	Time (min)
1	25	5
2	46	20
3	95	1
4	4	$\infty$

Furthermore, to determine gene expression levels of genes of interest in CD4+ T cells qRT-PCR was conducted. Primer pairs (forward and reverse, Table 9.3.) used were designed by the Primer-BLAST tool on NCBI (The National Center for Biotechnology Information) page. qRT-PCR was performed in Rotor-Gene Q cyclor (72-well rotor). Reaction mix (Table 13.3.), as well as cycling conditions for qRT-PCR (Table 13.4.), are shown below. For each sample, triplicates were used. As a negative control for each master mix, instead of cDNA, Ampuwa water was used.

## Materials and methods

**Table 13. 3.** Reaction mix for qRT-PCR.

Component	Volume (µL)
cDNA (dilution – 1:1)	1,0
Primer – forward (25 nM)	0,5
Primer – reverse (25 nM)	0,5
SYBER Green	5,0
RNAse-free water	3,0
Total volume	10,0

**Table 13. 4.** Cycling conditions for qRT-PCR.

Steps	Cycles	Temperature (°C)	Time (s/min)
Initial PCR activation step	1x	95	10 min
Denaturation	49x	95	10 s
Annealing		60	15 s
Extension		72	20 s
Melting curve	1x	72-95	0,5°C/step

Lastly, Rotor-Gene Q software was used to analyze the obtained data. Determined  $C_t$  values were further analysed in Microsoft Excel by  $\Delta C_t$  method for relative quantification ( $\Delta C_t = C_t(\text{target gene}) - C_t(\text{housekeeping gene}) \rightarrow 2^{(-\Delta C_t)}$ ).

### 2.2.10 Sample preparation and Immunoblotting

Tcon and Treg were isolated with CD4+CD25+ Regulatory T Cell Isolation Kit and cultured as described in Section 2.2.11. After 24 h in culture, cells were washed twice with ice-cold PBS and centrifuged at 400 x g for 4 min and +4°C. Cells were lysed in RIPA lysis buffer (Table 3.2.) supplemented with Halt protease inhibitor in addition to 4x Loading dye (Table 3.3.) and 10%  $\beta$ -mercaptoethanol. Every sample collection is based on determining cell number, which results in almost identical protein concentration. Next, cell lysate was boiled at 95°C for 5 min and stored at -20°C. Sodium dodecyl sulfate-polyacrylamide gel electrophoresis (SDS-PAGE) was used to separate proteins in correlation to their size. Stacking and separating gel were prepared as shown in Table 3.14. and 3.15. Protein ladder and samples were run in parallel at 130 V constantly for approx. 100 min by using electrophoresis equipment from BioRad together with 1x SDS Running buffer as reported in Table 3.8. Next, proteins were transferred from gel onto nitrocellulose membrane by assembling blotting sandwich set up in transfer

## Materials and methods

chamber from BioRad. For this purpose pre-cooled 1x Transfer buffer (Table 3.10.) supplemented with 20% methanol was used. Cold transfer was conducted at 100 V for 90 min. Membrane was cut at size 55 kDa so protein expression of protein of interest was checked as well as loading control (GAPDH) for the same sample set. Membrane pieces were incubated in blocking buffer (Table 3.13.) for 1 h at constant shaking, and afterward with primary antibody overnight in 50 mL falcon tube at tilting roller mixer at +4°C. On the following day, membranes were washed in 1x TBS-T buffer (Table 3.12.) three to four times at RT with constant shaking. Incubation with secondary antibody conjugated with horseradish peroxidase (HRP; Table 2.3.) was performed for 1 h at RT. Again, membranes were washed three to four times in 1x TBS-T buffer at RT. For the signal detection membranes were incubated with chemiluminescent reagents from SuperSignal West Pico PLUS Kit. Acquisition time between membranes and films varied upon primary antibody used (1 – 90 s). Scanned films were further used for densitometric analysis in ImageJ and Microsoft Excel.

### 2.2.11 T cells isolation and culture

Single-cell suspension was obtained from mouse spleen and or lymph nodes (superficial cervical, axillary, brachial, and inguinal). Splenocytes were further subjected to RBC lysis (Table 3.26.) for 2-3 min at RT. Cells were washed with ice-cold PBS and centrifuged at 400 x g, for 5 min at +4°C. Cell pellets from spleen and lymph nodes were determined with trypan blue stain (dilution – 1:10), and afterward kit-specific cell isolation protocol was applied according to the manufacturer's instructions. Incubation steps are executed at refrigerator (+4°C).

#### CD4+ T Cell Isolation Kit and CD25-Biotin antibody (for Live-cell imaging)

Splenocytes were incubated with antibodies as follows: 40  $\mu\text{L}/10^7$  cells of MACS buffer, 10  $\mu\text{L}/10^7$  cells for CD4+ T Cell Biotin-Antibody Cocktail, and incubated for 10 min. Next, 30  $\mu\text{L}/10^7$  of MACS buffer and 20  $\mu\text{L}/10^7$  of Anti-Biotin MicroBeads were added and further incubated for 15 min. CD4+ T cells were collected by negative selection upon magnetic separation. LD columns were used for this purpose and were pre-washed with 2 mL MACS buffer. Then, cell suspension was applied to the LD column. CD4+ T cells, as unlabeled cells go through column and are collected in falcon tube. Column is washed twice with 1 mL MACS buffer, cells were washed with PBS and centrifuged at 400 x g for 5 min at +4°C. CD4+ T cells were counted with trypan blue stain (dilution – 1:10) and further labeled with CD25-Biotin Antibody. Cell pellet was resuspended in 49  $\mu\text{L}/10^7$  cells of MACS buffer and 1  $\mu\text{L}/10^7$  cells of CD25-Biotin Antibody and incubated for 10 min. 30  $\mu\text{L}/10^7$  cells MACS buffer was added together with 20  $\mu\text{L}/10^7$  cells of Anti-Biotin MicroBeads. Two consecutive runs on different MS

## Materials and methods

column is equilibrated with 500  $\mu$ L MACS buffer. Cell suspension was applied to MS column and flow-through of first column is collected as a fraction of CD4+CD25- T cells. CD4+CD25+ T cells were flushed out from the column after removing column from the separator and run over second MACS column to increase the purity of obtained Treg cells. Both T cell subsets were washed in ice-cold PBS and centrifuged at 500 x g for 5 min at +4°C. T cells were resuspended in complete RPMI medium (Table 3.27.) and cell number was determined with trypan blue stain (dilution – 1:10). Lastly, cells were cultured overnight in presence of 10 IU/mL IL-2 and with or without anti-CD3/CD28 mouse Daynabeads (cell:bead=2:1).

### CD4+CD25+ Regulatory T Cells Isolation Kit (for Immunoblotting, Immunofluorescence, and qRT-PCR)

Splenocytes and cells from lymph nodes were incubated with antibodies as follows: 40  $\mu$ L/ $10^7$  cells of MACS buffer, 10  $\mu$ L/ $10^7$  cells for CD4+CD25+ Regulatory T Cell Biotin-Antibody Cocktail, and incubated for 10 min. Afterward, 38  $\mu$ L/ $10^7$  of MACS buffer, 20  $\mu$ L/ $10^7$  of Anti-Biotin MicroBeads and 2  $\mu$ L/ $10^7$  cells of CD25-PE antibody were added and further incubated for 15 min. CD4+ T cells were collected by negative selection upon magnetic separation. For this purpose, equilibrated LD columns were used. Next, cell suspension was applied to the LD column. CD4+ T cells, as unlabeled cells fraction, do not bind magnetic column and are collected in falcon tube. Column is washed twice with 1 mL MACS buffer and cells were washed with PBS. Centrifugation is carried at 400 x g for 5 min at +4°C. Obtained CD4+ T cell pellet was resuspended in 90  $\mu$ L/ $10^7$  cells of MACS buffer and 10  $\mu$ L/ $10^7$  cells of Anti-PE MicroBeads and incubated for 15 min. Two continuous runs over two pre-washed MS column is performed. Cell suspension was applied to MS column and flow-through of first column is collected as a fraction of CD4+CD25- T cells. CD4+CD25+ T cells were flushed out from the column after removing column from the separator and run over second MACS column to increase the purity of obtained Treg cells. Both T cell subsets were washed in ice-cold PBS and centrifuged at 500 x g for 5 min at +4°C. T cells were resuspended in complete RPMI medium (Table 3.27.) and cell number was determined with trypan blue stain (dilution – 1:10). Lastly, cells were cultured for 24 h in presence of 10 IU/mL IL-2 and with or without anti-CD3/CD28 mouse Daynabeads (cell:bead=2:1).

### MojoSort CD3 T Cell Isolation Kit (for FACS sorting – NanoString)

Single-cell suspensions from spleen and lymph nodes were resuspended in 100  $\mu$ L MACS buffer/ $10^7$  cells MACS. The biotinylated antibody cocktail was pre-diluted 1:10 in MACS buffer and used at 10  $\mu$ L/ $10^7$  cells. Cells were incubated on ice for 5 min. Streptavidin-conjugated nanobeads were vortexed and pre-diluted 1:15 in MACS buffer and used 10  $\mu$ L/ $10^7$  cells. Again, cells were incubated for 5 min on ice. LS column were equilibrated with 3 mL cold

## Materials and methods

MACS buffer and the cell suspension was applied. Flow-through was collected as a fraction of untouched CD3+ T cells. LS column was washed twice with 3 mL MACS buffer, and flow-through was collected and further used for surface staining and FACS-sorting to obtain Treg and Tcon cells.

### 2.2.12 Statistical analysis

In this PhD thesis, all data presented in bar graphs are shown as mean  $\pm$  standard error of the mean (SEM) or in whisker box plots. All statistical analyses were performed in GraphPad Prism software. Normal distribution was determined by the Kolmogorov-Smirnov test with Dallal-Wilkinson-Lille approximation to calculate the p value. Differences between groups and treatments were tested using one-way ANOVA followed by Sidak's multiple comparison tests, Student's t-test, and Mann-Whitney U, as indicated in the figure legends. Significant differences are marked as \* $p < 0.05$ , \*\* $p < 0.01$ , \*\*\* $p < 0.001$ , and \*\*\*\* $p < 0.0001$  in the graph and figure legends respectively.

### 3 Results

#### 3.1 Validation of cytosolic FRET-based sensor Epac1-camps in CD4+ T cells

To study the dynamics of cAMP changes at the single-cell level in murine CD4+ T cells, live-cell imaging via FRET was utilized as a fundamental technique. To conduct FRET measurements previously published and characterized transgenic mouse model CAG-Epac1-camps was used, ubiquitously expressing FRET-based biosensor, in all tissues and organs (Calebiri et al. 2009; Hübscher and Nikolaev 2015). Magnetically-sorted T cells were isolated from splenocytes and lymph nodes and cultured for 16 to 24 h in the absence (non-activated T cells) or presence (activated T cells) of anti-CD3/CD28 Dynabeads and IL-2. Firstly, the expression and distribution of the Epac1-camps sensor was validated with the FRET imaging system. The sensor was evenly expressed in the cytosol of non-activated (**Figure 5A**) and activated (**Figure 5B**) as shown on representative images of the YFP channel. To probe the Epac1-camps sensor's performance, FRET response was measured in murine CD4+ T cells. FRET measurements were performed upon stimulation with  $\beta$ -adrenergic receptor agonist drug, isoprenaline (ISO, 100 nM), the pan-PDE inhibitor 3-isobutyl-1-methylxanthine (IBMX, 100  $\mu$ M), and the addition of the AC-activator, Forskolin (FSK, 10  $\mu$ M). Stimulation with isoprenaline, in both non-activated (**Figure 5C,D**) and activated (**Figure 5E,F**) T cells resulted in increased donor molecule fluorescent intensity (CFP) and decreased acceptor molecule fluorescent intensity (YFP), indicative of a decrease in FRET. The maximal response was subsequently achieved by saturating concentrations of IBMX and Forskolin. Conducting real-time cAMP measurements in both non-activated and activated primary murine T cells upon diverse agonist and antagonist drug stimulation provided the unique possibility to investigate cAMP-signaling in T cell subsets which will be further elaborated through the present study.

## Results

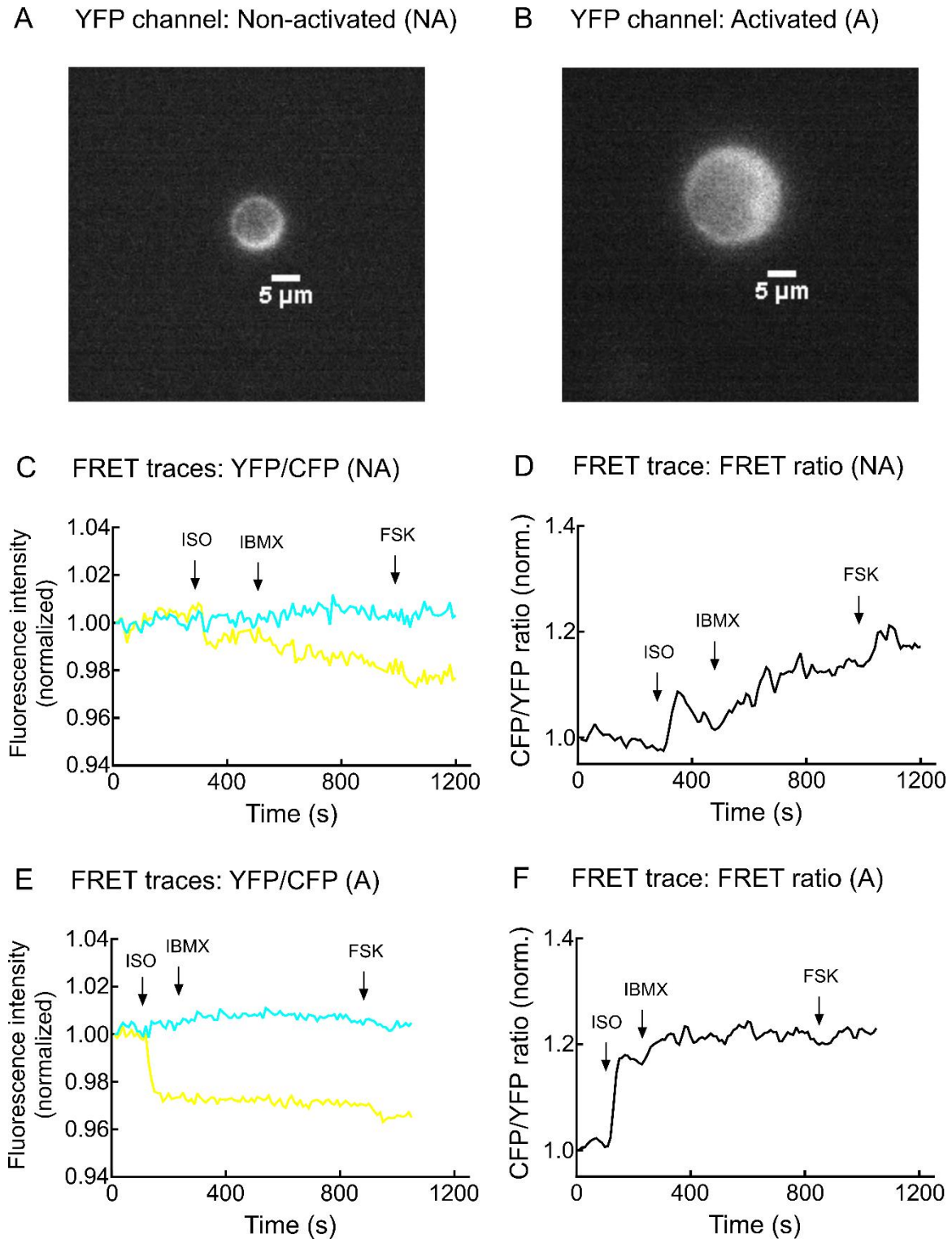


**Figure 5. T cells expressing Epac1-camps sensor.** Murine CD4<sup>+</sup> T cell isolated from CAG-Epac1-camps mice after overnight culture in **A**) absence (non-activated, NA) and **B**) presence (activated, A) anti-CD3/CD28 Dynabeads used for live-cell imaging via FRET are shown. Representative images of the YFP channel are depicted in **A**) and **B**) as indicated above. Representative FRET traces of individual channels (CFP in blue, YFP in yellow and FRET ratio trace in black), upon stimulation with isoprenaline (ISO, 100 nM), IBMX (100  $\mu$ M) and Forskolin (FSK, 10  $\mu$ M) are shown here for **C**) and **D**) non-activated and **E**) and **F**) for activated T cells. Scale bar: 5  $\mu$ m.

## Results

### 3.2 Probing cAMP levels and cAMP-relevant gene expression in CD4<sup>+</sup> T cells

#### 3.2.1 cAMP immunoassay

To determine the basal intracellular cAMP levels in whole cell lysate from CD4<sup>+</sup> T cell subsets, a commercially available cAMP immunoassay kit was used. Murine T cell subsets were MASC-purified from splenocytes and lymph nodes collected from 9-week-old (9 wo) GPR52-deficient mice (**Figure 6A**) and 16-week-old (16 wo) AC6-deficient mice with corresponding wild-type littermate controls (**Figure 6B**). Number of isolated T cell subsets per sample was adjusted to an equal quantity ( $10^6$  T cells/sample). Basal cAMP levels measured in regulatory T cells (9 wo:  $c=10,7$  pmol/ $10^6$  cells, 16wo:  $4,4$  pmol/ $10^6$  cells) were approximately 2-fold higher in comparison to conventional T cells (9 wo:  $c=6,3$  pmol/ $10^6$  cells, 16 wo:  $1,9$  pmol/ $10^6$  cells) in both 9-weeks-old (**Figure 6A**) and 16-weeks-old (**Figure 6B**) wild-type mice, although detected cAMP concentrations, in general, were lower in older mice. There was no difference observed comparing cAMP levels between T cell subsets from wild-type and GPR52-deficient mice (**Figure 6A**). On the other hand, a 2-fold increase in cAMP concentration was detected in Tcon isolated from AC6-deficient mice ( $c=4,1$  pmol/ $10^6$  cells) in comparison to Tcon from the wild-type group, while cAMP levels in Treg were constant (WT:  $4,4$  pmol/ $10^6$  cells, AC6-deficient:  $c=4,2$  pmol/ $10^6$  cells).

#### A cAMP immunoassay: GPR52-KO

#### B cAMP immunoassay: AC6-KO

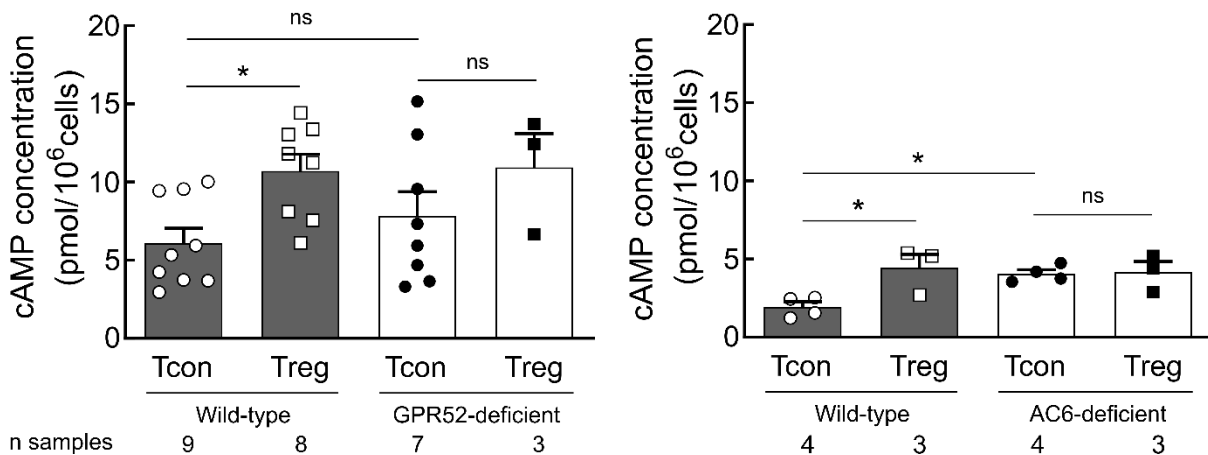


**Figure 6. Regulatory T cells have higher basal intracellular cAMP levels compared to conventional T cells.** Magnetically-sorted T cell subsets isolated from wild-type, **A**) GPR52-deficient, and **B**) AC6-deficient mice were used for cAMP immunoassay. cAMP concentration was quantified and depicted in bar graphs as the mean  $\pm$  SEM. Number of samples is indicated under bars and correlates with the number of mice used. \* $p < 0.05$ , ns—not significant by one-way ANOVA followed by Sidak's multiple comparison test.



## Results

### 3.2.2 NanoString analysis

To analyze the expression level of cAMP-relevant genes FACS-sorted naïve Tcon and Treg obtained from DREG mice were further used to isolate total RNA and prepared samples were examined via NanoString nCounter FLEX Analysis System. Significantly higher expression levels were observed for *Pde1b* and *Pde2a* in Treg, and for *Pde3b* and *Pde4b* in Tcon as compared to Treg (**Figure 7**). Also, there was no difference in the expression of the  $\beta$ -adrenergic receptors (*Adrb1* and *Adrb2*) between Tcon and Treg. Surprisingly, expression level of *Adcy9* was quite low and comparable between T cell subsets, while *Adcy6* and *Adcy7* indicated a trend for increased expression level in Tcon.

#### NanoString: cAMP-relevant genes

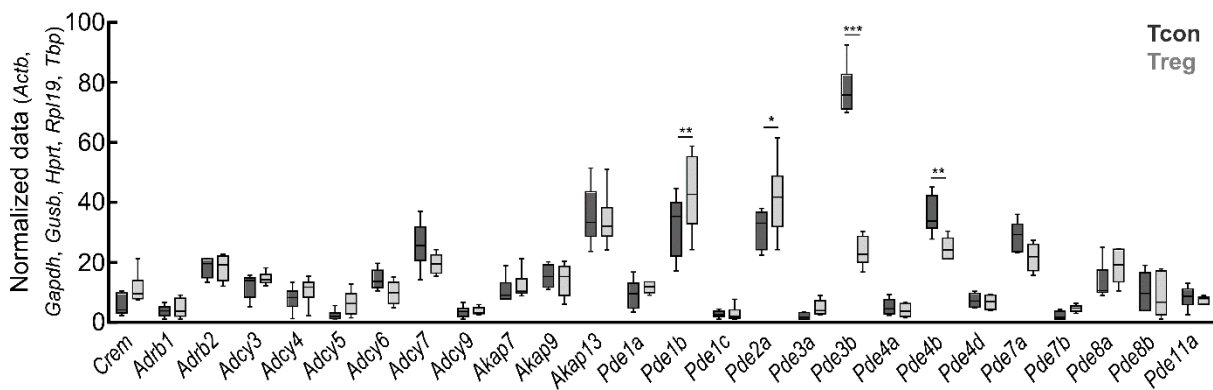


**Figure 7. Expression of cAMP-relevant genes in Tcon and Treg.** FACS-sorted T cells subsets were employed to determine the gene expression level of cAMP-relevant genes by NanoString nCounter FLEX Analysis System. Raw data were normalized to housekeeping genes (*Actb*, *Gapdh*, *Gusb*, *Hprt*, *Rpl19*, *Tbp*). Normalized data are demonstrated in whisker box plots. Number of samples correlates with the number of mice (n=6). \*p<0.05, \*\*p<0.01, \*\*\*p<0.001 by multiple t-tests (corrected by Benjamini-Hochberg Correction).

### 3.3 Orphan GPCRs – GPR52

To investigate the impact of orphan GPCRs on cAMP levels in T cell subsets, heat maps for the expression level data of different orphan GPCRs tasked from the ImmGene database were examined. During this analysis, GPR52 was identified as an interesting target since it showed significantly higher expression in Treg compared to Tcon and was not explored before in the context of T cell biology and function. As demonstrated before, cAMP immunoassay did not reveal any significant differences in basal intracellular cAMP levels from whole cell lysate between T cell subsets of wild-type and GPR52-deficient mice (**Figure 6A**). Furthermore, Nanostring analysis revealed a slightly higher expression level of *Gpr52* in Treg cells versus Tcon (data not shown). The unavailability of a specific GPR52 antibody for protein expression analysis resulted in conducting qRT-PCR to validate the difference in *Gpr52* expression upon T cell activation *in vitro*. Detected expression of *Gpr52* was 5-fold higher in non-activated Treg

## Results

compared to Tcon. Upon activation of T cells, the expression level of *Gpr52* in Treg was reduced and there were no significant difference detected between Tcon and Treg anymore (Figure 8).

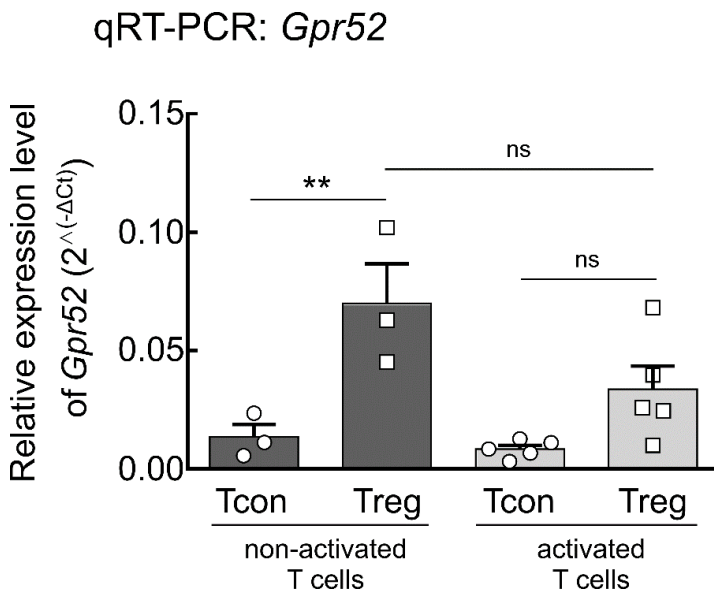


**Figure 8. *Gpr52* expression is increased in non-activated regulatory T cells versus Tcon.** Tcon and Treg were MACS-purified from mouse splenocytes and cultured for 24 h in the absence (non-activated) or presence (activated) of anti-CD3/CD28 Dynabeads. To measure the mRNA expression level of *Gpr52*, qRT-PCR was performed. *Tbp* was employed as a housekeeping gene for the normalization of each sample. Relative expression level is quantified by using obtained  $\Delta C_t$  values and demonstrated in bar graphs as mean  $\pm$  SEM of three (non-activated T cells) or five (activated T cells) individual experiments. \*\* $p < 0.01$ , ns—not significant by one-way ANOVA followed by Sidak's multiple comparison test.

### 3.3.1 Testing specificity of GPR52 agonist drug - FTBMT

FTBMT, as a selective GPR52 agonist drug, was already published for *in vitro* treatment of primary striatal neurons, where authors demonstrated how stimulation of GPR52 receptor with FTBMT modulates cAMP levels in a dose-dependent manner evaluated via cAMP ELISA (Nishiyama, Suzuki, Harasawa, et al. 2017). To test the specificity of the agonist drug in a live-cell imaging setting, FRET was employed. For this purpose, HEK293A cells were used since this cell line does not express GPR52 endogenously and could be efficiently transfected with plasmid DNA of interest. Firstly, restriction enzyme cloning was performed to fluorescently label the GPR52 construct with GFP. HEK293A cells were transfected with Epac1-camps sensor in order to measure FRET response in the cell cytosol. In addition, cells were co-transfected with an empty backbone vector, pCDNA3.1, as a control verifying the specificity of the FRET measurements or with a plasmid encoding for GPR52. Stimulation of HEK293A cells exogenously expressing GPR52 with 500 nM FTBMT resulted in 10-fold increase in

## Results

cAMP produced in comparison to the control group (**Figure 9A,C**). FRET response after FTBMT stimulation in HEK293A cells transfected with an empty backbone vector (Control) was negligible (**Figure 9A,B**). Maximal response of FRET sensor was induced by adding 10  $\mu$ M FSK and 100  $\mu$ M IBMX.

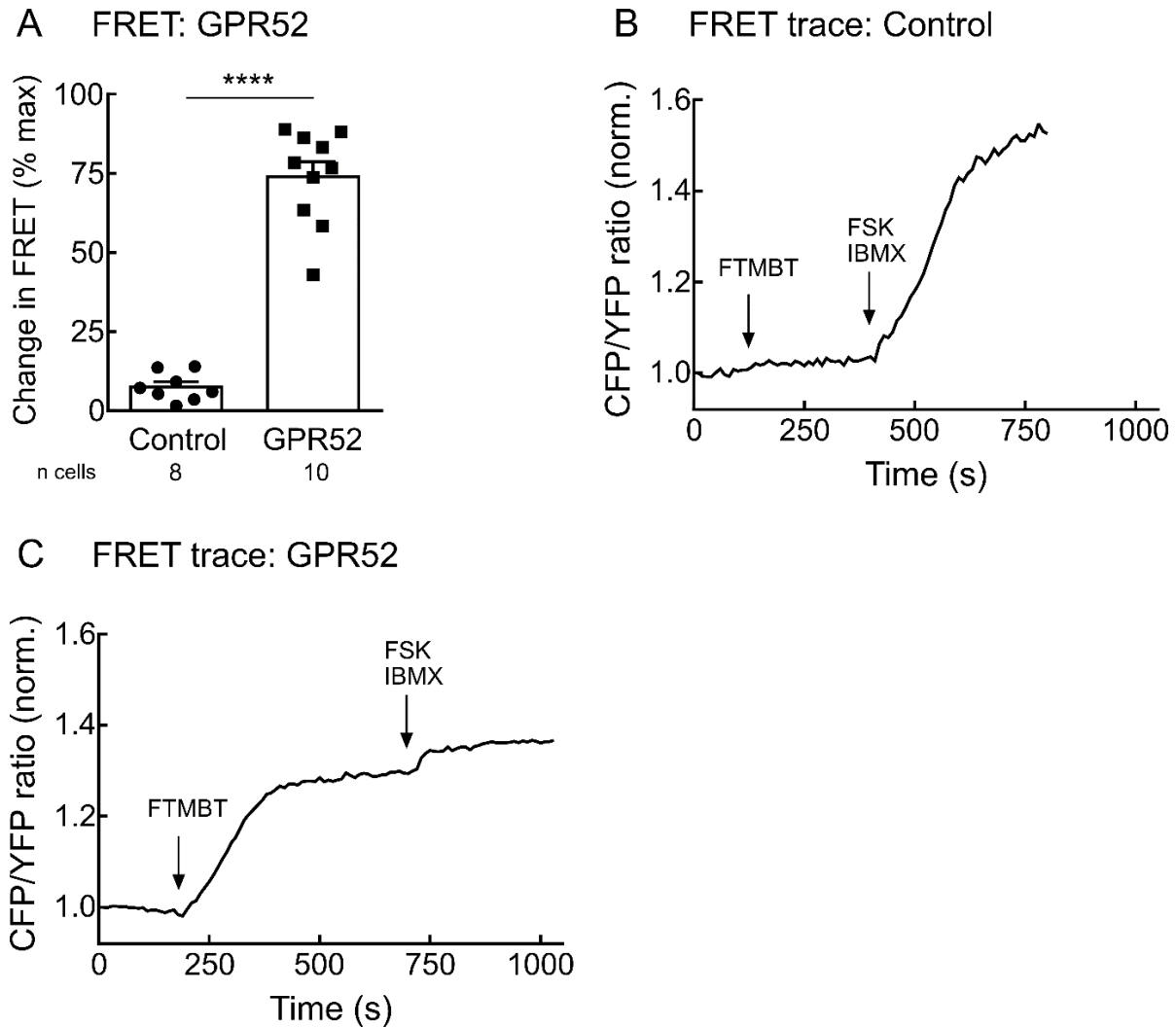


**Figure 9. FTBMT specifically activates GPR52 receptor to produce cAMP.** HEK293A were co-transfected with plasmid DNA encoding for GPR52 labeled with GFP or empty backbone vector for control and cytosolic FRET sensor Epac1-camps. After 36-48 h in culture, FRET response was measured and **A**) quantified as % of the change in FRET to GPR52 agonist drug stimulation (FTBMT, 500 nM) in comparison to maximal FRET response generated by Forskolin (FSK, 10  $\mu$ M) and IBMX (100  $\mu$ M). Representative FRET traces are revealed for **B**) control and **C**) GPR52-transfected HEK cells. Bar graphs are presented as mean  $\pm$  SEM. The number of cells measured per group is shown under the graph. \*\*\*\*p<0.0001 by Student's t-test.

## Results

### 3.3.2 Impact of GPR52 stimulation on cAMP levels in CD4+ T cells

To probe the impact of orphan GPR52 by stimulating receptor with published receptor-specific drugs (Song et al. 2018; Nishiyama, Suzuki, Harasawa, et al. 2017), impact of FTBMT (GPR52 agonist) and E7 (GPR52 antagonist) stimulation on cAMP production was tested in mouse T cell subsets via FRET. Tcon and Treg were isolated from splenocytes of CAG-Epac1-camps transgenic mice. FRET measurements were performed after overnight culture and in non-activated Treg higher cAMP level upon applying 500 nM FTBMT was observed compared to Tcon group (**Figure 10A,C,D**). Treatment of T cells at the start and during FRET measurement with GPR52 antagonist, 10  $\mu$ M E7, resulted in 3-fold decrease in FRET response to FTBMT stimulation in both T cells subsets (**Figure 10A,E,F**). Also, a difference in FRET response to GPR52 receptor stimulation with agonist drug was reduced in cells pretreated with E7. Upon activation of Tcon and Treg *in vitro*, an equal level of cAMP produced in response to FTBMT was detected in both T cell subsets. Similarly, the pretreatment of activated T cells with E7, throughout the life-cell imaging, resulted in a 4 to 5-fold decrease in FRET response observed in Tcon and Treg (**Figure 10B**), as demonstrated in non-activated T cells. FRET response was quantified upon maximal sensor response provoked by 10  $\mu$ M FSK and 100  $\mu$ M IBMX.

## Results

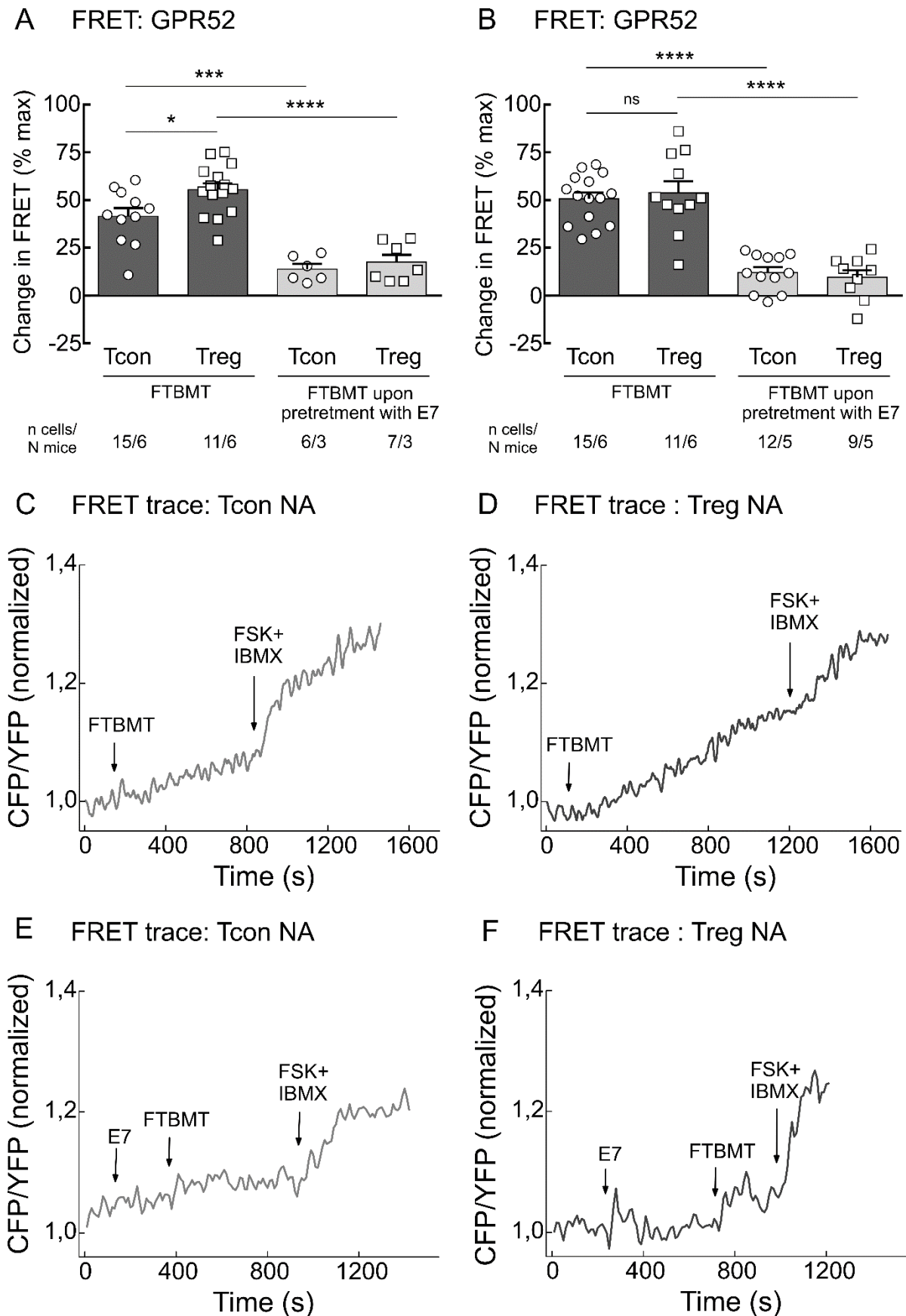


**Figure 10. Stimulation of non-activated Treg with GPR52 agonist results in a higher FRET change compared to Tcon.** MACS-sorted T cells isolated from the transgenic mouse model were cultured overnight with and without mouse anti-CD3/CD28 Dynabeads. The next day, FRET

## Results

measurements were performed and cells were stimulated with GPR52 agonist (FTBMT, 500 nM) in real-time. To test GPR52 antagonist effects cells were pretreated with inhibitor E7 (10  $\mu$ M). FRET response was measured for **A**) non-activated (NA) and **B**) activated (A) T cell subsets. Change in FRET is quantified as % of FRET response to agonist drug stimulation in comparison with maximal sensor response upon saturation by Forskolin (FSK, 10  $\mu$ M) and IBMX (100  $\mu$ M). Representative traces are presented for non-activated **C**) Tcon and **D**) Treg stimulated with FTBMT and non-activated **E**) Tcon and **F**) Treg stimulated with FTBMT after inhibition of GPR52 with E7 during live-cell imaging. Bar graphs are shown as mean  $\pm$  SEM. \* $p < 0.05$ , \*\*\* $p < 0.001$ , \*\*\*\* $p < 0.0001$ , ns—not significant by one-way ANOVA followed by Sidak's multiple comparison test.

### 3.4 PDE regulation during T cell activation in T cell subsets

#### 3.4.1 Provoking adenosine receptor activity in CD4+ T cells

CD4+ T cells express adenosine receptors on their surface, predominantly  $A_{2A}$  receptor. To study differences in adenosine receptor activity, FRET measurements were performed on T cell subsets expressing the Epac1-camps sensor. Non-activated Tcon cells exhibited a lower FRET response after 100  $\mu$ M ADO stimulation compared to Treg (**Figure 11A,C,D**). Next, there was no significant difference in response to ADO stimulation between activated Tcon and Treg. cAMP production in cells was saturated after applying 10  $\mu$ M FSK and 100  $\mu$ M IBMX. Next, to compare hydrolyzing activities of diverse PDEs, 100  $\mu$ M ADO was added to stimulate cAMP generation in activated T cells followed by inhibition of specific PDE. Sensor saturation was achieved by 100  $\mu$ M IBMX. After inhibiting PDE3 with 10  $\mu$ M Cilostamide (CILO), a tendency for higher FRET response was observed in activated Tcon. PDE2 inhibition by 100 nM BAY 60-7550 (BAY) revealed no difference in cAMP levels between activated T cell subsets. A significant difference in cAMP produced was detected in activated Tcon after PDE4 inhibition with 10  $\mu$ M Rolipram (ROLI, **Figure 11B,E,F**).

## Results

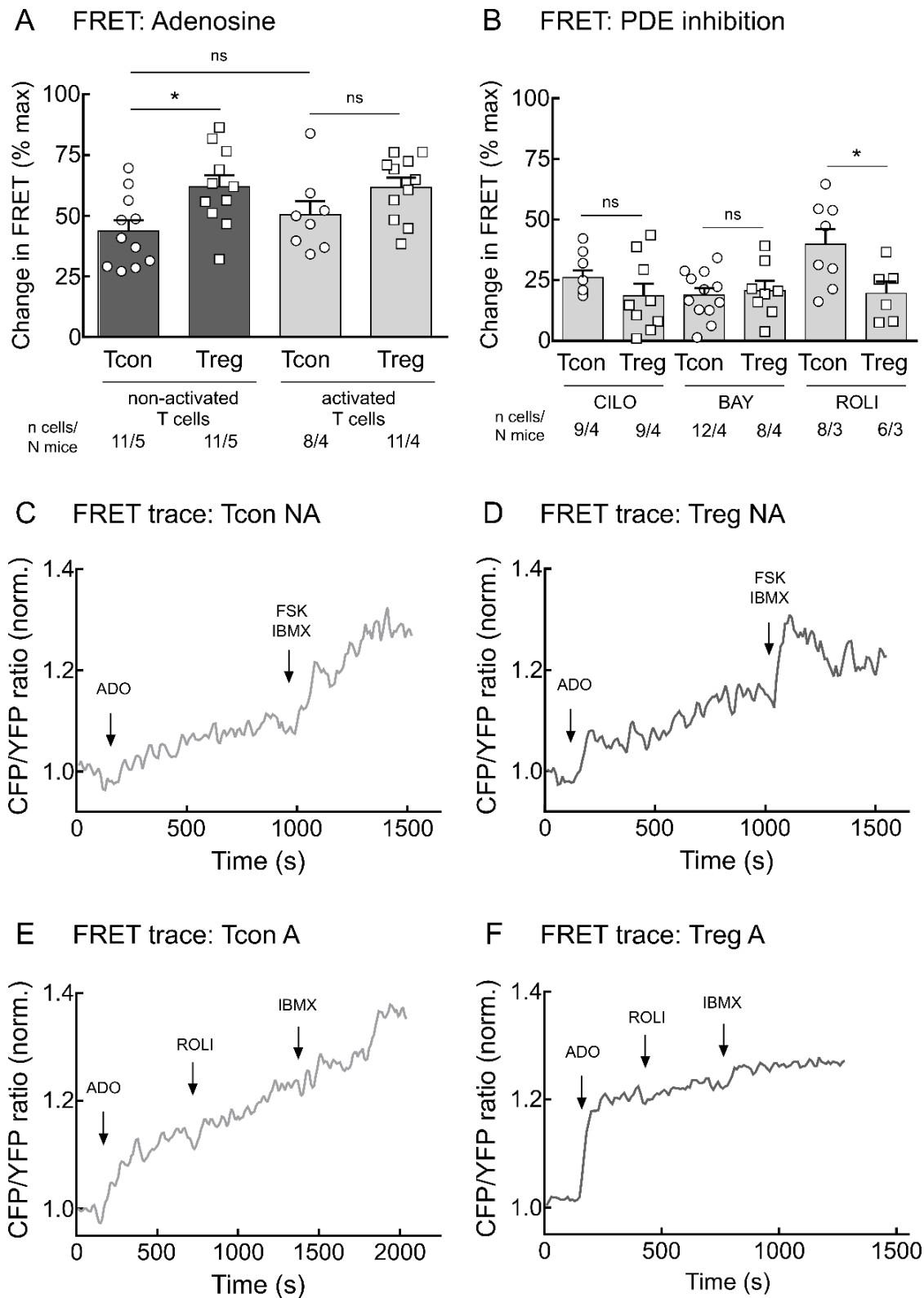


**Figure 11. Real-time measurements of FRET response in T cells upon adenosine stimulation.** T cell subsets expressing Epac1-camps sensor after overnight culture with IL-2 and activation by anti-CD3/CD28 Dynabeads were subjected to real-time measurements. **A)** T cells were stimulated with 100  $\mu$ M adenosine (ADO) and afterward with a combination of 10  $\mu$ M Forskolin (FSK) and 100  $\mu$ M IBMX. **B)** To evaluate individual PDE activity specific PDE inhibitor was applied (Cilostamide, CILO – 10  $\mu$ M, Bay 60-7550, BAY – 100 nM, and Rolipram, ROLI – 10  $\mu$ M) upon prestimulation of T cells with ADO (100  $\mu$ M). To fully saturate the sensor, a pan-PDE inhibitor was applied (IBMX, 100  $\mu$ M). Change in FRET is

## Results

shown as % of FRET response either to **A)** ADO or **B)** specific PDE inhibition in relation to the maximal response of the FRET sensor. Next, representative FRET traces showing T cell response to ADO stimulation in non-activated **C)** T con and **D)** Treg are presented together with FRET traces depicting PDE4 inhibition in activated **E)** Tcon and **F)** Treg. Bar graphs are revealed as mean  $\pm$  SEM and the number of cells and mice used per group are indicated under each bar. \* $p < 0.05$ , ns—not significant by one-way ANOVA followed by Sidak's multiple comparison test or Mann-Whitney U or Student's t-test.

### 3.4.2 Differences in PDE inhibition in activated vs. non-activated T cell subsets

#### 3.4.2.1 *Pan-PDE inhibition with IBMX in real-time*

Tcon and Treg cells were MACS-purified and further used for live-cell imaging performed on the day of isolation (D0), after overnight culture without (non-activated, D1) or with (activated, D1) anti-CD3/CD28 Dynabeads. To probe the effect of inhibiting PDE2, PDE3, and PDE4 at the same time in a basal setting, 100  $\mu$ M pan-PDE inhibitor IBMX was applied directly to T cells following 10  $\mu$ M FSK saturation. When FRET measurements were completed on the day of T cell isolation, increase cAMP levels were detected in Treg versus Tcon after IBMX, while lower cAMP levels were measured in non-activated Tcon after overnight culture compared to Treg cells (**Figure 12A,B,C**). Upon *in vitro* activation of Tcon, a shift in FRET response was observed. Additionally, activated Treg exhibited a non-significant reduction in response to treatment with IBMX (**Figure 12A,D**).



## Results

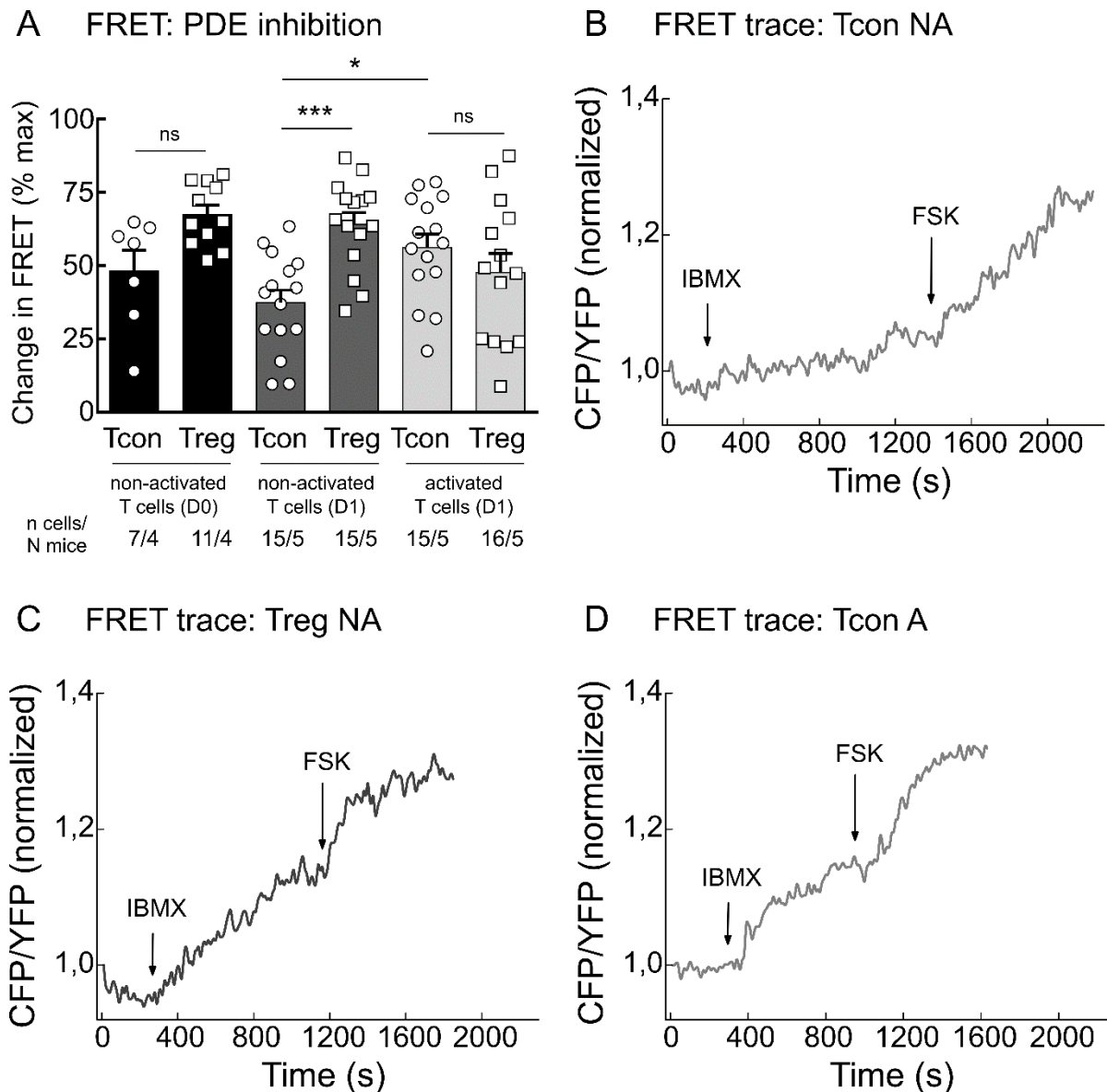


**Figure 12. Pan-PDE inhibitor IBMX differentially affects cAMP levels T cells subsets in activated vs. non-activated state.** T cell subsets were MACS-purified and utilized for FRET measurements either upon isolation (D0) or upon overnight culture and T cell activation (D1). Pan-PDE inhibitor, IBMX was used to inhibit PDEs followed by FRET sensor saturation with Forskolin (FSK, 10  $\mu$ M). FRET response was quantified and shown as % of the change in FRET after applying IBMX vs. maximal FRET sensor response. Representative FRET traces are depicted for non-activated **B**) Tcon (D1) and **C**) Treg (D1), as well for **D**) activated Tcon (D1) upon PDE inhibition by IBMX. Bar graphs are shown as mean  $\pm$  SEM. Number of cells and mice measured per group is shown below bars. \* $p < 0.05$ , \*\*\* $p < 0.001$ , ns—not significant by one-way ANOVA followed by Sidak's multiple comparison test.

## Results

### 3.4.2.2 PDE4 in T cells

To examine protein expression level of PDE4B and PDE4D in CD4<sup>+</sup> T cell subsets, immunoblotting analyses were conducted. MACS-sorted T cell subsets after 24 h in culture were further utilized to prepare protein lysates. Amount of protein quantified for each sample was normalized to the loading control, GAPDH. PDE4B (**Figure 13A**) and PDE4D (**Figure 13B**) were highly expressed in non-activated Tcon compared to Treg. Expression pattern observed in non-activated T cells did not change with overnight activation with anti-CD3/CD28 Dynabeads (**Figure 13A,B**).

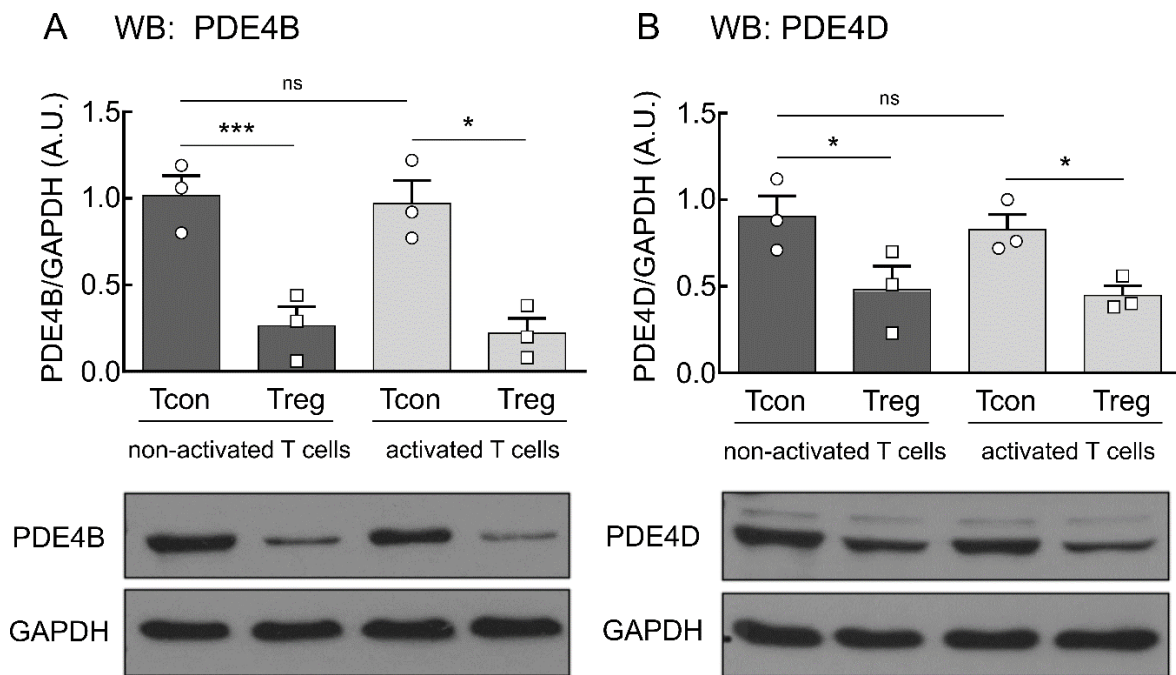


**Figure 13. Conventional T cells highly express PDE4B and PDE4D.** Isolated murine Tcon and Treg after 24 h in culture were used to perform immunoblot analysis. Quantification of protein expression for PDE4B and PDE4D is shown in bar graphs as mean  $\pm$  SEM from three separate experiments, along with representative immunoblots. As a loading control, GAPDH was used. A.U.—arbitrary unit. \* $p < 0.05$ , \*\*\* $p < 0.001$ , ns—not significant by one-way ANOVA followed by Sidak's multiple comparison test.

Real-time measurements were performed to test PDE4 hydrolyzing activity in T cell subsets in naïve versus activated state. Production of cAMP in T cells was stimulated via the  $\beta$ -adrenergic receptor with isoprenaline (ISO), used in different concentrations, 100 nM (**Figure 14A**) and 1  $\mu$ M (**Figure 14B**). When T cells were prestimulated with 100 nM ISO during FRET measurement, PDE4 inhibition in T cells resulted in comparable responses between Tcon and Treg (**Figure 14A**). Stimulation of T cells with 1  $\mu$ M ISO showed a constant cAMP production during measurements of PDE4 hydrolyzing activity among different T cell subsets and T cell activation status (**Figure 14B**). Maximal FRET response was achieved via 100  $\mu$ M IBMX.

## Results

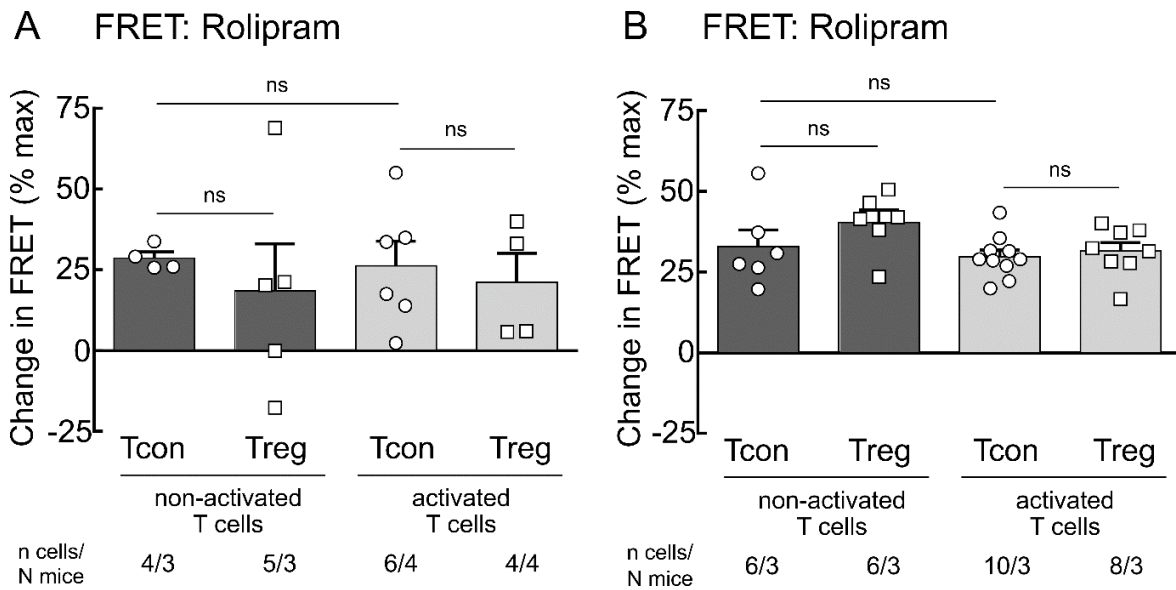


**Figure 14. Live-cell imaging of T cell subsets expressing Epac1-camps sensor upon PDE4 inhibition.** FRET measurements were conducted with non-activated and activated T cell subsets after overnight culture. Quantification of FRET response calculated is shown in **A**, **B**. T cells were initially stimulated with different concentrations of  $\beta$ -adrenoreceptor agonist, isoprenaline (ISO) **A**) 100 nM, and **B**) 1  $\mu$ M. 10  $\mu$ M Rolipram (ROLI) was applied to specifically inhibit PDE4 followed by FRET sensor saturation with a pan-PDE inhibitor 100  $\mu$ M IBMX. Change in FRET shows % of FRET response upon PDE4 inhibition in relation to maximal sensor response completed with IBMX. Bar graphs illustrate the mean  $\pm$  SEM of individual cells measured and number of mice as indicated under each bar. ns—not significant by one-way ANOVA followed by Sidak's multiple comparison test.

### 3.4.2.3 PDE3 in T cells

It was described in earlier publications that *Pde3b* expression is upregulated in Tcon vs Treg due to Foxp3-mediated transcriptional repression of *Pde3b* gene in Treg (Zheng et al. 2007), and this could be also confirmed with the NanoString analysis (**Figure 7**). Next, to further validate this data, protein expression of PDE3B was analyzed in the present study via immunoblotting in non-activated and activated T cell subsets. Protein level of PDE3B was elevated in Tcon, regardless of the T cell activation state. Again, expression of PDE3B in Treg was negligible and did not change upon T cell activation (**Figure 15**).

## Results

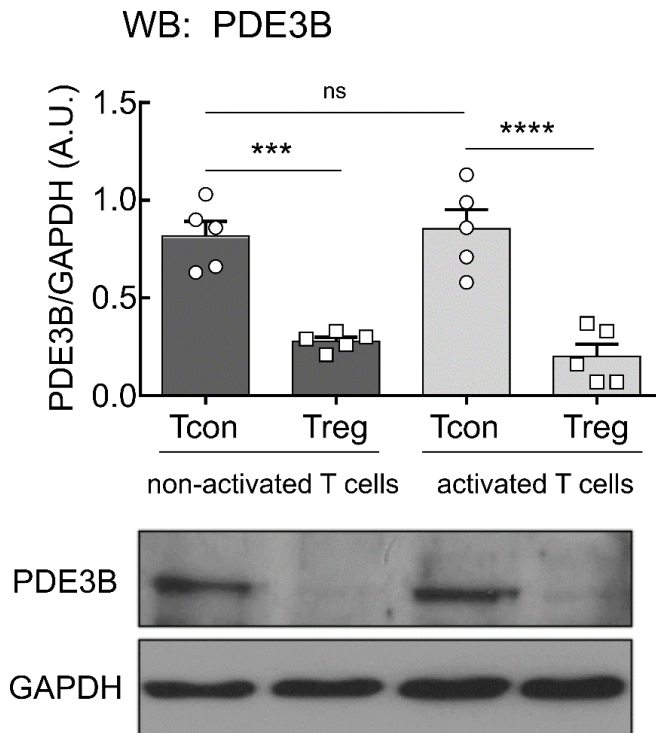


**Figure 15. PDE3B expression is elevated in conventional T cells vs regulatory T cells.** Magnetically-sorted Tcon and Treg were cultured for 24 h and further used for immunoblot analysis. PDE3B protein expression was quantified and indicated in bar graphs as mean  $\pm$  SEM from five individual experiments, together with representative immunoblot. GAPDH was used as a loading control. A.U.—arbitrary unit. \*\*\* $p < 0.001$ , \*\*\*\* $p < 0.0001$ , ns—not significant by one-way ANOVA followed by Sidak's multiple comparison test.

Alongside, FRET measurements were performed to probe hydrolyzing activity of PDE3 by using a specific inhibitor, Cilostamide and Cilostazol, after provoking cAMP production in T cells with agonist drugs, targeting either adenosine or  $\beta$ -adrenergic receptors on T cell surface.

Firstly, at the start of the FRET measurement, 10  $\mu$ M ADO was added to the cell to initiate cAMP generation in the cell cytosol. Next, PDE3 inhibitors, 10  $\mu$ M Cilostamide (**Figure 16A,C,D,E,F**), and 10  $\mu$ M Cilostazol (**PDE16B**) were used to assess PDE3 inhibition among different T cells subsets. After inhibiting PDE3 with Cilostamide and Cilostazol, a comparable FRET response was observed, verifying demonstrated results. Non-activated and activated Tcon exhibited a higher level of cAMP upon PDE3 inhibition in comparison to Treg cells. Likewise, there was no change in FRET response between matching subsets upon T cell activation (**Figure 16A,B**).

## Results

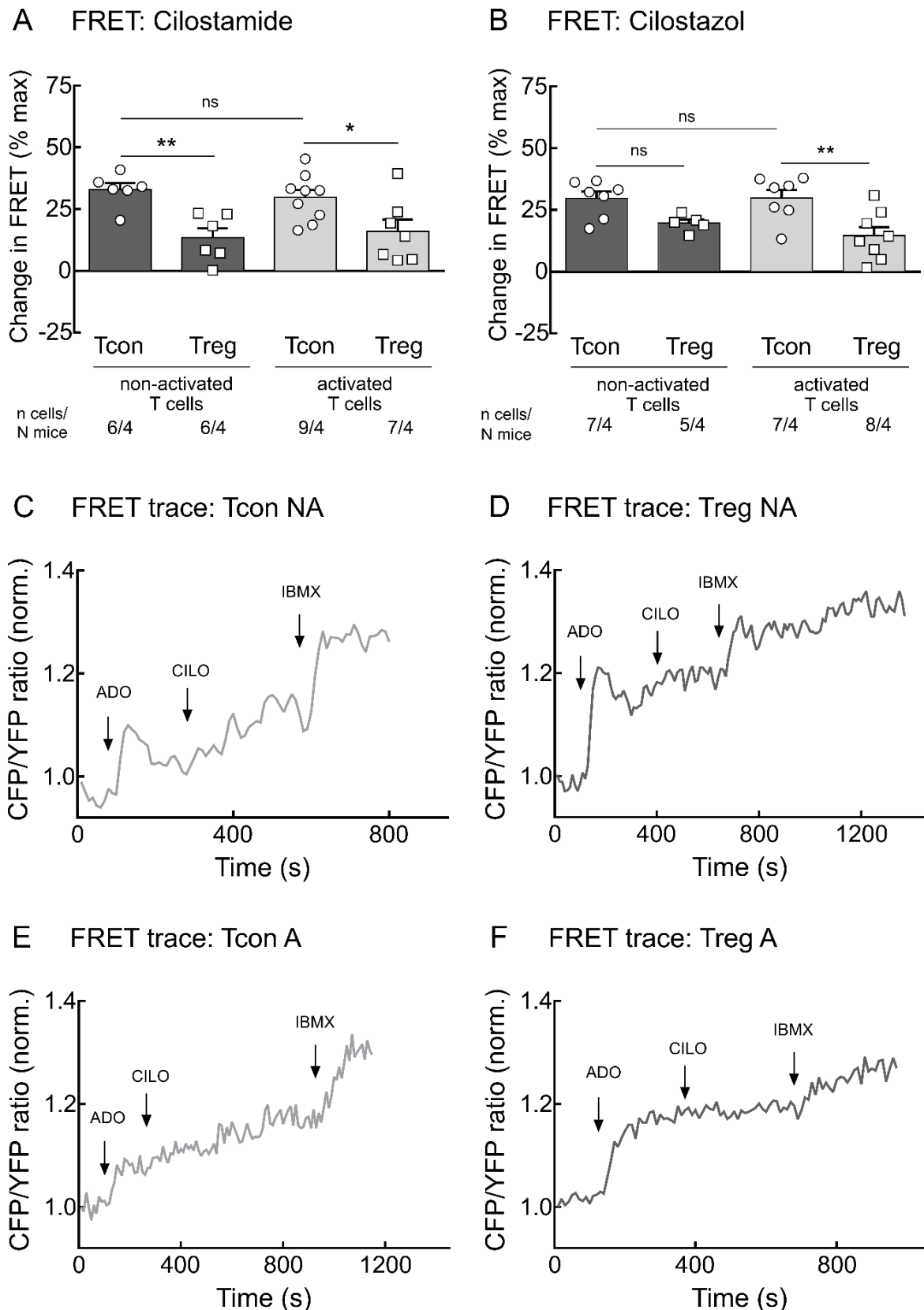


**Figure 16. Real-time measurements of PDE3 inhibitor effects in the cytosol of CD4<sup>+</sup> T cells via FRET.** MACS-purified T cell subsets expressing Epac1-camps sensor were cultured overnight to obtain non-activated and activated (in addition with anti-CD3/CD28 Dynabesd) T cell populations. Live-cell imaging was performed upon T cell stimulation with adenosine (ADO, 10  $\mu$ M) followed by inhibition of PDE3 specifically. As PDE3 inhibitor **A**) Cilostamide (CILO) and **B**) Cilostazol were used in concentration 10  $\mu$ M. FRET sensor was saturated with IBMX (100  $\mu$ M). Representative FRET traces

## Results

for non-activated **C**) Tcon and **D**) Treg together with activated **E**) Tcon and **F**) Treg are shown here. Change in FRET depicts % of FRET response after PDE3 inhibition in T cells vs. maximal cAMP produced. Bar graphs are shown as mean  $\pm$  SEM. Number of cells and mice measured are shown below each bar. \* $p < 0.05$ , ns—not significant by one-way ANOVA followed by Sidak's multiple comparison test.

Moreover, to investigate whether prestimulation of other surface receptors modifies PDE3 hydrolyzing activity, different concentrations of ISO were used to stimulate  $\beta$ -adrenoreceptors. After reaching a stable baseline, 100 nM (**Figure 17A**) or 1  $\mu$ M ISO (**Figure 17B**) was added to the measuring chamber. PDE3 was inhibited with 10  $\mu$ M Cilostamide. Although there was no significant difference in every group compared, there was a transparent trend confirming the above-mentioned findings (**Figure 16**) were non-activated Tcon together with activated equivalent subset, showed elevated cAMP level in comparison to Treg. Likewise, FRET response to PDE3 inhibition detected in Treg cells was low in non-activated and activated Treg (**Figure 17A,B**).

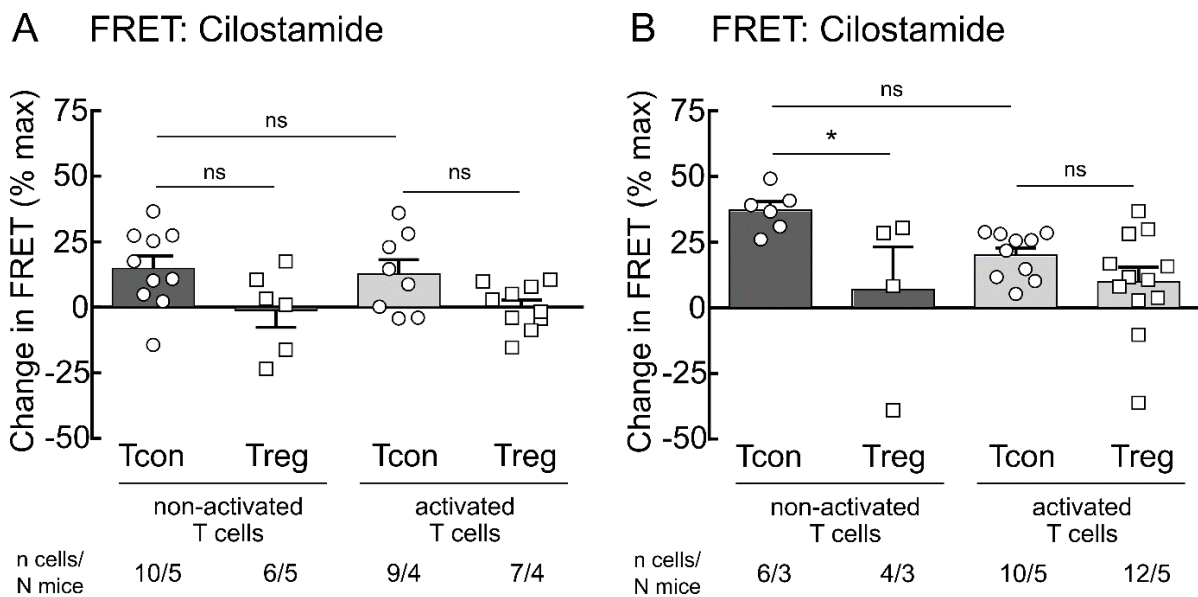


**Figure 17. Live-cell imaging of T cell subsets expressing Epac1-camps sensor upon PDE3 inhibition.** MACS-sorted T cell subsets expressing Epac1-camps after overnight culture and subsequent T cell activation were followed by FRET. Quantification of FRET response is indicated in **A**) and **B**). At the start of the measurement, T cells were prestimulated with  $\beta$ -adrenoreceptor agonist, isoprenaline (ISO) in various concentrations, **A**) 100 nM and **B**) 1  $\mu$ M. Maximal FRET response was utilized with IBMX (100  $\mu$ M). Change in FRET presents % of FRET response upon PDE3 inhibition to maximal sensor response. Bar graphs show the mean  $\pm$  SEM of individual cells and mice measured as defined below bars. \* $p < 0.05$ , ns—not significant by one-way ANOVA followed by Sidak's multiple comparison test.

## Results

### 3.4.2.4 PDE2 in T cells

The effects of PDE4 and PDE3 on modulating cAMP in T cells, as well as their impact on T cell function, have been shown earlier, through original research of other groups but also in the presented study. However, the role of PDE2A in producing cAMP in T cells has not been investigated adequately yet. In naïve T cell subsets, differential expression of *Pde2a* on a gene level was detected via Nanostring analysis (**Figure 7**). Moreover, immunoblotting analyses were conducted to compare PDE2A protein expression upon T cell activation. Protein expression of PDE2A showed a clear trend of elevated expression in non-activated Treg vs Tcon, but without significant impact. Surprisingly, strong upregulation in PDE2A expression was confirmed in Tcon subsets upon activation of T cells. Expression level of PDE2A in Treg remained constant in naïve and activated T cells (**Figure 18**).

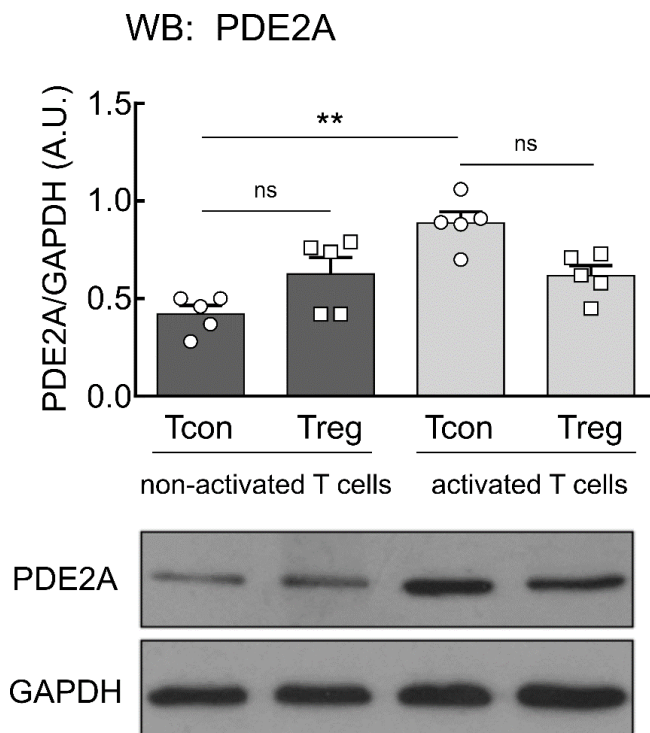


**Figure 18. Activation of conventional T cells in vitro results in upregulation of PDE2A on a protein level.** MASC-purified T con and Treg were subjected to immunoblotting analysis after 24 h in culture with and without murine anti-CD3/CD28 Dynabeads. Protein expression of PDE2A was quantified and normalized to loading control – GAPDH. Bar graphs are presented as mean  $\pm$  SEM from five separate experiments completed. A.U.–arbitrary unit. \*\* $p < 0.01$ , ns–not significant by one-way ANOVA followed by Sidak's multiple comparison test.



## Results

Next, FRET response was measured in T cells expressing Epac1-camps sensor in the cytosol to explore the impact of PDE2 hydrolyzing activity upon prestimulating  $\beta$ -adrenergic receptor or adenosine receptor with agonist drugs. Firstly, the level of cAMP was measured after triggering cAMP generation with 10  $\mu$ M ADO followed by PDE2A inhibition with 100 nM BAY (**Figure 19A**) or 100 nM PF-05180999 (**Figure 19B**) in addition to 100  $\mu$ M IBMX for sensor saturation. Upon treatment with BAY, an increase in FRET response was detected in activated Tcon in comparison to non-activated Tcon (**Figure 19A,C,E**). Inhibition of PDE2A resulted in a stable cAMP level in Treg, regardless of Treg activation status (**Figure 19A,D,F**). PF-05180999 was used to confirm this finding and although there was no significant difference between cAMP levels measured in non-activated and activated Tcon, evidently there was tendency after PDE2 inhibition with PF-05180999 (**Figure 19B**).



## Results

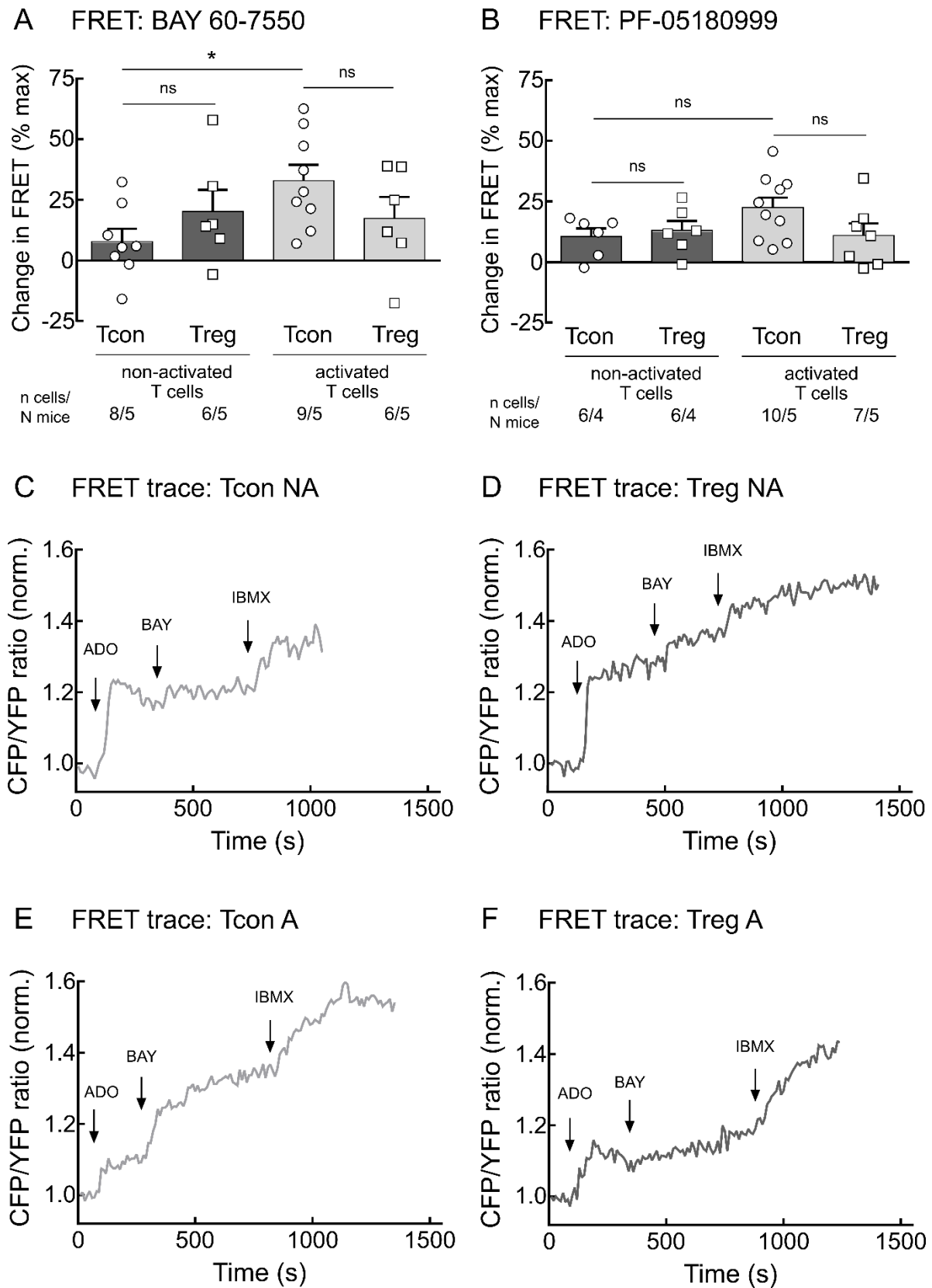


**Figure 19. Real-time measurements of PDE2 inhibitor effects in the cytosol of CD4<sup>+</sup> T cells via FRET.** Tcon and Treg isolated by MACS were cultured overnight with IL-2 and with (activated) or without (non-activated) anti-CD3/CD28 Dynbeads. T cells were prestimulated with adenosine (ADO, 10  $\mu$ M) and afterward PDE inhibitor was used in concentration 100 nM, **A**) BAY 60-7550 or **B**) PF-05180999.

## Results

Epac1-camps sensor was saturated with IBMX (100  $\mu$ M). Representative FRET traces of individual cells measured after inhibition with BAY are shown for non-activated (NA) **C**) Tcon and **D**) Treg together with activated (A) **E**) Tcon and **F**) Treg. FRET recordings were depicted in bar graphs as mean  $\pm$  SEM. % of the change in FRET after PDE2 inhibition is quantified in comparison to the maximal response of the sensor. Number of cells and mice per group as indicated under the individual bar. \* $p < 0.05$ ; ns—not significant by one-way ANOVA followed by Sidak's multiple comparison test.

Afterward, the level of cAMP was assessed in response to PDE2 inhibition with BAY after stimulation of  $\beta$ -adrenergic receptors with 1  $\mu$ M ISO. 2-fold increase in FRET response was detected in activated Tcon vs non-activated Tcon after treatment with BAY resembling augmentation observed upon T cell receptor mentioned earlier. Besides, a 4-fold elevation in cAMP level was measured in non-activated Treg vs. Tcon although without a significant effect (Figure 20).

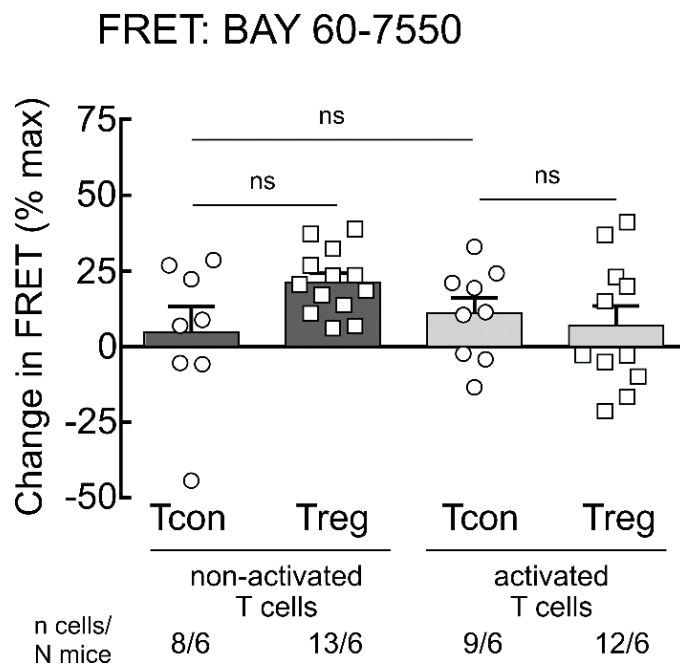


**Figure 20. Live-cell imaging of T cell subsets expressing Epac1-camps sensor upon PDE2 inhibition.** MACS-purified T cells from splenocytes isolated from transgenic mice were cultured overnight and afterward used for real-time measurements. Quantification of FRET response is depicted in bar graphs shown as mean  $\pm$  SEM of individual cells measured together with number of mice indicated under bar. At the start of the FRET measurement, cells were stimulated with an agonist drug for  $\beta$ -adrenergic receptor, 1  $\mu$ M isoprenaline (ISO). PDE2 inhibition was achieved by 100 nM BAY 60-7550 (BAY) and further saturation of the sensor by 100  $\mu$ M IBMX. Change in FRET represents % of FRET response upon PDE2 inhibition in comparison with maximal sensor response attained by applying IBMX. ns—not significant by one-way ANOVA followed by Sidak's multiple comparison test.

## Results

### 3.4.2.5 Regulation of cyclic nucleotide cross-talk in CD4<sup>+</sup> T cells

Since activity of PDE3 and PDE2A is modulated also by cGMP, cyclic nucleotide cross-talk was tested in T cells via FRET. Real-time measurements were conducted in order to study how provoking cGMP production with natriuretic peptides affects cAMP levels in non-activated versus activated T cell subsets expressing cytosolic FRET sensor, Epac1-camps.

Firstly, the expression of natriuretic peptide receptors, *Npr1* and *Npr2*, was tested in T cells via qRT-PCR to confirm findings demonstrated in earlier studies (Ma et al. 2013; Vollmar, Schmidt, and Schulz 1996). Level of gene expression was compared between bulk of CD4<sup>+</sup> T cells, both non-activated and activated. Expression of both genes, *Npra* and *Nprb*, was observed in T cells and level of expression was comparable between cells, independent of activation (**Figure 21**).

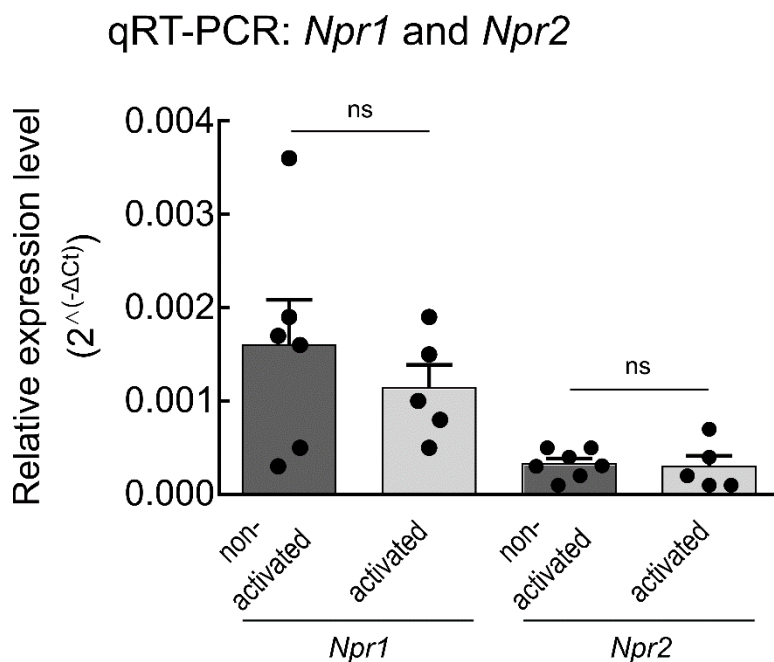


**Figure 21. Expression of *Npr1* and *Npr2* in CD4<sup>+</sup> T cells.** CD4<sup>+</sup> T cells isolated from mice were cultured 24 h in the presence (activated) or absence (non-activated) of CD3/CD28 Dynabeads and IL-2. qRT-PCR was performed to measure mRNA expression of *Npr1* and *Npr2*. Data were normalized to the housekeeping gene, *Tbp*. Bar graphs represent the quantification of the relative expression level of the gene of interest by using obtained  $\Delta C_t$  values. Results in bar graphs are depicted as mean  $\pm$  SEM of five (activated) or six to seven (non-activated) independent experiments. ns—not significant by Student's t-test.

Moreover, cGMP/cAMP cross-talk has been studied before in other cell types, such as cardiomyocytes (Götz et al. 2014) after stimulation of cells with  $\beta$ -adrenoreceptor agonist, followed by immediate stimulation of NP receptors. An identical protocol was applied while

## Results

measuring cAMP levels in T cells. T cells were prestimulated with an unselective  $\beta$ -AR agonist, 1  $\mu$ M ISO. Thereafter, saturating concentrations of natriuretic peptides, 200 nM ANP and 300 nM CNP, were added to initiate cGMP generation within the cell. FRET sensor saturation was achieved with a combination of 10  $\mu$ M FSK and 100  $\mu$ M IBMX. Real-time measurements of NP stimulus in non-activated Tcon showed an increase in cAMP response after both ANP and CNP (**Figure 22A,B,C**). Treatment of non-activated Tcon with a PDE3 inhibitor, Cilostamide, abrogated this effect (**Figure 22A,B,E**). Opposite to finding in non-activated Tcon, activated Tcon demonstrated a significant decrease in FRET response to cGMP produced after adding ANP and CNP (**Figure 22A,B,D**). This effect was particularly sensitive to the pretreatment of cells with a PDE2 inhibitor, BAY 60-7550, which resulted in a small increase in cAMP (**Figure 22A,B,F**). Non-activated and activated Treg exhibited negligible cAMP response after the addition of NPs to the measuring bath.

## Results

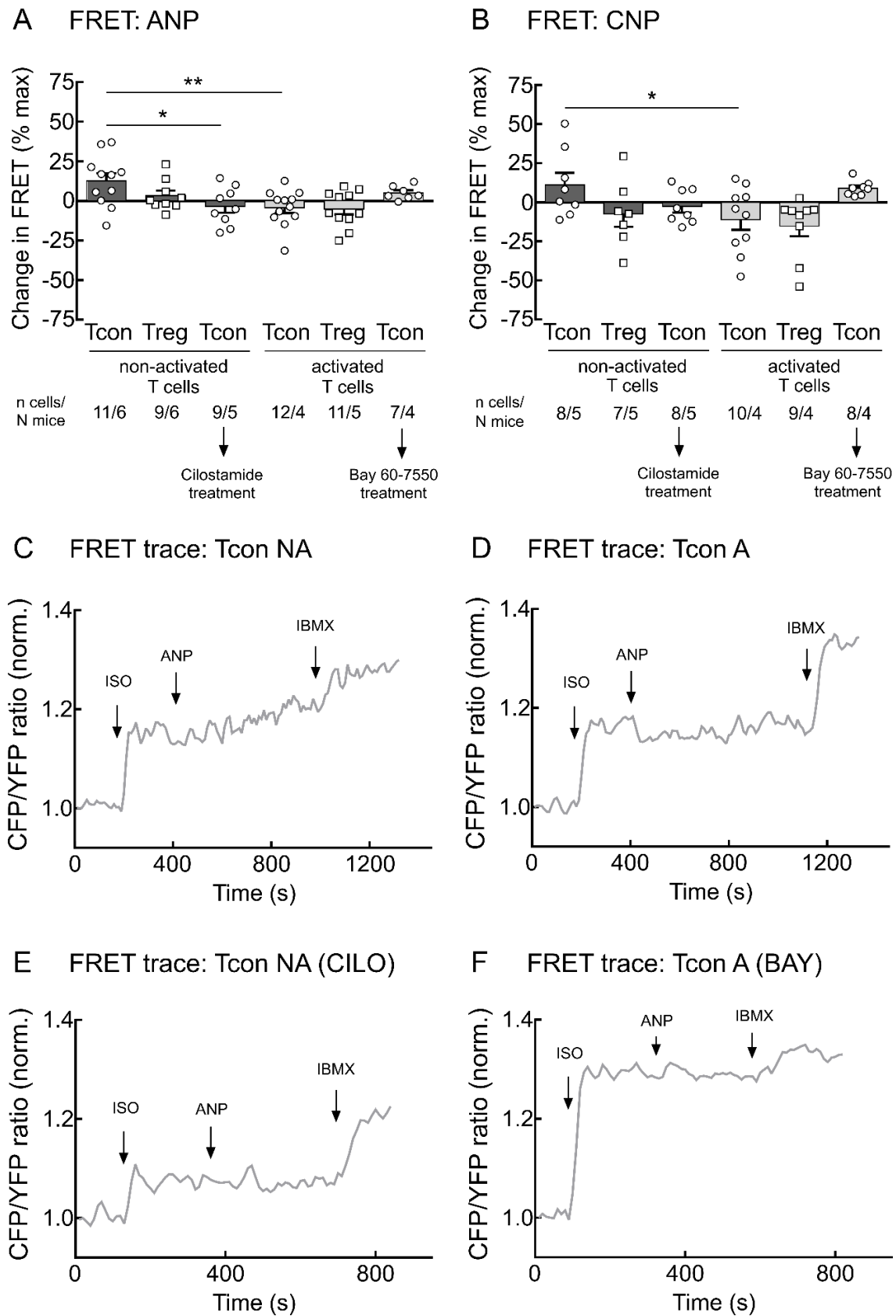


**Figure 22. Stimulation of T cells subsets with atrial and C-type natriuretic peptides changes cAMP levels measured via FRET.** Magnetically-sorted Tcon and Treg expressing FRET sensor Epac1-camps were cultured overnight with or without anti-CD3/CD28 Dynabeads and FRET measurements were performed on the following day. Quantification of FRET response is depicted in bar graphs as

## Results

mean  $\pm$  SEM. T cells were prestimulated with non-selective  $\beta$ -adrenergic receptor agonist 1  $\mu$ M isoprenaline (ISO) to provoke cAMP production. Change in FRET presents % of cAMP response to **A**) ANP (200 nM) and **B**) CNP (300 nM) stimulation of single cell in relation to maximal sensor response gained with FSK (10  $\mu$ M) and IBMX (100  $\mu$ M). Negative values represent a decrease in cAMP during real-time measurement. Representative FRET traces of Tcon cells measured upon ANP stimulation for **C**) non-activated (NA), **D**) activated (A), **E**) non-activated T con after CIL0-pretreatment and **F**) activated T cells after BAY pretreatment are shown. Number of cells and mice measured per group as indicated below the individual bar. \* $p < 0.05$ ; \*\* $p < 0.01$  by one-way ANOVA followed by Sidak's multiple comparison test.

### 3.4.3 Visualization of cAMP transfer between T cell subsets via live-cell imaging

Despite comprehensive research in the last decade on the function of connexins and gap junctions in the immune system, the exact mechanism of intracellular cAMP transfer between Treg and Tcon is not yet completely elucidated. Gap junction alpha-1 (*Gja1*) is a gene encoding for Connexin 43, a predominant GJ protein in both human and mouse immune systems (E. Oviedo-Orta, Hoy, and Evans 2000; Ernesto Oviedo-Orta and Howard Evans 2004). Initially, the relative expression level of *Gja1* was measured via qRT-PCR in bulk CD4+ T cells and there was no difference in *Gja1* expression among non-activated and activated CD4+ T cells (**Figure 23**).

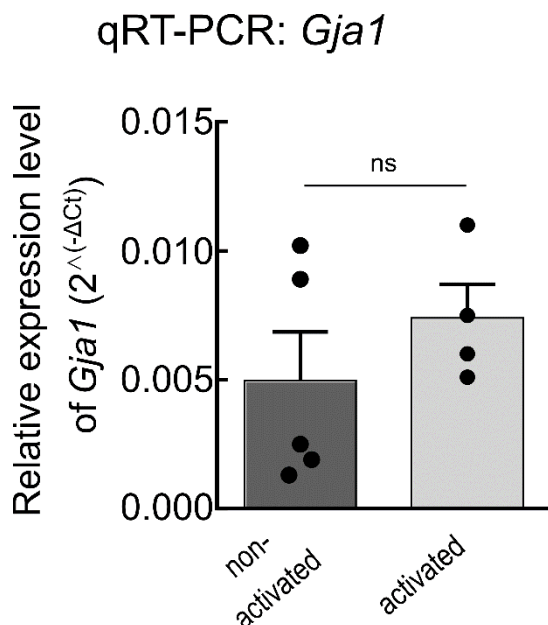


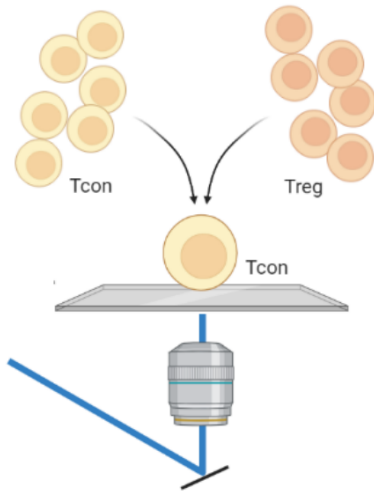
**Figure 23. Gene expression levels of Connexin 43 in non-activated and activated CD4+ T cells.** Murine CD4+ T cells were MACS-purified and cultured for 24 h in the presence (activated) or absence (non-activated) of CD3/CD28 Dynabeads. mRNA expression of *Gja1* in CD4+ T cells was evaluated by qRT-PCR. Quantification was performed upon normalization of obtained data with the housekeeping gene, *Tbp*, and bar graphs represent relative expression level of the gene of interest by using  $\Delta Ct$  values measured. Results in bar graphs are shown as mean  $\pm$  SEM of four (activated) or five (non-activated) independent experiments. ns—not significant by Student's t-test.

## Results

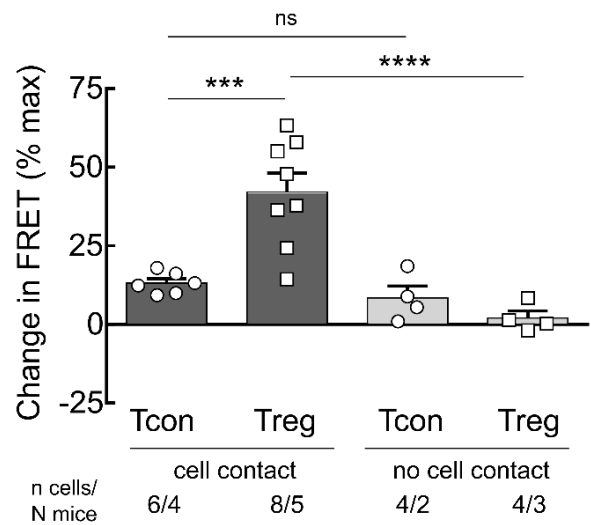
Previously it has been demonstrated how activated Tcon are competent to interact with Treg upon cell co-culture followed by FACS analysis (Bopp et al. 2007), but dynamics of the transfer process have not been visualized in real-time up to date. Experimental layout was established on an essential FRET imaging setup. To gain deeper insight into the mechanisms of Treg-to-Tcon cAMP transfer and to picture this process in real-time, activated Tcon expressing Epac1-camps sensor together with non-activated cell population were isolated and cultured overnight. Activated Tcon were plated for 30 min on glass coverslips before the start of the FRET measurement. Upon reaching the first baseline, either non-activated Tcon, as the control group, or non-activated Treg, as cells of interest, were added to the measuring bath and a change in FRET response was quantified compared to maximal FRET sensor response elicited with saturating concentrations of FSK and IBMX. A concept for this experiment originated from the idea of capturing the cAMP process in real-time, and for this cells in close proximity to each other were required for getting optimal measuring conditions. In order to land added cells closer to the activated measured cell, additional modifications were needed as the implementation of the nut, which reduced the area where cells could float and enhanced the actual experimental setup (**Figure 24A**). FRET data revealed a significant increase in cAMP levels upon cell contact between non-activated Treg and activated Tcon during real-time measurements (**Figure 24B,C,D**). Adding non-activated Tcon while measuring cAMP levels in activated Tcon, showed a minor response and comparable cAMP level when cell contact occurred as well as when there was no cell contact. When non-activated Treg were added to the measuring bath without direct cell contact, cAMP levels detected were negligible (**Figure 24B**).

## Results

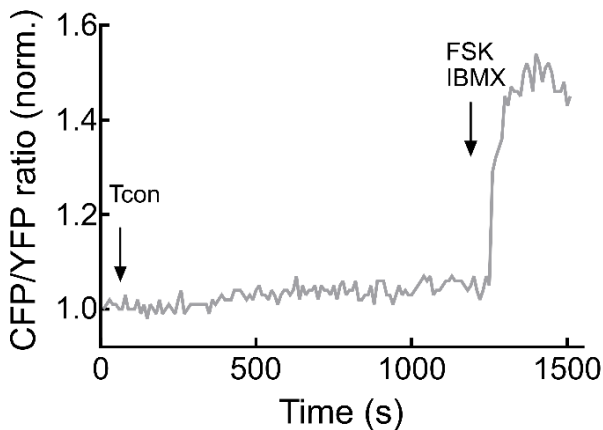
### A Experimental setup



### B FRET: Transfer



### C FRET trace: Tcon A and Tcon NA



### D FRET trace: Tcon A and Treg NA

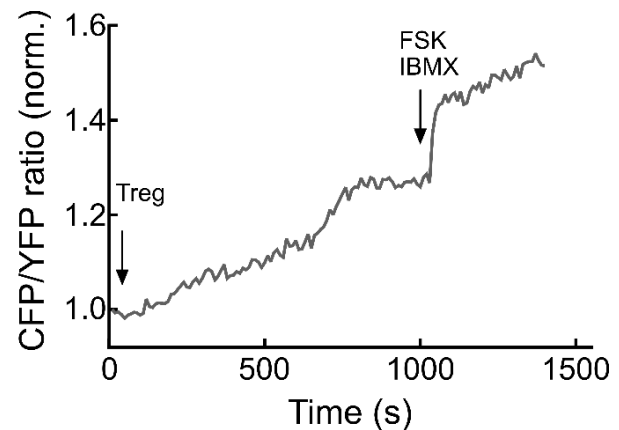


**Figure 24. Cell contact between regulatory and conventional T cells increases cAMP level in Tcon.** MACS-purified Tcon expressing Epac1-camps sensor were activated with CD3/CD28 murine Dynabeads in overnight culture in presence of IL-2. Non-activated Tcon and Treg were cultured with IL-2 and without Dynabeads. **A)** Scheme representing experimental layout for visualization of transfer process via live-cell imaging prepared in BioRender.com. Activated Tcon were on glass coverslips coated with Poly-D-lysine in a chamber for measuring. During real-time measurement, non-activated T cells were pipetted into the measuring chamber to monitor the interaction between cells upon direct contact. **B)** Quantification of FRET response is shown as % of the change in FRET upon cAMP production during contact between activated Tcon measured and non-activated T cell added. Sensor saturation was achieved concurrently with 10  $\mu$ M Forskolin and 100  $\mu$ M IBMX. **C)** Representative FRET traces for real-time measurement where cell-to-cell contact of measured and added T cells was observed. **D)** Activated Tcon under transmitted light at the start of FRET measurement (upper picture) and upon addition of non-activated T cells established cell-cell contact (lower picture) are depicted. Results in bar graphs are introduced as mean  $\pm$  SEM. Number of cells and mice used is stated under the bar graph. \*\*\* $p < 0.001$ , \*\*\*\* $p < 0.0001$ , ns—not significant by one-way ANOVA followed by Sidak's multiple comparison test.



## Results

To characterize the localization of GJ markers in T cells, immunofluorescence together with confocal microscopy was performed. For this set of experiments, splenocytes collected from wild-type mice were used to magnetically-sorted Tcon and Treg. Tcon were activated with anti-CD3/CD28 mouse Dynabeads and cultured overnight, on the side to non-activated T cell subsets. These experiments were anticipated to capture the moment of cell contact and to confirm the formation of GJs by staining for Connexin-43. As a marker for membrane staining, an anti-CD4 antibody was used. Confocal images revealed specific membrane staining on the cell surface of CD4<sup>+</sup> T cells. No differences in localization were observed between activated and non-activated T cells, with and without cell contact formation after staining for Connexin 43, as shown in representative images of individual channels and overlapping image (**Figure 25**).

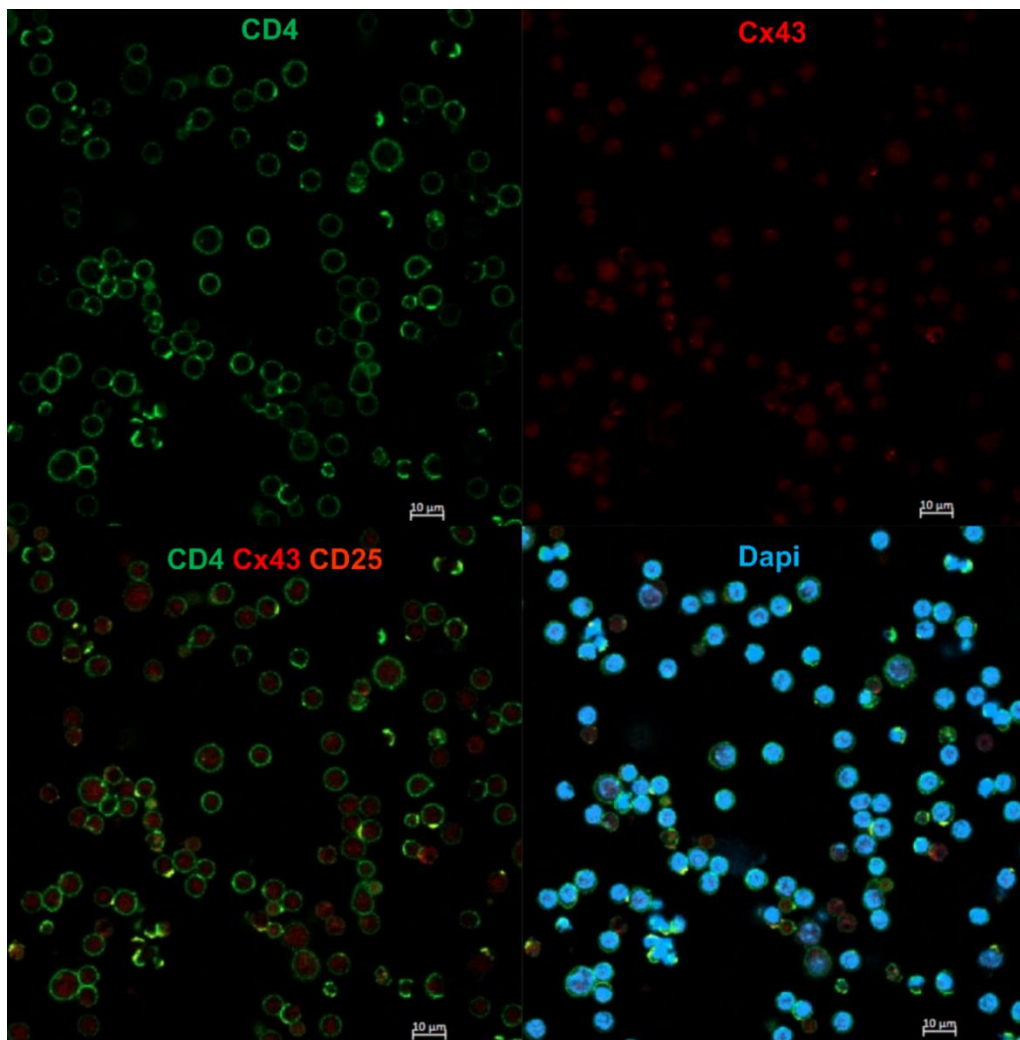


**Figure 25. Localization of Connexin 43 in T cells subsets.** Murine splenocytes obtained from wild-type mice upon overnight culture were used to mimic the FRET-base experimental setup and fixed afterward with Methanol. Immunofluorescence staining was performed for CD4 as a membrane marker of T cells (green), Connexin 43 to visualize gap junction assembled (red), CD25 as a marker of non-activated Treg (orange), and Dapi for nuclear staining (blue). Localization of the above-mentioned proteins was assessed via confocal microscopy. Scale bar: 10 µm.

### 4 Discussion

As aim of this PhD thesis was to delineate diverse expression and activation of cAMP pathway components in T cell subsets, different approaches were used with a focus on live-cell imaging via FRET. Generation of cAMP stimulated by various GPCRs or its degradation via PDEs brings interest in elucidating this orchestrated process behind multiple cellular responses in autoimmune diseases. Also, acknowledging the importance of cyclic nucleotides during inflammation promotes GPCRs and PDEs as great targets for possible therapeutic interventions.

#### 4.1 Establishing live-cell imaging in T cells

Live-cell imaging is a useful method for monitoring dynamics of spatiotemporal regulation of intracellular events in T cells, including polarization and migration of T cells (Hyun et al. 2009), cell-to-cell adhesion (Carlin et al. 2011) and TCR-dependent activation of T cells (Direnberger et al. 2012). Genetically encoded fluorescent biosensors are powerful tools widely used for performing live-cell imaging and are being continuously improved to achieve specific signal and greater performance. Downside of expressing fluorescent biosensors in T cells and/or other leukocytes is efficiency of the transduction process together with ubiquitous and applicable expression of the sensor since primary T cells are mostly quiescent. Proper transduction of T cells with retro- or lentiviral particles is TCR-dependent process that is vital for adequate infection. Thus, real-time measurements could be performed exclusively on activated T cells upon TCR activation and *in vitro* culture with viral particles. Another transduction pitfall comes from the use of unimolecular fluorescent biosensors flanked between two fluorophores. Fluorophores with high homology in nucleic acid sequence can show altered expression of fluorescent proteins due to recombination of homolog DNA sequence encoded in a lentiviral vector (Randriamampita and Lellouch 2014). To overcome the above-mentioned difficulties, generation of a transgenic animal model expressing fluorescent biosensors is a good solution. Transgenic animals are acknowledged for the potential of measuring intact and fresh primary cells ready to use for live-cell imaging instantly after isolation. Until now, cAMP has been indirectly measured in real-time in murine hybridoma T cell line (3A9 cells) upon nucleofection of DNA encoding the AKAR2 biosensor probe (Conche et al. 2009). AKAR2 probe reports PKA activity at the single-cell level following cAMP increase within the cell (Zhang et al. 2001). In this particular report, they could demonstrate that cAMP increases in 3A9 cells as a consequence of cell adhesion to fibronectin (Conche et al. 2009). Among different FRET probes, Epac1-camps sensor has already been published for measuring cytosolic cAMP levels in diverse primary murine cell types such as cells of

## Discussion

ovarian and thyroid follicles (Lyga et al. 2016), cardiomyocytes (Sprenger et al. 2016), etc. This biosensor was further used in this particular PhD thesis to study dynamics of intracellular cAMP changes under diverse cAMP-agonizing and -antagonizing stimuli (Figure 5). Available transgenic animal model was used to conduct live-cell imaging in T cells. In this particular animal model, Epac1-camps biosensor is expressed under the control of the CAG promoter in all cells and tissues uniformly (excluding erythrocytes and hair) (Calebiro et al. 2009). Final challenge in performing live-cell imaging in T cells is their rather small size and high motility which makes FRET measurements very challenging compared to other primary cells. All things considered, although setting up real-time FRET measurement when using T cells can be demeaning, valuable information can be obtained when performing live-cell imaging.

### 4.2 Relevance of GPR52 in the context of T cell biology

As described in the introduction, activation of GPCRs is mostly regulated through the binding of specific ligands, such as hormones, ions, neurotransmitters, or photons. But, there is also a family of GPCRs called orphan GPCRs, due to an unknown ligand specific to that particular receptor (Wootten et al. 2018). Expression of constitutively active orphan GPCRs was first explored through the ImmGen database search for GPR candidate genes, such as *Gpr65*, *Gpr52*, *Gpr21*, *Gpr12*, *Gpr6*, and *Gpr3* (data not shown). High expression of *Gpr52* in Treg subset caught interest for studying this gene in the context of T cell biology. Gene expression level of *Gpr52* was analyzed on murine T cell subsets upon activation with anti-CD3/CD28 via qRT-PCR. This analysis revealed a 5-fold higher level of expression of *Gpr52* in non-activated Treg compared to Tcon. Upon activation, *Gpr52* was unchanged in Tcon, while a decrease was observed in activated Treg compared to non-activated cells although without significance (Figure 8). These data are the first connection of this particular orphan GPCR with the immune system. Previously, expression of *Gpr52* was detected in the murine striatum where it colocalized with pyramidal neurons expressing dopamine D1 receptor and medium spiny projection neurons expressing dopamine D2 receptor evidencing involvement of GPR52 in several neuropsychiatric disorders (Komatsu et al. 2014). As GPR52 was already profiled to be a drug target in neuropsychiatric disorders, like schizophrenia and Huntington's disease, researchers obtained structure of human GPR52 in the ligand-free state and complex with synthetic receptor agonist molecule, c17. Interestingly, they discovered high basal activity of the GPR52 receptor due to unusual structural elements (Krumm and Roth 2020). To further investigate the effects of GPR52 on modulating cAMP levels, already published agonist and antagonist drugs were examined. Specificity of FTBMT, GPR52 agonist drug, was previously tested in the CHO cell line expressing DNA encoding for human, mouse, or rat GPR52. cAMP increase was measured via cAMP ELISA, and addition of nanomolar concentrations of FTBMT

## Discussion

resulted in the promotion of cAMP generation (Nishiyama, Suzuki, Harasawa, et al. 2017). To confirm agonist drug specificity, in this PhD thesis fluorescently labeled GPR52 construct or empty backbone vector were used to transiently transfect HEK293A cell line. This cell line does not express GPR52 endogenously and changes in the cAMP response upon FTBMT stimuli could be measured in real-time to directly assess drug specificity. For this purpose, HEK293A were double-transfected with FRET biosensor, Epac1-camps. Upon stimulation with 500 nM FTBMT, no change or dispensable rise in FRET response was detected in the control group while cells expressing human GPR52 construct upon addition of FTBMT revealed elevation in cAMP confirming, FTBMT specificity for GPR52 (Figure 9). Identical concentrations were used while performing live-cell imaging in primary murine T cells, upon overnight culture with and without anti-CD3/CD28. In non-activated Treg, the increased cAMP response was observed compared to Tcon, while upon activation of T cell subsets this difference in cAMP was diminished (Figure 10). On the other hand, GPR52 antagonist drug, E7, was published as a highly specific drug for GPR52, and it was tested in HEK293 cell line exogenously expressing GPR52. The intracellular cAMP level was assessed by HTRF and inhibition of cAMP response upon stimulation with 100 nM WO-459, another GPR52 agonist, was detected in the low micromolar range (Song et al. 2018). Hence, E7 was examined in T cell subsets via FRET. Indeed was confirmed that preincubation of T cells with 10  $\mu$ M E7 abolished cAMP response to FTBMT treatment during real-time measurements in both non-activated and activated T cell subsets (Figure 10). Stimulation of GPR52 was also achieved *in vivo* with compound 7m, reported as an additional GPR52 agonist small molecule. Agonist treatment was tested in animal studies associated with psychostimulant-induced hyperactivity and beneficial effects were confirmed when applying GPR52 agonist drug together in treating diseases such as schizophrenia (Nishiyama, Suzuki, Maruyama, et al. 2017; Spark et al. 2020). Since *Gpr52* was highly expressed not only in the brain and spleen but also in the liver and adipose tissue of WT mice, additional research was carried out on *Gpr52*-deficient mice to characterize the physiological role of GPR52 in controlling energy metabolism. Results revealed that *Gpr52*-deficient mice have lower weight compared to littermate controls, in addition to decreased fat and liver weight but also elevated insulin sensitivity (Wada et al. 2021). Next, the role of GPR52 in Treg-mediated immunosuppression was studied *in vivo* in collaboration with A06 project partners from CRC1328 (Research group of Prof. Dr. Fries). Mice lacking GPR52 together with both sex- and age-matched littermate controls were subjected to EAE, the well-established mouse model of MS. Disease severity was not affected by GPR52 deficiency indicating that presence of GPR52 in T cells and potential immunosuppression do not have any impact on functional level (Krieg et al. 2022).

## Discussion

### 4.3 cAMP immunoassay analysis of murine T cell subsets

To assess basal cAMP levels in T cell subsets derived from wild-type mice, cAMP immunoassay was performed. MACS-sorted T cells were lysed directly upon adjusting samples obtained from multiple mice to equal number of cells. Tcon demonstrated 2-fold lower basal cAMP level in comparison to Treg cells (Figure 6). It has been shown before that intracellular cAMP levels differ between Tcon and Treg cells which could be confirmed with this experimental readout. In previous reports, cAMP ELISA has been performed on FACS-sorted T cells where 20-fold higher cAMP level have been detected in Treg compared to Tcon. Upon short-term activation (4 hours) of TCR *in vitro* by using an anti-CD3 monoclonal antibody, cAMP levels in Treg further increased while Tcon cells maintained a low level of cAMP (Bopp et al. 2007). Interesting finding reported in that study was that upon co-culture of preactivated Treg and Tcon (20 hours) cAMP level in Tcon increased to comparable results as treatment of Tcon cells with 1  $\mu$ M forskolin. Another group also compared levels of cAMP between T cell subsets and they could show that freshly isolated Treg have high level of cAMP. Additionally, 4 hours incubation of both T cell subsets with forskolin or IBMX (final concentrations 100  $\mu$ M) upon *in vitro* T cell activation with anti-CD3/CD28 promoted elevation of cAMP levels (Vaeth et al. 2011). On the other hand, no difference in cAMP levels between T cell subsets was shown in the study where authors measured similarly low cAMP concentrations in both subsets (Bazhin et al. 2010). To address the hypothesis that GPR52 partly drives higher cAMP levels in Treg cells, cAMP immunoassay was performed in GPR52-deficient mice and corresponding littermate controls. Opposite to the presented hypothesis that Treg cells isolated from GPR52-deficient mice have a lower cAMP level in comparison to Treg cells from WT mice, both T cell subsets isolated from mice lacking GPR52 revealed no difference in cAMP level compared to WT mice (Figure 6A). This finding suggests the presence of unexplored additional compensatory mechanisms occurring in T cells upon knocking out of the *Gpr52* receptor gene which could influence basal cAMP level. In addition, cAMP immunoassay was performed on a mouse model with global AC6 deficiency and its littermate control. Direct comparison to previously discussed data can not be drawn since the mice used in completed experiments differ in age. Still, higher cAMP levels were confirmed in WT Treg cells in comparison to WT Tcon, as shown before. Furthermore, upon knocking out AC6, upregulation of cAMP levels was observed in Tcon while Treg cells maintained their cAMP levels as seen in WT Treg (Figure 6B). Previous contribution of AC7 on cAMP levels in CD3<sup>+</sup> T cells was examined also via one of the available cAMP assays. Both WT and AC7-deficient mice revealed comparable levels of cAMP, while upon stimulation with 100 nM ISO (1 minute stimulation), AC7-KO derived T cells exhibited a significantly lower cAMP response to a stimulus versus WT T cells (Duan et al. 2010). Next, concentration of cAMP measured in



## Discussion

8-week-old WT mice was at least 2-fold higher for both T cell subsets in relation to cAMP concentrations detected in 16-week-old WT mice. Various measurements of cAMP levels summarised above were completed on WT mice at a comparable age but cAMP concentrations detected highly vary between different research groups. This could be partly due to the use of diverse commercially available kits each suggesting sample collection and preparation in presence of chemical inhibitors of ACs or PDEs. To sum up, traditional assays, like RIA or EIA, discussed above, usually require presence of IBMX to prevent degradation of cAMP and augment cAMP levels to reach detection limit making it difficult to assess basal level of cAMP within the cell but also the dynamics of cAMP level changes at the single cell level in real-time. For this study, a cAMP immunoassay was performed on freshly isolated T cells without additional drug stimulation to allow interpretation of data as basal cAMP levels detected in T cell subsets of WT and available global KO mice. An additional disadvantage of cAMP ELISA and similar traditional assays is a high number of T cells per sample required to obtain concentration of cAMP within the detection of assay.

### 4.4 Real-time dynamics of cAMP in T cells

To analyze the expression of cAMP-relevant genes in naïve murine T cell subsets, NanoString analysis has been performed. Among various genes, such as ACs, AKAPs, and PDEs, differential expression between T cell subsets was observed specifically in the expression of PDE isoforms. While in Treg cells expression of *Pde1b* and *Pde2a* was upregulated, Tcon showed higher expression of *Pde3b* and *Pde4b* (Figure 7). In brief, multiple research groups probed expression of diverse PDE isoforms in both T cell subsets, either on mRNA or protein level (Bazhin et al. 2010; A. G. Vang et al. 2013; Torphy 1998). Particularly, a question was directed toward expression levels of PDEs after *in vitro* activation of specific T cell subset. To address this question, T cells were cultured for 24 hours in the presence or absence of anti-CD3/CD28 coated beads, followed by immunoblot analysis. PDE4B and PDE4D were differentially expressed in naïve murine T cell subsets, and the same expression level was observed upon TCR activation, where Tcon showed higher expression of both PDE4 isoforms (Figure 13). Accordingly, activation of short isoforms of PDE4B and PDE4D was assessed upon *in vitro* culture of human CD4<sup>+</sup> T cells in presence of anti-CD3/CD28 on the gene level. Upon 24-48 hours of TCR activation, downregulation of *Pde4d* was observed compared to non-activated cells, while after 72-120 h, higher gene expression was detected for *Pde4d* isoform. Upregulation of *Pde4b* was detected after 24 h culture with anti-CD3/CD28 but the effect was diminished after prolonged culturing (Peter et al. 2007). In line with previous results for PDE4B and PDE4D, the same pattern was detected for PDE3B, where the difference in expression between Tcon and Treg was more dramatic, regardless of their

## Discussion

activation status (Figure 15). This finding has already been described after identifying transcriptional repression of *Pde3b* gene in Treg mediated by Foxp3 (B. Huang et al. 2009; Gavin et al. 2007; Anandagoda et al. 2019). Expression of PDE2A in naïve T cell subsets revealed tendency but no significant difference between Tcon and Treg. Strikingly, upon activation of Tcon, PDE2A expression level was upregulated in comparison to non-activated Tcon, while Treg cell maintained identical expression level before and after TCR activation (Figure 18). Moreover, PDE2, together with PDE4, was earlier identified as prominent contributor to total PDE activity in murine thymocytes (Michie et al. 1996) but this novel finding towards PDE2A upregulation in activated Tcon was not documented before and was further elaborated in this particular thesis through monitoring cAMP responses in real-time after specific PDE inhibition. Functionally, impact of inhibition of specific PDE was investigated in T cell proliferation assay designed to answer a question whether cAMP plays a role in Treg-mediated Graft-versus-host Disease (GvHD). Authors could show that different concentrations of specific inhibitors used, BAY 60-7550 for PDE2A, Cilostazol for PDE3, and Rolipram for PDE4 suppressed allogeneic T cell activation, either via inactivating DC and inhibiting proliferation of responder T cells, thus directly confirming involvement of cAMP (M. Weber et al. 2013). PDE4, as a predominately studied PDE in immune system, was analyzed in multiple *in vivo* and *in vitro* settings. In brief, one study revealed that blocking the degradation of cAMP by the PDE4 inhibitor Rolipram can result in elevation of the suppressive capacity of Treg towards Th2 cells due to increased cAMP (Bopp et al. 2009). The impact of PDE4 inhibition in T cell subsets expressing cytosolic Epac1-camps sensor after *in vitro* activation was measured via FRET. Since cAMP is predominantly bound under basal conditions, leading to a relatively low concentration of free cAMP, measured T cells were firstly stimulated with ISO or ADO (Bock et al. 2020). In essence, ISO prestimulation of T cells, nor activated or non-activated, did not affect cAMP response in T cell subsets upon PDE4 inhibition with Rolipram (Figure 14). FRET response upon PDE4 inhibition differed between Tcon and Treg in activated T cells which were first stimulated with ADO (Figure 11B). This implies that stimulation of different GPCRs on the T cell surface differently controls localized PDE activity within the cell. Gradients of cAMP around specific GPCRs were already identified as receptor-associated independent cAMP nanodomains (RAINs) which can function as autonomous signaling units. By contrast, strong stimulation of receptors could induce fusion of distinct RAINs and a rise in bulk cAMP levels (Anton et al. 2022). Furthermore, when FRET imaging was conducted in non-activated Tcon and Treg subsets, a similar pattern of cAMP response to PDE3-specific inhibition with Cilostamide or Cilostazol was observed. Regardless of the receptor agonist drug (ISO or ADO) or its concentrations used for stimulating cAMP production in real-time, both non-activated and activated Tcon showed increased cAMP response after inhibiting PDE3 (Figure 16, 17). This repetitively observed result could be possibly attributed to strong

## Discussion

transcriptional repression of the *Pde3b* on a gene level mediated by Treg-specific marker FOXP3. Again, the same protocol was applied while performing live-cell imaging upon inhibition of PDE2A with BAY 60-7550 or PF-05180999. Interestingly, increased cAMP response was detected in activated Tcon compared to non-activated Tcon upon PDE2A inhibition, while Treg cells revealed lower FRET response to BAY stimulation (Figure 19). Provoking cAMP production via  $\beta$ -adrenergic receptor or adenosine receptor did not have a tremendous impact on inhibiting PDE2 activity (Figure 19, 20). Compared to PDE2A and PDE3B which are only members of their superfamily expressed in CD4<sup>+</sup> T cells, PDE4 has multiple isoforms expressed together with the fact that each isoform encodes for diverse variants. When Rolipram, as a global inhibitor was applied during FRET measurements, this could identify very high but comparable PDE4 activity upon inhibition among different non-activated and activated T cell subsets. Alternatively, the compartmentation of cAMP in T cells would be a crucial segment to study for a better understanding of downstream signaling events intervened by individual cAMP pools. Exact localization of specific ACs, AKAPs, PDEs, and PKAs during T cell activation could reveal information about directed cAMP responses. Main obstacle in conducting this experimental outlook would be the small T cell volume of primary cells which could be overcome in the future by improvements in super-resolution microscopy performance together with refinements in FRET-based biosensors whose bright signal and specific sensor targeting would allow more detailed information upon real-time measurements.

### 4.5 Regulation of cyclic nucleotide cross-talk in T cell subsets

Upon detected upregulation of PDE2A in activated Tcon, together with sustained expression level of PDE3B in both activated and non-activated Tcon, the next step in experimental plan was directed towards live-cell imaging of cAMP response after stimulation of cGMP generation within the T cell cytosol. Cyclic nucleotide cross-talk was analyzed before in cardiomyocytes via FRET, and there is a well-established protocol that was adopted for T cells also. The FRET protocol for studying cGMP/cAMP cross-talk in cardiomyocytes expressing Epac1-camps was tested in a TG mouse model expressing cytosolic Epac1-camps biosensor. FRET response was examined in cells that were stimulated with 100 nM ISO and upon reaching a stable baseline, 100 nM ANP or CNP was added. High concentrations of 10  $\mu$ M FSK and/or 100  $\mu$ M IBMX were used to achieve the maximal response of the sensor. Data analysis showed augmentation of cAMP response detected after consecutive stimulation with NPs. When cardiomyocytes were preincubated with 10  $\mu$ M CILO, FRET responses to NPs were showing less cAMP measured in comparison to the untreated group and demonstrated positive cGMP/cAMP cross-talk loop in cardiomyocytes which was dependent on PDE2 (Götz et al.



## Discussion

2014; Bork et al. 2021). Another example of cGMP/cAMP cross-talk was previously revealed in cardiomyocytes expressing Epac1-camps targeted to the plasma membrane to assess difference in PDE redistribution between healthy controls and mice that underwent transaortic constriction surgery (TAC). FRET protocol included 3 nM ISO, followed by 100 nM ANP and sensor saturation with FSK and IBMX. Key finding of that study was that ANP stimulation generated a small cAMP response in the control group compared to the TAC group due to the subcellular redistribution of crucial PDEs, PDE2A and PDE3, after early cardiac hypertrophy (Perera et al. 2015). Studying cross-talk between cGMP and cAMP, including remodeling of PDEs within the cell, has been a topic of significant interest for elucidating underlying mechanisms of cardiovascular diseases (Calamera et al. 2022). To test whether the redistribution of cGMP-sensitive PDEs have an impact on regulating cyclic nucleotide cross-talk in T cells, real-time measurement in non-activated and activated T cell subsets expressing cytosolic Epac1-camps sensor were performed. cAMP response was measured upon stimulation of T cells with 1  $\mu$ M ISO, and 200 nM ANP or 300 nM CNP were applied to increase cGMP with the cell. As mentioned earlier, FSK and IBMX were used to reach maximal FRET response of the biosensor. Upon stimulation of non-activated Tcon with NPs, positive values for FRET response could be measured corresponding to rise in cAMP, opposite to activated Tcon where cAMP response was diminished. No significant effect on changing FRET response after cGMP production induced via NPs was observed in Treg cells, regardless of activation status. Accordingly, PDE3 selective inhibitor, CILLO, reversed the FRET response in non-activated Tcon upon stimulation with NPs, and identical pattern was observed in activated Tcon after using PDE2A-specific inhibitor BAY (Figure 22). These data suggest that the upregulation of PDE2 on a protein level in activated Tcon promotes PDE2A activity in these cells but functional relevance of these findings has not been addressed in connection to T cell physiology until now. Simultaneously, gene expression of *Npr1* and *Npr2*, receptors for ANP/BNP and CNP, was assessed in murine CD4<sup>+</sup> T cells via qRT-PCR. Expression pattern was detected in both activated and non-activated T cells (Figure 21), which goes in the line with previous findings where *Npr1* expression was shown in naïve T cells derived from mouse spleen (Ma et al. 2013). Previously, importance of NP in the early stages of T cell development was examined in rat thymocytes after showing the expression of NP receptor on a gene level (*Npr1*, *Npr2*, and *Npr3*) via PCR and Northern blot. Next, cGMP increase after stimulation of thymic cells with ANP and CNP confirmed the functional relevance of these receptors via cGMP ELISA. However, stimulation of rat thymocytes with ANP but not CNP led to inhibition of the proliferation of mitogen-activated thymocytes (Vollmar, Schmidt, and Schulz 1996). Functional assays in murine CD4<sup>+</sup> T cells were performed in collaboration with A06 project partners from CRC1328 (Research group of Prof. Dr. Friesen). Since activation of TCR has been already reported to encourage a transient rise of cAMP levels within T cells, while a

## Discussion

sustained rise in cAMP abolish T cell proliferation, activation, and chemotaxis (K. Taskén and Stokka 2006) hypothesis was formed that stimulation with ANP will benefit higher T cell activation via cAMP hydrolysis mediated through PDE2A. Substantial increase in expression of early activation markers, CD25 and CD69, was reported *in vitro* after stimulation of CD4+ T cells with ANP in comparison to the non-treated group (Kurelic et al. 2021). Similarly, the functional aspect of NP stimulation was studied before in Th17 cells. Treatment of naïve CD4+ T cells derived from mouse spleen with ANP suppressed differentiation of Th17 cells and production of IL-17, respectively (Ma et al. 2013). *In vivo* study performed by the same research group on a mouse model of acute allergic asthma demonstrated augmented inflammatory cytokines production in the lung as well as an increased inflammatory response after stimulation with ANP. Effect was partially reversed after inhibiting the NPRA receptor by specific antagonist A71915 (Ma et al. 2015). To fully uncover the role of NP actions in T cell biology, additional functional assays are needed to be performed *in vitro* and *in vivo* for an adequate interpretation of its role in inflammation and autoimmunity.

### 4.6 Connection between Connexin 43 and cAMP transfer

Although the shift of cAMP between the cells was shown earlier via cAMP ELISA upon 16 hour co-culture of Treg and Tcon resulting in accumulation of cAMP in Tcon, dynamics of the intracellular cAMP transfer itself were never visualized in real-time. The same research group confirmed involvement of gap junction intracellular communication since Cx43 specific antagonizing peptide, GAP27, reduced transfer of calcein from calcein-loaded Treg to Tcon by 2-fold, while scrambled peptide used as a control revealed maintained level of calcein dye measured in Tcon (Bopp et al. 2007). Similar approach was conducted to confirm formation of GJIC between T cells and bone marrow-derived dendritic cells (BMDC), where an increase in calcein dye was observed upon co-culture of calcein-loaded Treg cells with DC or responder T cells while effect was reversed by using GAP27 (M. Weber et al. 2013). Expression of Cx43 was measured in this thesis via qRT-PCR, and relative expression level of *Gja1*, gene encoding for Cx43, was reported. There was no significant difference detected between non-activated and activated CD4+ T cell samples, although a tendency in expressing *Gja1* gene at a higher level in activated cells was observed (Figure 23). In the previous study, gene expression of Cx43 was confirmed in human T, B, and NK cells isolated from peripheral blood and tonsils (E. Oviedo-Orta, Hoy, and Evans 2000). Also, both FACS and ELISA analysis of Cx43 levels showed upregulation of activated human CD4+ T cells upon 24-48 hour-long culture with anti-CD3/CD28 compared to unstimulated T cells (Ernesto Oviedo-Orta et al. 2010). Expression of Cx43 was analyzed via qRT-PCR in murine T cell subsets by another group, before and after activation with anti-CD3. While in non-activated Tcon and Treg

## Discussion

expression was negligible, upon *in vitro* activation Cx43 levels were increased (Kuczma, Lee, and Kraj 2011). Next, immunofluorescent staining was performed in T cell subsets upon short-term (1 hour) co-culture of T cell subsets to mimic conditions similar to performing FRET. As a control membrane staining, anti-CD4 was used. Although Cx43 was expected to be localized exclusively at the plasma membrane upon cell contact, partially cytosolic staining was observed (Figure 25). As compared to previously shown data where Cx43 was accumulated in T cells at the contact site with e.g. magnetic beads coated with anti-CD3 and/or anti-CD28 (Mendoza-Naranjo et al. 2011), this leads to the conclusion that protocol used requires further improvements. Localization of Cx43 at the contact site was also shown via scanning ion conductance microscopy (SICM) and immunofluorescence in neonatal rat cardiomyocytes upon cell contact among second cardiomyocyte or myofibroblast (Schultz et al. 2019). In addition, previously established FRET imaging setup was adopted to measure cAMP response in activated Tcon upon the addition of another T cell subset, Tcon as control and Treg cells. Cells were further analyzed and subdivided into groups with or without established contact between Tcon measured and T cell added. This data suggested that cell-to-cell contact between activated Tcon and Treg cells results in a rise of cAMP compared to contact between Tcon-Tcon or when cell contact was lacking (Figure 24). Additional real-time measurements should be carried out in presence of a specific inhibitor for GJ (e.g. Cx43 mimetic peptides, GAP26 or GAP27) or adenosine receptors (e.g. antagonist for A<sub>2A</sub>R, Preladenant) to confirm wheater this discovery is due to gap junction intracellular communication or surrounding adenosine has also impact on increased FRET response upon Tcon-Treg cell contact. Since transfer of cAMP itself between pairs of interacting T cells has not been directly visualized until now, this could be a suitable approach to depict this process. Furthermore, importance of Cx43 hemichannels and GJs was also recognized in inflammatory disease pathogenesis. While gap junction intracellular communication is sought to be crucial for immune homeostasis, opened Cx hemichannels can result in membrane leaking and tissue damage due to inflammation, respectively. These findings were tested during ischemic injuries of brain and heart. In fetal sheep, at high gestation phase, blocking of Cx43 with a low concentration of peptide inhibitor (50-100  $\mu$ M Peptide 5) showed a neuroprotective effect during cerebral ischemia while 5 to 10-fold higher concentrations of Peptide 5 (500  $\mu$ M), sufficient to block GJIC, led to increased ischemic injury (P. Yang et al. 2020). In the context of the heart, where CxHC are opened during ischemia/hypoxia, treatment with mimetic peptides of Cx, e.g. GAP26, reduced the damage in the rat heart after ischemic injury (Hawat et al. 2010). It has been also shown that the formation of functional GJ can be established between immune and endothelial cells. This was confirmed by two-photon laser scanning microscopy in an experimental setup *in vitro* where endothelial cells were loaded with calcein dye. Upon migration on T cells across the endothelium, an increase in calcein dye was

## Discussion

detected as rise in green fluorescence, corresponding to T cell contact occurring with endothelial cells (Ernesto Oviedo-Orta and Howard Evans 2004). Since T cells, like other immune cells, are highly motile, they are couriers of information obtained through GJIC with multiple cells in residing tissue to other parts of the organism which allows them to prepare for adequate immune response by cell activation of expansions of specific T cell subsets (Neijssen, Pang, and Neefjes 2007). To sum up, despite comprehensive research in the last decades in elucidating function of Cx and GJs in the immune system, the underlying mechanisms of the cAMP transfer process are not yet been fully understood, and visualizing this process could be a step forward in gaining more knowledge.

### 4.7 Summary and Conclusion

In brief, differential cAMP levels in naïve murine T cell subsets were confirmed via cAMP immunoassay. Experimental plan was further focused on delineating the impact of individual protein/gene candidates on modulating cAMP level in diverse T cell subsets. Successful live-cell imaging via FRET was established in non-activated and activated T cells and further employed to study changes in cAMP dynamics in T cells on a single-cell level.

In summary, the first promising candidate, GPR52, showed elevated expression in Treg compared to Tcon, and upon activation of T cells, this was descending in Treg. Pharmacological manipulation of GPR52 by FTBMT in primary murine T cells resulted in elevated cAMP response in Treg vs. Tcon while activation of T cells led to comparable FRET response between subsets. On the other hand, inhibition of GPR52 by the antagonist drug, E7, clearly diminished cAMP response in both non-activated and activated T cells. Additional *in vitro* and *in vivo* experiments, led to the conclusion that GPR52 has a redundant role in T cell function and Treg-mediated immunosuppression as well.

A designed NanoString panel was utilized to acquire the gene expression level of diverse cAMP-relevant genes in non-activated T cell subsets, and an increase in *Pde1b* and *Pde2a* was detected in Treg while *Pde3b* and *Pde4d* were upregulated in Tcon. To further validate our tools immunoblotting analysis were next performed by exploring PDE3B, PDE4B, and PDE4D in T cell subsets. Immunoblotting revealed higher expression of PDE3B, PDE4B, and PDE4D in both active and non-activated Tcon, compared to Treg. While real-time measurements upon PDE4 inhibition by Rolipram did not result in change between T cell subsets of diverse activation status, inhibition of PDE3 via Cilostamide or Cilostazol demonstrated higher FRET response after PDE3 inhibition in Tcon vs. Treg. Strikingly, PDE2A was upregulated in activated Tcon compared to non-activated Tcon, while Treg cells showed

## Discussion

compared PDE2A expression before and after activation. Similarly, FRET imaging showed a higher rise in cAMP upon PDE2A inhibition with BAY 60-7550 in activated T con. This finding was further tested by stimulating T cells with agonists of particulate guanylyl cyclase (pGC), natriuretic peptides. Stimulation with NPs resulted in augmented cAMP levels in non-activated T cells opposite to the activated T cell response measured, which suggested the conversion of PDE3B-dependent positive to PDE2A-dependent negative cyclic nucleotide cross-talk. In summary, this mode of action is an interesting and novel finding in T cells whose impact could be further explored in T cell biology and its possible role in modulating inflammatory response in the immune system and heart.

Established live-cell imaging protocol was further used to investigate cAMP response in activated Tcon after cell contact between Treg or Tcon subsets. Interestingly, the addition of Treg and cell contact formation results in increased FRET response in activated Tcon compared to Tcon cells used as a negative control. This can be conceivably due to intracellular communication between cells enabled by gap junction formation and adenosine stimulation of adenosine receptors. This part of the project requires additional experiments to further explore the exact underlying mechanism behind observed cAMP increase.

Employing new techniques, such as live-cell imaging via FRET, together with traditional assays *in vitro* and *in vivo* assays performed in T cells is essential for identification and validation of possible novel targets, for solving the puzzle of underlying mechanisms of Treg-mediated suppression and immune responses occurring during inflammation.

### 5 Bibliography

Abrahamsen, Hilde, George Baillie, Jacob Ngai, Torkel Vang, Konstantina Nika, Anja Ruppelt, Tomas Mustelin, Manuela Zaccolo, Miles Houslay, and Kjetil Taskén. 2004. "TCR- and CD28-Mediated Recruitment of Phosphodiesterase 4 to Lipid Rafts Potentiates TCR Signaling." *Journal of Immunology (Baltimore, Md.: 1950)* 173 (8): 4847–58. <https://doi.org/10.4049/jimmunol.173.8.4847>.

Anandagoda, Nelomi, Joanna Cd Willis, Arnulf Hertweck, Luke B. Roberts, Ian Jackson, M. Refik Gökmen, Richard G. Jenner, Jane K. Howard, and Graham M. Lord. 2019. "MicroRNA-142-Mediated Repression of Phosphodiesterase 3B Critically Regulates Peripheral Immune Tolerance." *The Journal of Clinical Investigation* 129 (3): 1257–71. <https://doi.org/10.1172/JCI124725>.

Anton, Selma E., Charlotte Kayser, Isabella Maiellaro, Katarina Nemec, Jan Möller, Andreas Koschinski, Manuela Zaccolo, et al. 2022. "Receptor-Associated Independent CAMP Nanodomains Mediate Spatiotemporal Specificity of GPCR Signaling." *Cell* 185 (7): 1130–1142.e11. <https://doi.org/10.1016/j.cell.2022.02.011>.

Aranami, Toshimasa, and Takashi Yamamura. 2008. "Th17 Cells and Autoimmune Encephalomyelitis (EAE/MS)." *Allergology International: Official Journal of the Japanese Society of Allergology* 57 (2): 115–20. <https://doi.org/10.2332/allergolint.R-07-159>.

Ariazi, Jennifer, Andrew Benowitz, Vern De Biasi, Monique L. Den Boer, Stephanie Cherqui, Haifeng Cui, Nathalie Douillet, et al. 2017. "Tunneling Nanotubes and Gap Junctions—Their Role in Long-Range Intercellular Communication during Development, Health, and Disease Conditions." *Frontiers in Molecular Neuroscience* 10. <https://www.frontiersin.org/articles/10.3389/fnmol.2017.00333>.

Arp, Jacqueline, Mark G. Kirchhof, Miren L. Baroja, Steven H. Nazarian, Thu A. Chau, Craig A. Strathdee, Eric H. Ball, and Joaquín Madrenas. 2003. "Regulation of T-Cell Activation by Phosphodiesterase 4B2 Requires Its Dynamic Redistribution during Immunological Synapse Formation." *Molecular and Cellular Biology* 23 (22): 8042–57. <https://doi.org/10.1128/MCB.23.22.8042-8057.2003>.

Arumugham, Vijay Bharathi, and Cosima T. Baldari. 2017. "CAMP: A Multifaceted Modulator of Immune Synapse Assembly and T Cell Activation." *Journal of Leukocyte Biology* 101 (6): 1301–16. <https://doi.org/10.1189/jlb.2RU1116-474R>.

## Bibliography

- Axelrod, Sara, and Leonard Bielory. 2007. "Beta2-Agonists and Paresthesias in Multiple Sclerosis." *Annals of Allergy, Asthma & Immunology: Official Publication of the American College of Allergy, Asthma, & Immunology* 98 (1): 100. [https://doi.org/10.1016/S1081-1206\(10\)60871-X](https://doi.org/10.1016/S1081-1206(10)60871-X).
- Baillie, George S., Gonzalo S. Tejada, and Michy P. Kelly. 2019. "Therapeutic Targeting of 3',5'-Cyclic Nucleotide Phosphodiesterases: Inhibition and Beyond." *Nature Reviews. Drug Discovery* 18 (10): 770–96. <https://doi.org/10.1038/s41573-019-0033-4>.
- Baroja, M. L., L. B. Cieslinski, T. J. Torphy, R. L. Wange, and J. Madrenas. 1999. "Specific CD3 Epsilon Association of a Phosphodiesterase 4B Isoform Determines Its Selective Tyrosine Phosphorylation after CD3 Ligation." *Journal of Immunology (Baltimore, Md.: 1950)* 162 (4): 2016–23.
- Basole, Chaitali P., Rebecca K. Nguyen, Katie Lamothe, Puja Billis, Mai Fujiwara, Amanda G. Vang, Robert B. Clark, Paul M. Epstein, and Stefan Brocke. 2022. "Treatment of Experimental Autoimmune Encephalomyelitis with an Inhibitor of Phosphodiesterase-8 (PDE8)." *Cells* 11 (4): 660. <https://doi.org/10.3390/cells11040660>.
- Basole, Chaitali P., Rebecca K. Nguyen, Katie Lamothe, Amanda Vang, Robert Clark, George S. Baillie, Paul M. Epstein, and Stefan Brocke. 2017. "PDE8 Controls CD4+ T Cell Motility through the PDE8A-Raf-1 Kinase Signaling Complex." *Cellular Signalling* 40 (December): 62–72. <https://doi.org/10.1016/j.cellsig.2017.08.007>.
- Bazhin, Alexandr V., Sarah Kahnert, Silvia Kimpfler, Dirk Schadendorf, and Viktor Umansky. 2010. "Distinct Metabolism of Cyclic Adenosine Monophosphate in Regulatory and Helper CD4+ T Cells." *Molecular Immunology* 47 (4): 678–84. <https://doi.org/10.1016/j.molimm.2009.10.032>.
- Beavo, Joseph A., and Laurence L. Brunton. 2002. "Cyclic Nucleotide Research — Still Expanding after Half a Century." *Nature Reviews Molecular Cell Biology* 3 (9): 710–17. <https://doi.org/10.1038/nrm911>.
- Becker, Christian, Sabine Stoll, Tobias Bopp, Edgar Schmitt, and Helmut Jonuleit. 2006. "Regulatory T Cells: Present Facts and Future Hopes." *Medical Microbiology and Immunology* 195 (3): 113–24. <https://doi.org/10.1007/s00430-006-0017-y>.
- Bender, Andrew T., and Joseph A. Beavo. 2006. "Cyclic Nucleotide Phosphodiesterases: Molecular Regulation to Clinical Use." *Pharmacological Reviews* 58 (3): 488–520. <https://doi.org/10.1124/pr.58.3.5>.

## Bibliography

- Bermudez-Fajardo, Alexandra, Minna Ylihärsilä, W. Howard Evans, Andrew C. Newby, and Ernesto Oviedo-Orta. 2007. "CD4+ T Lymphocyte Subsets Express Connexin 43 and Establish Gap Junction Channel Communication with Macrophages in Vitro." *Journal of Leukocyte Biology* 82 (3): 608–12. <https://doi.org/10.1189/jlb.0307134>.
- Billington, Charlotte K., Oluwaseun O. Ojo, Raymond B. Penn, and Satoru Ito. 2013. "CAMP Regulation of Airway Smooth Muscle Function." *Pulmonary Pharmacology & Therapeutics* 26 (1): 112–20. <https://doi.org/10.1016/j.pupt.2012.05.007>.
- Bluestone, Jeffrey A., and Qizhi Tang. 2005. "How Do CD4+CD25+ Regulatory T Cells Control Autoimmunity?" *Current Opinion in Immunology* 17 (6): 638–42. <https://doi.org/10.1016/j.coi.2005.09.002>.
- Bock, Andreas, Paolo Annibale, Charlotte Konrad, Annette Hannawacker, Selma E. Anton, Isabella Maiellaro, Ulrike Zabel, Sivaraj Sivaramakrishnan, Martin Falcke, and Martin J. Lohse. 2020. "Optical Mapping of CAMP Signaling at the Nanometer Scale." *Cell* 182 (6): 1519–1530.e17. <https://doi.org/10.1016/j.cell.2020.07.035>.
- Boelhouwer, Eric, Jerry Davis, Ana Franco-Watkins, Nathan Dorris, and Claudiu Lungu. 2013. "Comprehension of Hazard Communication: Effects of Pictograms on Safety Data Sheets and Labels." *Journal of Safety Research* 46 (September): 145–55. <https://doi.org/10.1016/j.jsr.2013.06.001>.
- Bopp, Tobias, Christian Becker, Matthias Klein, Stefan Klein-Hessling, Alois Palmetshofer, Edgar Serfling, Valeska Heib, et al. 2007. "Cyclic Adenosine Monophosphate Is a Key Component of Regulatory T Cell-Mediated Suppression." *The Journal of Experimental Medicine* 204 (6): 1303–10. <https://doi.org/10.1084/jem.20062129>.
- Bopp, Tobias, Nina Dehzad, Sebastian Reuter, Matthias Klein, Nina Ullrich, Michael Stassen, Hansjörg Schild, Roland Buhl, Edgar Schmitt, and Christian Taube. 2009. "Inhibition of CAMP Degradation Improves Regulatory T Cell-Mediated Suppression." *Journal of Immunology (Baltimore, Md.: 1950)* 182 (7): 4017–24. <https://doi.org/10.4049/jimmunol.0803310>.
- Borea, Pier Andrea, Stefania Gessi, Stefania Merighi, Fabrizio Vincenzi, and Katia Varani. 2018. "Pharmacology of Adenosine Receptors: The State of the Art." *Physiological Reviews* 98 (3): 1591–1625. <https://doi.org/10.1152/physrev.00049.2017>.
- Bork, Nadja I., Anna Kuret, Melanie Cruz Santos, Cristina E. Molina, Beate Reiter, Hermann Reichenspurner, Andreas Friebe, et al. 2021. "Rise of CGMP by Partial Phosphodiesterase-



## Bibliography

3A Degradation Enhances Cardioprotection during Hypoxia.” *Redox Biology* 48 (December): 102179. <https://doi.org/10.1016/j.redox.2021.102179>.

Börner, Sebastian, Frank Schwede, Angela Schlipp, Filip Berisha, Davide Calebiro, Martin J. Lohse, and Viacheslav O. Nikolaev. 2011. “FRET Measurements of Intracellular CAMP Concentrations and CAMP Analog Permeability in Intact Cells.” *Nature Protocols* 6 (4): 427–38. <https://doi.org/10.1038/nprot.2010.198>.

Brooker, G., W. L. Terasaki, and M. G. Price. 1976. “Gammaflow: A Completely Automated Radioimmunoassay System.” *Science; (United States)* 194:4262 (October). <https://doi.org/10.1126/science.184530>.

Brunkow, M. E., E. W. Jeffery, K. A. Hjerrild, B. Paeper, L. B. Clark, S. A. Yasayko, J. E. Wilkinson, D. Galas, S. F. Ziegler, and F. Ramsdell. 2001. “Disruption of a New Forkhead/Winged-Helix Protein, Scurfin, Results in the Fatal Lymphoproliferative Disorder of the Scurfy Mouse.” *Nature Genetics* 27 (1): 68–73. <https://doi.org/10.1038/83784>.

Calamera, Gaia, Lise Román Moltzau, Finn Olav Levy, and Kjetil Wessel Andressen. 2022. “Phosphodiesterases and Compartmentation of CAMP and CGMP Signaling in Regulation of Cardiac Contractility in Normal and Failing Hearts.” *International Journal of Molecular Sciences* 23 (4): 2145. <https://doi.org/10.3390/ijms23042145>.

Calebiro, Davide, and Zsombor Koszegi. 2019. “The Subcellular Dynamics of GPCR Signaling.” *Molecular and Cellular Endocrinology* 483 (March): 24–30. <https://doi.org/10.1016/j.mce.2018.12.020>.

Calebiro, Davide, Viacheslav O. Nikolaev, Maria Cristina Gagliani, Tiziana de Filippis, Christian Dees, Carlo Tacchetti, Luca Persani, and Martin J. Lohse. 2009. “Persistent CAMP-Signals Triggered by Internalized G-Protein-Coupled Receptors.” *PLoS Biology* 7 (8): e1000172. <https://doi.org/10.1371/journal.pbio.1000172>.

Carlin, Leo M., Rachel Evans, Hanna Milewicz, Luis Fernandes, Daniel R. Matthews, Michela Perani, James Levitt, et al. 2011. “A Targeted SiRNA Screen Identifies Regulators of Cdc42 Activity at the Natural Killer Cell Immunological Synapse.” *Science Signaling* 4 (201): ra81. <https://doi.org/10.1126/scisignal.2001729>.

Coffman, R. L., and J. Carty. 1986. “A T Cell Activity That Enhances Polyclonal IgE Production and Its Inhibition by Interferon-Gamma.” *The Journal of Immunology* 136 (3): 949–54. <https://www.jimmunol.org/content/136/3/949>.

## Bibliography

- Collison, Lauren W., Creg J. Workman, Timothy T. Kuo, Kelli Boyd, Yao Wang, Kate M. Vignali, Richard Cross, David Sehy, Richard S. Blumberg, and Dario A. A. Vignali. 2007. "The Inhibitory Cytokine IL-35 Contributes to Regulatory T-Cell Function." *Nature* 450 (7169): 566–69. <https://doi.org/10.1038/nature06306>.
- Conche, Claire, Geneviève Boulla, Alain Trautmann, and Clotilde Randriamampita. 2009. "T Cell Adhesion Primes Antigen Receptor-Induced Calcium Responses through a Transient Rise in Adenosine 3',5'-Cyclic Monophosphate." *Immunity* 30 (1): 33–43. <https://doi.org/10.1016/j.immuni.2008.10.020>.
- Conti, M., and S. L. Jin. 1999. "The Molecular Biology of Cyclic Nucleotide Phosphodiesterases." *Progress in Nucleic Acid Research and Molecular Biology* 63: 1–38. [https://doi.org/10.1016/s0079-6603\(08\)60718-7](https://doi.org/10.1016/s0079-6603(08)60718-7).
- Conti, Marco, and Joseph Beavo. 2007. "Biochemistry and Physiology of Cyclic Nucleotide Phosphodiesterases: Essential Components in Cyclic Nucleotide Signaling." *Annual Review of Biochemistry* 76: 481–511. <https://doi.org/10.1146/annurev.biochem.76.060305.150444>.
- Coombes, Janine L., Karima R. R. Siddiqui, Carolina V. Arancibia-Cárcamo, Jason Hall, Cheng-Ming Sun, Yasmine Belkaid, and Fiona Powrie. 2007. "A Functionally Specialized Population of Mucosal CD103+ DCs Induces Foxp3+ Regulatory T Cells via a TGF-Beta and Retinoic Acid-Dependent Mechanism." *The Journal of Experimental Medicine* 204 (8): 1757–64. <https://doi.org/10.1084/jem.20070590>.
- Deaglio, Silvia, Karen M. Dwyer, Wenda Gao, David Friedman, Anny Usheva, Anna Erat, Jiang-Fan Chen, et al. 2007. "Adenosine Generation Catalyzed by CD39 and CD73 Expressed on Regulatory T Cells Mediates Immune Suppression." *The Journal of Experimental Medicine* 204 (6): 1257–65. <https://doi.org/10.1084/jem.20062512>.
- Direnberger, Stephan, Marsilius Mues, Vincenzo Micale, Carsten T. Wotjak, Steffen Dietzel, Michael Schubert, Andreas Scharr, et al. 2012. "Biocompatibility of a Genetically Encoded Calcium Indicator in a Transgenic Mouse Model." *Nature Communications* 3: 1031. <https://doi.org/10.1038/ncomms2035>.
- Dong, Hongli, Christof Zitt, Cornelia Auriga, Armin Hatzelmann, and Paul M. Epstein. 2010. "Inhibition of PDE3, PDE4 and PDE7 Potentiates Glucocorticoid-Induced Apoptosis and Overcomes Glucocorticoid Resistance in CEM T Leukemic Cells." *Biochemical Pharmacology* 79 (3): 321–29. <https://doi.org/10.1016/j.bcp.2009.09.001>.

## Bibliography

Doulatov, Sergei, Faiyaz Notta, Kolja Eppert, Linh T. Nguyen, Pamela S. Ohashi, and John E. Dick. 2010. "Revised Map of the Human Progenitor Hierarchy Shows the Origin of Macrophages and Dendritic Cells in Early Lymphoid Development." *Nature Immunology* 11 (7): 585–93. <https://doi.org/10.1038/ni.1889>.

Duan, Biyan, Richard Davis, Eva L. Sadat, Julie Collins, Paul C. Sternweis, Dorothy Yuan, and Lily I. Jiang. 2010. "Distinct Roles of Adenylyl Cyclase VII in Regulating the Immune Responses in Mice." *Journal of Immunology* 185 (1): 335–44. <https://doi.org/10.4049/jimmunol.0903474>.

Dustin, Michael L. 2014. "The Immunological Synapse." *Cancer Immunology Research* 2 (11): 1023–33. <https://doi.org/10.1158/2326-6066.CIR-14-0161>.

Epstein, Paul M., Chaitali Basole, and Stefan Brocke. 2021. "The Role of PDE8 in T Cell Recruitment and Function in Inflammation." *Frontiers in Cell and Developmental Biology* 9: 636778. <https://doi.org/10.3389/fcell.2021.636778>.

Erdogan, S., and M. D. Houslay. 1997. "Challenge of Human Jurkat T-Cells with the Adenylate Cyclase Activator Forskolin Elicits Major Changes in CAMP Phosphodiesterase (PDE) Expression by up-Regulating PDE3 and Inducing PDE4D1 and PDE4D2 Splice Variants as Well as down-Regulating a Novel PDE4A Splice Variant." *The Biochemical Journal* 321 ( Pt 1) (January): 165–75. <https://doi.org/10.1042/bj3210165>.

Ernst, Peter B., James C. Garrison, and Linda F. Thompson. 2010. "Much Ado about Adenosine: Adenosine Synthesis and Function in Regulatory T Cell Biology." *Journal of Immunology* (Baltimore, Md. : 1950) 185 (4): 1993–98. <https://doi.org/10.4049/jimmunol.1000108>.

Essayan, David M. 2001. "Cyclic Nucleotide Phosphodiesterases." *Journal of Allergy and Clinical Immunology* 108 (5): 671–80. <https://doi.org/10.1067/mai.2001.119555>.

Feng, Gang, Satish N. Nadig, Liselotte Bäckdahl, Stephan Beck, Ross S. Francis, Alexandru Schiopu, Andrew Whatcott, Kathryn J. Wood, and Andrew Bushell. 2011. "Functional Regulatory T Cells Produced by Inhibiting Cyclic Nucleotide Phosphodiesterase Type 3 Prevent Allograft Rejection." *Science Translational Medicine* 3 (83): 83ra40. <https://doi.org/10.1126/scitranslmed.3002099>.

Fontenot, Jason D., Jeffrey P. Rasmussen, Luke M. Williams, James L. Dooley, Andrew G. Farr, and Alexander Y. Rudensky. 2005. "Regulatory T Cell Lineage Specification by the

## Bibliography

Forkhead Transcription Factor Foxp3." *Immunity* 22 (3): 329–41. <https://doi.org/10.1016/j.immuni.2005.01.016>.

Foord, Steven M., Tom I. Bonner, Richard R. Neubig, Edward M. Rosser, Jean-Phillipe Pin, Anthony P. Davenport, Michael Spedding, and Anthony J. Harmar. 2005. "International Union of Pharmacology. XLVI. G Protein-Coupled Receptor List." *Pharmacological Reviews* 57 (2): 279–88. <https://doi.org/10.1124/pr.57.2.5>.

Förster, Th. 1948. "Zwischenmolekulare Energiewanderung und Fluoreszenz." *Annalen der Physik* 437 (1–2): 55–75. <https://doi.org/10.1002/andp.19484370105>.

Francis, Sharron H., Mitsi A. Blount, and Jackie D. Corbin. 2011. "Mammalian Cyclic Nucleotide Phosphodiesterases: Molecular Mechanisms and Physiological Functions." *Physiological Reviews* 91 (2): 651–90. <https://doi.org/10.1152/physrev.00030.2010>.

Fredriksson, Robert, Malin C. Lagerström, Lars-Gustav Lundin, and Helgi B. Schiöth. 2003. "The G-Protein-Coupled Receptors in the Human Genome Form Five Main Families. Phylogenetic Analysis, Paralogon Groups, and Fingerprints." *Molecular Pharmacology* 63 (6): 1256–72. <https://doi.org/10.1124/mol.63.6.1256>.

Fus-Kujawa, Agnieszka, Pawel Prus, Karolina Bajdak-Rusinek, Paulina Teper, Katarzyna Gawron, Agnieszka Kowalczyk, and Aleksander L. Sieron. 2021. "An Overview of Methods and Tools for Transfection of Eukaryotic Cells in Vitro." *Frontiers in Bioengineering and Biotechnology* 9. <https://www.frontiersin.org/articles/10.3389/fbioe.2021.701031>.

Gajewski, T. F., and F. W. Fitch. 1988. "Anti-Proliferative Effect of IFN-Gamma in Immune Regulation. I. IFN-Gamma Inhibits the Proliferation of Th2 but Not Th1 Murine Helper T Lymphocyte Clones." *Journal of Immunology (Baltimore, Md.: 1950)* 140 (12): 4245–52.

Gavin, Marc A., Jeffrey P. Rasmussen, Jason D. Fontenot, Valeria Vasta, Vincent C. Manganiello, Joseph A. Beavo, and Alexander Y. Rudensky. 2007. "Foxp3-Dependent Programme of Regulatory T-Cell Differentiation." *Nature* 445 (7129): 771–75. <https://doi.org/10.1038/nature05543>.

Germain, Ronald N. 2002. "T-Cell Development and the CD4–CD8 Lineage Decision." *Nature Reviews Immunology* 2 (5): 309–22. <https://doi.org/10.1038/nri798>.

Getnet, Derese, Joseph F. Grosso, Monica V. Goldberg, Timothy J. Harris, Hung-Rong Yen, Tullia C. Bruno, Nicholas M. Durham, et al. 2010. "A Role for the Transcription Factor Helios

## Bibliography

in Human CD4(+)CD25(+) Regulatory T Cells.” *Molecular Immunology* 47 (7–8): 1595–1600. <https://doi.org/10.1016/j.molimm.2010.02.001>.

Ghani, Saeed, Markus Feuerer, Cornelia Doebis, Uta Lauer, Christoph Loddenkemper, Jochen Huehn, Alf Hamann, and Uta Syrbe. 2009. “T Cells as Pioneers: Antigen-Specific T Cells Condition Inflamed Sites for High-Rate Antigen-Non-Specific Effector Cell Recruitment.” *Immunology* 128 (1 Suppl): e870-880. <https://doi.org/10.1111/j.1365-2567.2009.03096.x>.

Glavas, N. A., C. Ostenson, J. B. Schaefer, V. Vasta, and J. A. Beavo. 2001. “T Cell Activation Up-Regulates Cyclic Nucleotide Phosphodiesterases 8A1 and 7A3.” *Proceedings of the National Academy of Sciences of the United States of America* 98 (11): 6319–24. <https://doi.org/10.1073/pnas.101131098>.

Godfrey, D. I., J. Kennedy, T. Suda, and A. Zlotnik. 1993. “A Developmental Pathway Involving Four Phenotypically and Functionally Distinct Subsets of CD3-CD4-CD8- Triple-Negative Adult Mouse Thymocytes Defined by CD44 and CD25 Expression.” *Journal of Immunology (Baltimore, Md.: 1950)* 150 (10): 4244–52.

Gondek, David C., Li-Fan Lu, Sergio A. Quezada, Shimon Sakaguchi, and Randolph J. Noelle. 2005. “Cutting Edge: Contact-Mediated Suppression by CD4+CD25+ Regulatory Cells Involves a Granzyme B-Dependent, Perforin-Independent Mechanism.” *Journal of Immunology (Baltimore, Md.: 1950)* 174 (4): 1783–86. <https://doi.org/10.4049/jimmunol.174.4.1783>.

Goodenough, D. A., J. A. Goliger, and D. L. Paul. 1996. “Connexins, Connexons, and Intercellular Communication.” *Annual Review of Biochemistry* 65: 475–502. <https://doi.org/10.1146/annurev.bi.65.070196.002355>.

Götz, Konrad R., Julia U. Sprenger, Ruwan K. Perera, Julia H. Steinbrecher, Stephan E. Lehnart, Michaela Kuhn, Julia Gorelik, Jean-Luc Balligand, and Viacheslav O. Nikolaev. 2014. “Transgenic Mice for Real-Time Visualization of CGMP in Intact Adult Cardiomyocytes.” *Circulation Research* 114 (8): 1235–45. <https://doi.org/10.1161/CIRCRESAHA.114.302437>.

Gouirand, Victoire, Ireneusz Habrylo, and Michael D. Rosenblum. 2022. “Regulatory T Cells and Inflammatory Mediators in Autoimmune Disease.” *The Journal of Investigative Dermatology* 142 (3 Pt B): 774–80. <https://doi.org/10.1016/j.jid.2021.05.010>.

Gowans, J. L., and E. J. Knight. 1964. “THE ROUTE OF RE-CIRCULATION OF LYMPHOCYTES IN THE RAT.” *Proceedings of the Royal Society of London. Series B, Biological Sciences* 159 (January): 257–82. <https://doi.org/10.1098/rspb.1964.0001>.

## Bibliography

- Guereschi, Marcia G., Leandro P. Araujo, Juliana T. Maricato, Maisa C. Takenaka, Vanessa M. Nascimento, Bruno C. Vivanco, Vanessa O. Reis, Alexandre C. Keller, Patrícia C. Brum, and Alexandre S. Basso. 2013. "Beta2-Adrenergic Receptor Signaling in CD4<sup>+</sup> Foxp3<sup>+</sup> Regulatory T Cells Enhances Their Suppressive Function in a PKA-Dependent Manner." *European Journal of Immunology* 43 (4): 1001–12. <https://doi.org/10.1002/eji.201243005>.
- Hall, Bruce M. 2015. "T Cells: Soldiers and Spies--The Surveillance and Control of Effector T Cells by Regulatory T Cells." *Clinical Journal of the American Society of Nephrology: CJASN* 10 (11): 2050–64. <https://doi.org/10.2215/CJN.06620714>.
- Harding, F. A., J. G. McArthur, J. A. Gross, D. H. Raulet, and J. P. Allison. 1992. "CD28-Mediated Signalling Co-Stimulates Murine T Cells and Prevents Induction of Anergy in T-Cell Clones." *Nature* 356 (6370): 607–9. <https://doi.org/10.1038/356607a0>.
- Hawat, Ghayda, Mohamed Benderdour, Guy Rousseau, and Ghayath Baroudi. 2010. "Connexin 43 Mimetic Peptide Gap26 Confers Protection to Intact Heart against Myocardial Ischemia Injury." *Pflugers Archiv: European Journal of Physiology* 460 (3): 583–92. <https://doi.org/10.1007/s00424-010-0849-6>.
- Hilger, Daniel, Matthieu Masureel, and Brian K. Kobilka. 2018. "Structure and Dynamics of GPCR Signaling Complexes." *Nature Structural & Molecular Biology* 25 (1): 4–12. <https://doi.org/10.1038/s41594-017-0011-7>.
- Houslay, Miles D., George S. Baillie, and Donald H. Maurice. 2007. "CAMP-Specific Phosphodiesterase-4 Enzymes in the Cardiovascular System: A Molecular Toolbox for Generating Compartmentalized CAMP Signaling." *Circulation Research* 100 (7): 950–66. <https://doi.org/10.1161/01.RES.0000261934.56938.38>.
- Huang, Bo, Jie Zhao, Zhang Lei, Shiqian Shen, Dong Li, Guan-Xin Shen, Gui-Mei Zhang, and Zuo-Hua Feng. 2009. "MiR-142-3p Restricts CAMP Production in CD4<sup>+</sup>CD25<sup>–</sup> T Cells and CD4<sup>+</sup>CD25<sup>+</sup> TREG Cells by Targeting AC9 mRNA." *EMBO Reports* 10 (2): 180–85. <https://doi.org/10.1038/embor.2008.224>.
- Huang, S., S. Apasov, M. Koshiba, and M. Sitkovsky. 1997. "Role of A2a Extracellular Adenosine Receptor-Mediated Signaling in Adenosine-Mediated Inhibition of T-Cell Activation and Expansion." *Blood* 90 (4): 1600–1610.
- Hübscher, Daniela, and Viacheslav O. Nikolaev. 2015. "Generation of Transgenic Mice Expressing FRET Biosensors." *Methods in Molecular Biology (Clifton, N.J.)* 1294: 117–29. [https://doi.org/10.1007/978-1-4939-2537-7\\_9](https://doi.org/10.1007/978-1-4939-2537-7_9).

## Bibliography

- Hyun, Young-Min, Hung-Li Chung, James L. McGrath, Richard E. Waugh, and Minsoo Kim. 2009. "Activated Integrin VLA-4 Localizes to the Lamellipodia and Mediates T Cell Migration on VCAM-1." *Journal of Immunology (Baltimore, Md.: 1950)* 183 (1): 359–69. <https://doi.org/10.4049/jimmunol.0803388>.
- Ingwersen, J., B. Wingerath, J. Graf, K. Lepka, M. Hofrichter, F. Schröter, F. Wedekind, et al. 2016. "Dual Roles of the Adenosine A2a Receptor in Autoimmune Neuroinflammation." *Journal of Neuroinflammation* 13 (February): 48. <https://doi.org/10.1186/s12974-016-0512-z>.
- Jiang, Lily I., Julie Collins, Richard Davis, Iain D. Fraser, and Paul C. Sternweis. 2008. "Regulation of CAMP Responses by the G12/13 Pathway Converges on Adenylyl Cyclase VII." *The Journal of Biological Chemistry* 283 (34): 23429–39. <https://doi.org/10.1074/jbc.M803281200>.
- Josefowicz, Steven Z., and Alexander Rudensky. 2009. "Control of Regulatory T Cell Lineage Commitment and Maintenance." *Immunity* 30 (5): 616–25. <https://doi.org/10.1016/j.immuni.2009.04.009>.
- Juilfs, D. M., S. Soderling, F. Burns, and J. A. Beavo. 1999. "Cyclic GMP as Substrate and Regulator of Cyclic Nucleotide Phosphodiesterases (PDEs)." In *Reviews of Physiology, Biochemistry and Pharmacology, Volume 135*, 67–104. Reviews of Physiology, Biochemistry and Pharmacology. Berlin, Heidelberg: Springer. <https://doi.org/10.1007/BFb0033670>.
- Kamenetsky, Margarita, Sabine Middelhaufe, Erin M. Bank, Lonny R. Levin, Jochen Buck, and Clemens Steegborn. 2006. "Molecular Details of CAMP Generation in Mammalian Cells: A Tale of Two Systems." *Journal of Molecular Biology* 362 (4): 623–39. <https://doi.org/10.1016/j.jmb.2006.07.045>.
- Kanda, Naoko, and Shinichi Watanabe. 2001. "Regulatory Roles of Adenylate Cyclase and Cyclic Nucleotide Phosphodiesterases 1 and 4 in Interleukin-13 Production by Activated Human T Cells." *Biochemical Pharmacology* 62 (4): 495–507. [https://doi.org/10.1016/S0006-2952\(01\)00688-8](https://doi.org/10.1016/S0006-2952(01)00688-8).
- Kandel, Eric R. 2012. "The Molecular Biology of Memory: CAMP, PKA, CRE, CREB-1, CREB-2, and CPEB." *Molecular Brain* 5 (1): 14. <https://doi.org/10.1186/1756-6606-5-14>.
- Kaplan, M. H., and M. J. Grusby. 1998. "Regulation of T Helper Cell Differentiation by STAT Molecules." *Journal of Leukocyte Biology* 64 (1): 2–5. <https://doi.org/10.1002/jlb.64.1.2>.

## Bibliography

Khan, Uqba, and Hareem Ghazanfar. 2018. "T Lymphocytes and Autoimmunity." *International Review of Cell and Molecular Biology* 341: 125–68. <https://doi.org/10.1016/bs.ircmb.2018.05.008>.

Klarenbeek, Jeffrey, Joachim Goedhart, Aernoud van Batenburg, Daniella Groenewald, and Kees Jalink. 2015. "Fourth-Generation Epac-Based FRET Sensors for CAMP Feature Exceptional Brightness, Photostability and Dynamic Range: Characterization of Dedicated Sensors for FLIM, for Ratiometry and with High Affinity." *PLOS ONE* 10 (4): e0122513. <https://doi.org/10.1371/journal.pone.0122513>.

Klein, Matthias, and Tobias Bopp. 2016. "Cyclic AMP Represents a Crucial Component of Treg Cell-Mediated Immune Regulation." *Frontiers in Immunology* 7: 315. <https://doi.org/10.3389/fimmu.2016.00315>.

Komatsu, Hidetoshi, Minoru Maruyama, Shuuhei Yao, Tokuyuki Shinohara, Kensuke Sakuma, Sachiko Imaichi, Tomoko Chikatsu, et al. 2014. "Anatomical Transcriptome of G Protein-Coupled Receptors Leads to the Identification of a Novel Therapeutic Candidate GPR52 for Psychiatric Disorders." *PLOS ONE* 9 (2): e90134. <https://doi.org/10.1371/journal.pone.0090134>.

Krieg, Paula F., Jana K. Sonner, Roberta Kurelic, Jan Broder Engler, Marlena F. Scharenberg, Simone Bauer, Viacheslav O. Nikolaev, and Manuel A. Friese. 2022. "GPR52 Regulates CAMP in T Cells but Is Dispensable for Encephalitogenic Responses." *Frontiers in Immunology* 13: 1113348. <https://doi.org/10.3389/fimmu.2022.1113348>.

Krumm, Brian, and Bryan L. Roth. 2020. "A Self-Activating Orphan Receptor." *Nature* 579 (7797): 35–36. <https://doi.org/10.1038/d41586-020-00411-y>.

Krupinski, John, Françoise Coussen, Heather A. Bakalyar, Wei-Jen Tang, Paul G. Feinstein, Kim Orth, Clive Slaughter, Randall R. Reed, and Alfred G. Gilman. 1989. "Adenylyl Cyclase Amino Acid Sequence: Possible Channel- or Transporter-Like Structure." *Science* 244 (4912): 1558–64. <https://doi.org/10.1126/science.2472670>.

Kuczma, Michal, Jeffrey R. Lee, and Piotr Kraj. 2011. "Connexin 43 Signaling Enhances the Generation of Foxp3+ Regulatory T Cells." *Journal of Immunology (Baltimore, Md.: 1950)* 187 (1): 248–57. <https://doi.org/10.4049/jimmunol.1003785>.

Kuczma, Michal, Cong-Yi Wang, Leszek Ignatowicz, Robert Gourdie, and Piotr Kraj. 2015. "Altered Connexin 43 Expression Underlies Age-Dependent Decrease of Regulatory T Cell



## Bibliography

Suppressor Function in Nonobese Diabetic Mice.” *Journal of Immunology (Baltimore, Md.: 1950)* 194 (11): 5261–71. <https://doi.org/10.4049/jimmunol.1400887>.

Kuhn, Michaela. 2016. “Molecular Physiology of Membrane Guanylyl Cyclase Receptors.” *Physiological Reviews* 96 (2): 751–804. <https://doi.org/10.1152/physrev.00022.2015>.

Kurelic, Roberta, Paula F. Krieg, Jana K. Sonner, Gloria Bhaiyan, Gustavo C. Ramos, Stefan Frantz, Manuel A. Friese, and Viacheslav O. Nikolaev. 2021. “Upregulation of Phosphodiesterase 2A Augments T Cell Activation by Changing CGMP/CAMP Cross-Talk.” *Frontiers in Pharmacology* 12: 748798. <https://doi.org/10.3389/fphar.2021.748798>.

Lahl, Katharina, Christoph Loddenkemper, Cathy Drouin, Jennifer Freyer, Jon Arnason, Gérard Eberl, Alf Hamann, Hermann Wagner, Jochen Huehn, and Tim Sparwasser. 2007. “Selective Depletion of Foxp3+ Regulatory T Cells Induces a Scurfy-like Disease.” *The Journal of Experimental Medicine* 204 (1): 57–63. <https://doi.org/10.1084/jem.20061852>.

Laird, Dale W., and Paul D. Lampe. 2018. “Therapeutic Strategies Targeting Connexins.” *Nature Reviews. Drug Discovery* 17 (12): 905–21. <https://doi.org/10.1038/nrd.2018.138>.

Lakowicz, Joseph R. 1999. “Introduction to Fluorescence.” In *Principles of Fluorescence Spectroscopy*, edited by Joseph R. Lakowicz, 1–23. Boston, MA: Springer US. [https://doi.org/10.1007/978-1-4757-3061-6\\_1](https://doi.org/10.1007/978-1-4757-3061-6_1).

Landells, L. J., C. M. Szilagy, N. A. Jones, K. H. Banner, J. M. Allen, A. Doherty, B. J. O'Connor, D. Spina, and C. P. Page. 2001. “Identification and Quantification of Phosphodiesterase 4 Subtypes in CD4 and CD8 Lymphocytes from Healthy and Asthmatic Subjects.” *British Journal of Pharmacology* 133 (5): 722–29. <https://doi.org/10.1038/sj.bjp.0704120>.

Lappas, Courtney M., Jayson M. Rieger, and Joel Linden. 2005. “A2A Adenosine Receptor Induction Inhibits IFN-Gamma Production in Murine CD4+ T Cells.” *Journal of Immunology (Baltimore, Md.: 1950)* 174 (2): 1073–80. <https://doi.org/10.4049/jimmunol.174.2.1073>.

Li, L., C. Yee, and J. A. Beavo. 1999. “CD3- and CD28-Dependent Induction of PDE7 Required for T Cell Activation.” *Science (New York, N.Y.)* 283 (5403): 848–51. <https://doi.org/10.1126/science.283.5403.848>.

Lighvani, A. A., D. M. Frucht, D. Jankovic, H. Yamane, J. Aliberti, B. D. Hissong, B. V. Nguyen, et al. 2001. “T-Bet Is Rapidly Induced by Interferon-Gamma in Lymphoid and Myeloid Cells.”

## Bibliography

*Proceedings of the National Academy of Sciences of the United States of America* 98 (26): 15137–42. <https://doi.org/10.1073/pnas.261570598>.

Liston, Adrian, and Daniel H. D. Gray. 2014. “Homeostatic Control of Regulatory T Cell Diversity.” *Nature Reviews. Immunology* 14 (3): 154–65. <https://doi.org/10.1038/nri3605>.

Lohse, Martin J., Stefan Engelhardt, and Thomas Eschenhagen. 2003. “What Is the Role of  $\beta$ -Adrenergic Signaling in Heart Failure?” *Circulation Research* 93 (10): 896–906. <https://doi.org/10.1161/01.RES.0000102042.83024.CA>.

Lorton, Dianne, and Denise L Bellinger. 2015. “Sympathetic Nervous System Regulation of Th Cells in Autoimmunity: Beyond Th1 and Th2 Cell Balance” 6 (5): 23.

Lu, Li-Fan, Marc A. Gavin, Jeffrey P. Rasmussen, and Alexander Y. Rudensky. 2007. “G Protein-Coupled Receptor 83 Is Dispensable for the Development and Function of Regulatory T Cells.” *Molecular and Cellular Biology* 27 (23): 8065–72. <https://doi.org/10.1128/MCB.01075-07>.

Lubahn, Cheri L., Dianne Lorton, Jill A. Schaller, Sarah J. Sweeney, and Denise L. Bellinger. 2014. “Targeting  $\alpha$ - and  $\beta$ -Adrenergic Receptors Differentially Shifts Th1, Th2, and Inflammatory Cytokine Profiles in Immune Organs to Attenuate Adjuvant Arthritis.” *Frontiers in Immunology* 5. <https://www.frontiersin.org/articles/10.3389/fimmu.2014.00346>.

Lyga, Sandra, Silvia Volpe, Ruth C. Werthmann, Konrad Götz, Titiwat Sungkaworn, Martin J. Lohse, and Davide Calebiro. 2016. “Persistent CAMP Signaling by Internalized LH Receptors in Ovarian Follicles.” *Endocrinology* 157 (4): 1613–21. <https://doi.org/10.1210/en.2015-1945>.

Ma, Libing, Jinxiu Li, Guyi Wang, Subo Gong, Li Zhang, Keng Li, Xiaoying Ji, Yi Liu, Ping Chen, and Xudong Xiang. 2013. “Atrial Natriuretic Peptide Suppresses Th17 Development through Regulation of CGMP-Dependent Protein Kinase and PI3K-Akt Signaling Pathways.” *Regulatory Peptides* 181 (February): 9–16. <https://doi.org/10.1016/j.regpep.2012.12.003>.

Ma, Libing, Jinrong Zeng, Biwen Mo, Changming Wang, Yabing Sun, Meng Zhang, Shaokun Liu, Xudong Xiang, and Cong-Yi Wang. 2015. “ANP/NPRA Signaling Preferentially Mediates Th2 Responses in Favor of Pathological Processes during the Course of Acute Allergic Asthma.” *International Journal of Clinical and Experimental Medicine* 8 (4): 5121–28.

Martinez, Gustavo J., Roza I. Nurieva, Xuexian O. Yang, and Chen Dong. 2008. “Regulation and Function of Proinflammatory TH17 Cells.” *Annals of the New York Academy of Sciences* 1143 (November): 188–211. <https://doi.org/10.1196/annals.1443.021>.

## Bibliography

- Martins, T. J., M. C. Mumby, and J. A. Beavo. 1982. "Purification and Characterization of a Cyclic GMP-Stimulated Cyclic Nucleotide Phosphodiesterase from Bovine Tissues." *Journal of Biological Chemistry* 257 (4): 1973–79. [https://doi.org/10.1016/S0021-9258\(19\)68134-2](https://doi.org/10.1016/S0021-9258(19)68134-2).
- Massengill, Crystian I., Landon Bayless-Edwards, Cesar C. Ceballos, Elizabeth R. Cebul, Maozhen Qin, Matthew R. Whorton, Bing Ye, Tianyi Mao, and Haining Zhong. 2021. "Highly Sensitive Genetically-Encoded Sensors for Population and Subcellular Imaging of cAMP in Vivo." *bioRxiv*. <https://doi.org/10.1101/2021.08.27.457999>.
- Mendoza-Naranjo, Ariadna, Gerben Bouma, Cristián Pereda, Marcos Ramírez, Kevin F. Webb, Andrés Tittarelli, Mercedes N. López, et al. 2011. "Functional Gap Junctions Accumulate at the Immunological Synapse and Contribute to T Cell Activation." *Journal of Immunology (Baltimore, Md.: 1950)* 187 (6): 3121–32. <https://doi.org/10.4049/jimmunol.1100378>.
- Michie, A. M., M. Lobban, T. Müller, M. M. Harnett, and M. D. Houslay. 1996. "Rapid Regulation of PDE-2 and PDE-4 Cyclic AMP Phosphodiesterase Activity Following Ligation of the T Cell Antigen Receptor on Thymocytes: Analysis Using the Selective Inhibitors Erythro-9-(2-Hydroxy-3-Nonyl)-Adenine (EHNA) and Rolipram." *Cellular Signalling* 8 (2): 97–110. [https://doi.org/10.1016/0898-6568\(95\)02032-2](https://doi.org/10.1016/0898-6568(95)02032-2).
- Mosmann, T. R., H. Cherwinski, M. W. Bond, M. A. Giedlin, and R. L. Coffman. 1986. "Two Types of Murine Helper T Cell Clone. I. Definition According to Profiles of Lymphokine Activities and Secreted Proteins." *Journal of Immunology (Baltimore, Md.: 1950)* 136 (7): 2348–57.
- Murphy, Kenneth. 2014. *Janeway's Immunobiology*. 8th edition. Place of publication not identified: Garland Science.
- Nadeem, Ahmed, Ming Fan, Habib R. Ansari, Catherine Ledent, and S. Jamal Mustafa. 2007. "Enhanced Airway Reactivity and Inflammation in A2A Adenosine Receptor-Deficient Allergic Mice." *American Journal of Physiology. Lung Cellular and Molecular Physiology* 292 (6): L1335-1344. <https://doi.org/10.1152/ajplung.00416.2006>.
- Neijssen, Joost, Baoxu Pang, and Jacques Neefjes. 2007. "Gap Junction-Mediated Intercellular Communication in the Immune System." *Progress in Biophysics and Molecular Biology* 94 (1–2): 207–18. <https://doi.org/10.1016/j.pbiomolbio.2007.03.008>.
- Neves, Susana R., Prahlad T. Ram, and Ravi Iyengar. 2002. "G Protein Pathways." *Science (New York, N.Y.)* 296 (5573): 1636–39. <https://doi.org/10.1126/science.1071550>.

## Bibliography

Nielsen, Morten Schak, Lene Nygaard Axelsen, Paul L. Sorgen, Vandana Verma, Mario Delmar, and Niels-Henrik Holstein-Rathlou. 2012. "Gap Junctions." *Comprehensive Physiology* 2 (3): 1981–2035. <https://doi.org/10.1002/cphy.c110051>.

Nikolaev, Viacheslav O., Moritz Bünemann, Lutz Hein, Annette Hannawacker, and Martin J. Lohse. 2004. "Novel Single Chain CAMP Sensors for Receptor-Induced Signal Propagation." *The Journal of Biological Chemistry* 279 (36): 37215–18. <https://doi.org/10.1074/jbc.C400302200>.

Nikolaev, Viacheslav O., Moritz Bünemann, Eva Schmitteckert, Martin J. Lohse, and Stefan Engelhardt. 2006. "Cyclic AMP Imaging in Adult Cardiac Myocytes Reveals Far-Reaching Beta1-Adrenergic but Locally Confined Beta2-Adrenergic Receptor-Mediated Signaling." *Circulation Research* 99 (10): 1084–91. <https://doi.org/10.1161/01.RES.0000250046.69918.d5>.

Nikolaev, Viacheslav O., and Martin J. Lohse. 2006. "Monitoring of CAMP Synthesis and Degradation in Living Cells." *Physiology* 21 (2): 86–92. <https://doi.org/10.1152/physiol.00057.2005>.

Nikolaev, Viacheslav O., Alexey Moshkov, Alexander R. Lyon, Michele Miragoli, Pavel Novak, Helen Paur, Martin J. Lohse, Yuri E. Korchev, Sian E. Harding, and Julia Gorelik. 2010. "B2-Adrenergic Receptor Redistribution in Heart Failure Changes CAMP Compartmentation." *Science* 327 (5973): 1653–57. <https://doi.org/10.1126/science.1185988>.

Nishiyama, Keiji, Hirobumi Suzuki, Toshiya Harasawa, Noriko Suzuki, Emi Kurimoto, Takayuki Kawai, Minoru Maruyama, et al. 2017. "FTBMT, a Novel and Selective GPR52 Agonist, Demonstrates Antipsychotic-Like and Procognitive Effects in Rodents, Revealing a Potential Therapeutic Agent for Schizophrenia." *The Journal of Pharmacology and Experimental Therapeutics* 363 (2): 253–64. <https://doi.org/10.1124/jpet.117.242925>.

Nishiyama, Keiji, Hirobumi Suzuki, Minoru Maruyama, Tomoki Yoshihara, and Hiroyuki Ohta. 2017. "Genetic Deletion of GPR52 Enhances the Locomotor-Stimulating Effect of an Adenosine A2A Receptor Antagonist in Mice: A Potential Role of GPR52 in the Function of Striatopallidal Neurons." *Brain Research* 1670 (September): 24–31. <https://doi.org/10.1016/j.brainres.2017.05.031>.

Onnis, Anna, and Cosima T. Baldari. 2019. "Orchestration of Immunological Synapse Assembly by Vesicular Trafficking." *Frontiers in Cell and Developmental Biology* 7. <https://www.frontiersin.org/articles/10.3389/fcell.2019.00110>.

## Bibliography

- Oviedo-Orta, E., T. Hoy, and W. H. Evans. 2000. "Intercellular Communication in the Immune System: Differential Expression of Connexin40 and 43, and Perturbation of Gap Junction Channel Functions in Peripheral Blood and Tonsil Human Lymphocyte Subpopulations." *Immunology* 99 (4): 578–90. <https://doi.org/10.1046/j.1365-2567.2000.00991.x>.
- Oviedo-Orta, Ernesto, and W. Howard Evans. 2004. "Gap Junctions and Connexin-Mediated Communication in the Immune System." *Biochimica Et Biophysica Acta* 1662 (1–2): 102–12. <https://doi.org/10.1016/j.bbamem.2003.10.021>.
- Oviedo-Orta, Ernesto, Matthieu Perreau, W. Howard Evans, and Ilaria Potoicchio. 2010. "Control of the Proliferation of Activated CD4+ T Cells by Connexins." *Journal of Leukocyte Biology* 88 (1): 79–86. <https://doi.org/10.1189/jlb.0909613>.
- Park, Heon, Zhaoxia Li, Xuexian O. Yang, Seon Hee Chang, Roza Nurieva, Yi-Hong Wang, Ying Wang, et al. 2005. "A Distinct Lineage of CD4 T Cells Regulates Tissue Inflammation by Producing Interleukin 17." *Nature Immunology* 6 (11): 1133–41. <https://doi.org/10.1038/ni1261>.
- Pavlaki, Nikoleta, and Viacheslav O. Nikolaev. 2018. "Imaging of PDE2- and PDE3-Mediated CGMP-to-CAMP Cross-Talk in Cardiomyocytes." *Journal of Cardiovascular Development and Disease* 5 (1). <https://doi.org/10.3390/jcdd5010004>.
- Perera, Ruwan K., Julia U. Sprenger, Julia H. Steinbrecher, Daniela Hübscher, Stephan E. Lehnart, Marco Abesser, Kai Schuh, Ali El-Armouche, and Viacheslav O. Nikolaev. 2015. "Microdomain Switch of CGMP-Regulated Phosphodiesterases Leads to ANP-Induced Augmentation of  $\beta$ -Adrenoceptor-Stimulated Contractility in Early Cardiac Hypertrophy." *Circulation Research* 116 (8): 1304–11. <https://doi.org/10.1161/CIRCRESAHA.116.306082>.
- Peter, Daniel, S. L. Catherine Jin, Marco Conti, Armin Hatzelmann, and Christof Zitt. 2007. "Differential Expression and Function of Phosphodiesterase 4 (PDE4) Subtypes in Human Primary CD4+ T Cells: Predominant Role of PDE4D." *Journal of Immunology (Baltimore, Md.: 1950)* 178 (8): 4820–31. <https://doi.org/10.4049/jimmunol.178.8.4820>.
- Pietraszewska-Bogiel, A., and T.w.j. Gadella. 2011. "FRET Microscopy: From Principle to Routine Technology in Cell Biology." *Journal of Microscopy* 241 (2): 111–18. <https://doi.org/10.1111/j.1365-2818.2010.03437.x>.
- Powrie, F., J. Carlino, M. W. Leach, S. Mauze, and R. L. Coffman. 1996. "A Critical Role for Transforming Growth Factor-Beta but Not Interleukin 4 in the Suppression of T Helper Type

## Bibliography

1-Mediated Colitis by CD45RB(Low) CD4+ T Cells." *The Journal of Experimental Medicine* 183 (6): 2669–74. <https://doi.org/10.1084/jem.183.6.2669>.

Qureshi, Omar S., Yong Zheng, Kyoko Nakamura, Kesley Attridge, Claire Manzotti, Emily M. Schmidt, Jennifer Baker, et al. 2011. "Trans-Endocytosis of CD80 and CD86: A Molecular Basis for the Cell-Extrinsic Function of CTLA-4." *Science (New York, N.Y.)* 332 (6029): 600–603. <https://doi.org/10.1126/science.1202947>.

Raker, Verena Katharina, Christian Becker, and Kerstin Steinbrink. 2016. "The CAMP Pathway as Therapeutic Target in Autoimmune and Inflammatory Diseases." *Frontiers in Immunology* 7 (March): 123. <https://doi.org/10.3389/fimmu.2016.00123>.

Randriamampita, Clotilde, and Annemarie C. Lellouch. 2014. "Imaging Early Signaling Events in T Lymphocytes with Fluorescent Biosensors." *Biotechnology Journal* 9 (2): 203–12. <https://doi.org/10.1002/biot.201300195>.

Redondo, Miriam, José Brea, Daniel I. Perez, Ignacio Soteras, Cristina Val, Concepción Perez, Jose A. Morales-García, et al. 2012. "Effect of Phosphodiesterase 7 (PDE7) Inhibitors in Experimental Autoimmune Encephalomyelitis Mice. Discovery of a New Chemically Diverse Family of Compounds." *Journal of Medicinal Chemistry* 55 (7): 3274–84. <https://doi.org/10.1021/jm201720d>.

Rooij, Johan de, Fried J. T. Zwartkruis, Mark H. G. Verheijen, Robbert H. Cool, Sebastian M. B. Nijman, Alfred Wittinghofer, and Johannes L. Bos. 1998. "Epac Is a Rap1 Guanine-Nucleotide-Exchange Factor Directly Activated by Cyclic AMP." *Nature* 396 (6710): 474–77. <https://doi.org/10.1038/24884>.

Rothenberg, Ellen V., Jonathan E. Moore, and Mary A. Yui. 2008. "Launching the T-Cell-Lineage Developmental Programme." *Nature Reviews. Immunology* 8 (1): 9–21. <https://doi.org/10.1038/nri2232>.

Rueda, Cesar M., Courtney M. Jackson, and Claire A. Chougnet. 2016. "Regulatory T-Cell-Mediated Suppression of Conventional T-Cells and Dendritic Cells by Different CAMP Intracellular Pathways." *Frontiers in Immunology* 7: 216. <https://doi.org/10.3389/fimmu.2016.00216>.

Sadek, Mirna S., Eleder Cachorro, Ali El-Armouche, and Susanne Kämmerer. 2020. "Therapeutic Implications for PDE2 and CGMP/CAMP Mediated Crosstalk in Cardiovascular Diseases." *International Journal of Molecular Sciences* 21 (20): E7462. <https://doi.org/10.3390/ijms21207462>.

## Bibliography

Sáez, Juan C., Viviana M. Berthoud, María C. Brañes, Agustín D. Martínez, and Eric C. Beyer. 2003. "Plasma Membrane Channels Formed by Connexins: Their Regulation and Functions." *Physiological Reviews* 83 (4): 1359–1400. <https://doi.org/10.1152/physrev.00007.2003>.

Sakaguchi, S., N. Sakaguchi, M. Asano, M. Itoh, and M. Toda. 1995. "Immunologic Self-Tolerance Maintained by Activated T Cells Expressing IL-2 Receptor Alpha-Chains (CD25). Breakdown of a Single Mechanism of Self-Tolerance Causes Various Autoimmune Diseases." *Journal of Immunology (Baltimore, Md.: 1950)* 155 (3): 1151–64.

Sanders, V. M., R. A. Baker, D. S. Ramer-Quinn, D. J. Kasproicz, B. A. Fuchs, and N. E. Street. 1997. "Differential Expression of the Beta2-Adrenergic Receptor by Th1 and Th2 Clones: Implications for Cytokine Production and B Cell Help." *Journal of Immunology (Baltimore, Md.: 1950)* 158 (9): 4200–4210.

Schmidt, Angelika, Nina Oberle, and Peter Krammer. 2012. "Molecular Mechanisms of Treg-Mediated T Cell Suppression." *Frontiers in Immunology* 3. <https://www.frontiersin.org/articles/10.3389/fimmu.2012.00051>.

Schultz, Francisca, Pamela Swiatlowska, Anita Alvarez-Laviada, Jose L. Sanchez-Alonso, Qianqian Song, Antoine A. F. de Vries, Daniël A. Pijnappels, et al. 2019. "Cardiomyocyte-Myofibroblast Contact Dynamism Is Modulated by Connexin-43." *FASEB Journal: Official Publication of the Federation of American Societies for Experimental Biology* 33 (9): 10453–68. <https://doi.org/10.1096/fj.201802740RR>.

Scott, J. D. 1991. "Cyclic Nucleotide-Dependent Protein Kinases." *Pharmacology & Therapeutics* 50 (1): 123–45. [https://doi.org/10.1016/0163-7258\(91\)90075-w](https://doi.org/10.1016/0163-7258(91)90075-w).

Shabb, J. B. 2001. "Physiological Substrates of CAMP-Dependent Protein Kinase." *Chemical Reviews* 101 (8): 2381–2411. <https://doi.org/10.1021/cr000236l>.

Shimoda, Kazuya, Jan van Deursent, Mark Y. Sangster, Sally R. Sarawar, Richard T. Carson, Ralph A. Tripp, Charles Chu, et al. 1996. "Lack of IL-4-Induced Th2 Response and IgE Class Switching in Mice with Disrupted State6 Gene." *Nature* 380 (6575): 630–33. <https://doi.org/10.1038/380630a0>.

Shrestha, Dilip, Attila Jenei, Péter Nagy, György Vereb, and János Szöllősi. 2015. "Understanding FRET as a Research Tool for Cellular Studies." *International Journal of Molecular Sciences* 16 (4): 6718–56. <https://doi.org/10.3390/ijms16046718>.

## Bibliography

Söhl, Goran, and Klaus Willecke. 2004. "Gap Junctions and the Connexin Protein Family." *Cardiovascular Research* 62 (2): 228–32. <https://doi.org/10.1016/j.cardiores.2003.11.013>.

Sompayrac, Lauren. 2019. *How the Immune System Works / Lauren Sompayrac*. Sixth edition. The How It Works Ser. Hoboken, NJ: Wiley Blackwell.

Song, Haikun, Hexuan Li, Shimeng Guo, Yuyin Pan, Yuhua Fu, Zijian Zhou, Zhaoyang Li, et al. 2018. "Targeting Gpr52 Lowers Mutant HTT Levels and Rescues Huntington's Disease-Associated Phenotypes." *Brain: A Journal of Neurology* 141 (6): 1782–98. <https://doi.org/10.1093/brain/awy081>.

Spark, Daisy L., Miaomiao Mao, Sherie Ma, Mohsin Sarwar, Cameron J. Nowell, David M. Shackleford, Patrick M. Sexton, Jess Nithianantharajah, Gregory D. Stewart, and Christopher J. Langmead. 2020. "In the Loop: Extrastriatal Regulation of Spiny Projection Neurons by GPR52." *ACS Chemical Neuroscience* 11 (14): 2066–76. <https://doi.org/10.1021/acscchemneuro.0c00197>.

Špiranec Spes, Katarina, Wen Chen, Lisa Krebs, Katharina Völker, Marco Abeßer, Petra Eder Negrin, Antonella Cellini, et al. 2020. "Heart-Microcirculation Connection." *Hypertension* 76 (5): 1637–48. <https://doi.org/10.1161/HYPERTENSIONAHA.120.15772>.

Sprenger, Julia U., Nadja I. Bork, Jonas Herting, Thomas H. Fischer, and Viacheslav O. Nikolaev. 2016. "Interactions of Calcium Fluctuations during Cardiomyocyte Contraction with Real-Time CAMP Dynamics Detected by FRET." *PLOS ONE* 11 (12): e0167974. <https://doi.org/10.1371/journal.pone.0167974>.

Sprenger, Julia U., and Viacheslav O. Nikolaev. 2013. "Biophysical Techniques for Detection of CAMP and CGMP in Living Cells." *International Journal of Molecular Sciences* 14 (4): 8025–46. <https://doi.org/10.3390/ijms14048025>.

Sprenger, Julia U., Ruwan K. Perera, Konrad R. Götz, and Viacheslav O. Nikolaev. 2012. "FRET Microscopy for Real-Time Monitoring of Signaling Events in Live Cells Using Unimolecular Biosensors." *Journal of Visualized Experiments: JoVE*, no. 66 (August): e4081. <https://doi.org/10.3791/4081>.

Sprenger, Julia U., Ruwan K. Perera, Julia H. Steinbrecher, Stephan E. Lehnart, Lars S. Maier, Gerd Hasenfuss, and Viacheslav O. Nikolaev. 2015. "In Vivo Model with Targeted CAMP Biosensor Reveals Changes in Receptor–Microdomain Communication in Cardiac Disease." *Nature Communications* 6 (1): 6965. <https://doi.org/10.1038/ncomms7965>.



## Bibliography

- Sunahara, Roger K., and Ron Taussig. 2002. "Isoforms of Mammalian Adenylyl Cyclase: Multiplicities of Signaling." *Molecular Interventions* 2 (3): 168–84. <https://doi.org/10.1124/mi.2.3.168>.
- Sutherland, E. W., and T. W. Rall. 1958. "Fractionation and Characterization of a Cyclic Adenine Ribonucleotide Formed by Tissue Particles." *The Journal of Biological Chemistry* 232 (2): 1077–91.
- Swain, S. L., A. D. Weinberg, M. English, and G. Huston. 1990. "IL-4 Directs the Development of Th2-like Helper Effectors." *Journal of Immunology (Baltimore, Md.: 1950)* 145 (11): 3796–3806.
- Swanson, M. A., W. T. Lee, and V. M. Sanders. 2001. "IFN-Gamma Production by Th1 Cells Generated from Naive CD4+ T Cells Exposed to Norepinephrine." *Journal of Immunology (Baltimore, Md.: 1950)* 166 (1): 232–40. <https://doi.org/10.4049/jimmunol.166.1.232>.
- Szczypka, Marianna. 2020. "Role of Phosphodiesterase 7 (PDE7) in T Cell Activity. Effects of Selective PDE7 Inhibitors and Dual PDE4/7 Inhibitors on T Cell Functions." *International Journal of Molecular Sciences* 21 (17): E6118. <https://doi.org/10.3390/ijms21176118>.
- Takahashi, T., T. Tagami, S. Yamazaki, T. Uede, J. Shimizu, N. Sakaguchi, T. W. Mak, and S. Sakaguchi. 2000. "Immunologic Self-Tolerance Maintained by CD25(+)CD4(+) Regulatory T Cells Constitutively Expressing Cytotoxic T Lymphocyte-Associated Antigen 4." *The Journal of Experimental Medicine* 192 (2): 303–10. <https://doi.org/10.1084/jem.192.2.303>.
- Tanaka, Shigeru, Ken Ishii, Kazue Kasai, Sung Ok Yoon, and Yoshinaga Saeki. 2007. "Neural Expression of G Protein-Coupled Receptors GPR3, GPR6, and GPR12 up-Regulates Cyclic AMP Levels and Promotes Neurite Outgrowth." *The Journal of Biological Chemistry* 282 (14): 10506–15. <https://doi.org/10.1074/jbc.M700911200>.
- Tang, Tong, Mei Hua Gao, N. Chin Lai, Amy L. Firth, Toshiyuki Takahashi, Tracy Guo, Jason X.-J. Yuan, David M. Roth, and H. Kirk Hammond. 2008. "Adenylyl Cyclase Type 6 Deletion Decreases Left Ventricular Function via Impaired Calcium Handling." *Circulation* 117 (1): 61–69. <https://doi.org/10.1161/CIRCULATIONAHA.107.730069>.
- Taskén, K., and A. J. Stokka. 2006. "The Molecular Machinery for cAMP-Dependent Immunomodulation in T-Cells." *Biochemical Society Transactions* 34 (Pt 4): 476–79. <https://doi.org/10.1042/BST0340476>.

## Bibliography

- Taskén, Kjetil, and Einar Martin Aandahl. 2004. "Localized Effects of CAMP Mediated by Distinct Routes of Protein Kinase A." *Physiological Reviews* 84 (1): 137–67. <https://doi.org/10.1152/physrev.00021.2003>.
- Taylor, S. S., D. R. Knighton, J. Zheng, L. F. Ten Eyck, and J. M. Sowadski. 1992. "Structural Framework for the Protein Kinase Family." *Annual Review of Cell Biology* 8: 429–62. <https://doi.org/10.1146/annurev.cb.08.110192.002241>.
- Thornton, A. M., and E. M. Shevach. 1998. "CD4+CD25+ Immunoregulatory T Cells Suppress Polyclonal T Cell Activation in Vitro by Inhibiting Interleukin 2 Production." *The Journal of Experimental Medicine* 188 (2): 287–96. <https://doi.org/10.1084/jem.188.2.287>.
- Tittarelli, Andrés, Mariela Navarrete, María Alejandra Gleisner, Peter Gebicke-Haerter, and Flavio Salazar-Onfray. 2020. "Connexin-Mediated Signaling at the Immunological Synapse." *International Journal of Molecular Sciences* 21 (10): 3736. <https://doi.org/10.3390/ijms21103736>.
- Togashi, Yosuke, Kohei Shitara, and Hiroyoshi Nishikawa. 2019. "Regulatory T Cells in Cancer Immunosuppression - Implications for Anticancer Therapy." *Nature Reviews. Clinical Oncology* 16 (6): 356–71. <https://doi.org/10.1038/s41571-019-0175-7>.
- Torphy, Theodore J. 1998. "Phosphodiesterase Isozymes." *American Journal of Respiratory and Critical Care Medicine* 157 (2): 351–70. <https://doi.org/10.1164/ajrccm.157.2.9708012>.
- Uhl, Lion F. K., and Audrey Gérard. 2020. "Modes of Communication between T Cells and Relevance for Immune Responses." *International Journal of Molecular Sciences* 21 (8): E2674. <https://doi.org/10.3390/ijms21082674>.
- Vaeth, Martin, Tea Gogishvili, Tobias Bopp, Matthias Klein, Friederike Berberich-Siebelt, Stefan Gattenloehner, Andris Avots, et al. 2011. "Regulatory T Cells Facilitate the Nuclear Accumulation of Inducible CAMP Early Repressor (ICER) and Suppress Nuclear Factor of Activated T Cell C1 (NFATc1)." *Proceedings of the National Academy of Sciences of the United States of America* 108 (6): 2480–85. <https://doi.org/10.1073/pnas.1009463108>.
- Vang, Amanda G., Shlomo Z. Ben-Sasson, Hongli Dong, Barbara Kream, Michael P. DeNinno, Michelle M. Claffey, William Housley, Robert B. Clark, Paul M. Epstein, and Stefan Brocke. 2010. "PDE8 Regulates Rapid T cell Adhesion and Proliferation Independent of ICER." *PloS One* 5 (8): e12011. <https://doi.org/10.1371/journal.pone.0012011>.

## Bibliography

- Vang, Amanda G., William Housley, Hongli Dong, Chaitali Basole, Shlomo Z. Ben-Sasson, Barbara E. Kream, Paul M. Epstein, Robert B. Clark, and Stefan Brocke. 2013. "Regulatory T-Cells and CAMP Suppress Effector T-Cells Independently of PKA-CREM/ICER: A Potential Role for Epac." *The Biochemical Journal* 456 (3): 463–73. <https://doi.org/10.1042/BJ20130064>.
- Vang, T., K. M. Torgersen, V. Sundvold, M. Saxena, F. O. Levy, B. S. Skålhegg, V. Hansson, T. Mustelin, and K. Taskén. 2001. "Activation of the COOH-Terminal Src Kinase (Csk) by CAMP-Dependent Protein Kinase Inhibits Signaling through the T Cell Receptor." *The Journal of Experimental Medicine* 193 (4): 497–507. <https://doi.org/10.1084/jem.193.4.497>.
- Vollmar, A. M. 1997. "Influence of Atrial Natriuretic Peptide on Thymocyte Development in Fetal Thymic Organ Culture." *Journal of Neuroimmunology* 78 (1–2): 90–96. [https://doi.org/10.1016/s0165-5728\(97\)00086-6](https://doi.org/10.1016/s0165-5728(97)00086-6).
- Vollmar, A. M., K. N. Schmidt, and R. Schulz. 1996. "Natriuretic Peptide Receptors on Rat Thymocytes: Inhibition of Proliferation by Atrial Natriuretic Peptide." *Endocrinology* 137 (5): 1706–13. <https://doi.org/10.1210/endo.137.5.8612505>.
- Wachter, S. Blake, and Edward M. Gilbert. 2012. "Beta-Adrenergic Receptors, from Their Discovery and Characterization through Their Manipulation to Beneficial Clinical Application." *Cardiology* 122 (2): 104–12. <https://doi.org/10.1159/000339271>.
- Wada, Mitsuo, Kayo Yukawa, Hiroyuki Ogasawara, Koichi Suzawa, Tatsuya Maekawa, Yoshihisa Yamamoto, Takeshi Ohta, Eunyoung Lee, and Takashi Miki. 2021. "GPR52 Accelerates Fatty Acid Biosynthesis in a Ligand-Dependent Manner in Hepatocytes and in Response to Excessive Fat Intake in Mice." *IScience* 24 (4): 102260. <https://doi.org/10.1016/j.isci.2021.102260>.
- Wan, Yisong Y., and Richard A. Flavell. 2009. "How Diverse--CD4 Effector T Cells and Their Functions." *Journal of Molecular Cell Biology* 1 (1): 20–36. <https://doi.org/10.1093/jmcb/mjp001>.
- Weber, Michael, Corinna Lupp, Pamela Stein, Andreas Kreft, Tobias Bopp, Thomas C. Wehler, Edgar Schmitt, Hansjörg Schild, and Markus P. Radsak. 2013. "Mechanisms of Cyclic Nucleotide Phosphodiesterases in Modulating T Cell Responses in Murine Graft-versus-Host Disease." *PLOS ONE* 8 (3): e58110. <https://doi.org/10.1371/journal.pone.0058110>.

## Bibliography

- Weber, Silvio, Miriam Zeller, Kaomei Guan, Frank Wunder, Michael Wagner, and Ali El-Armouche. 2017. "PDE2 at the Crossway between CAMP and CGMP Signalling in the Heart." *Cellular Signalling* 38 (October): 76–84. <https://doi.org/10.1016/j.cellsig.2017.06.020>.
- Wehbi, Vanessa L., and Kjetil Taskén. 2016. "Molecular Mechanisms for CAMP-Mediated Immunoregulation in T Cells - Role of Anchored Protein Kinase A Signaling Units." *Frontiers in Immunology* 7: 222. <https://doi.org/10.3389/fimmu.2016.00222>.
- Weis, William I., and Brian K. Kobilka. 2018. "The Molecular Basis of G Protein-Coupled Receptor Activation." *Annual Review of Biochemistry* 87 (June): 897–919. <https://doi.org/10.1146/annurev-biochem-060614-033910>.
- Wildin, R. S., F. Ramsdell, J. Peake, F. Faravelli, J. L. Casanova, N. Buist, E. Levy-Lahad, et al. 2001. "X-Linked Neonatal Diabetes Mellitus, Enteropathy and Endocrinopathy Syndrome Is the Human Equivalent of Mouse Scurfy." *Nature Genetics* 27 (1): 18–20. <https://doi.org/10.1038/83707>.
- Willoughby, Debbie, and Dermot M. F. Cooper. 2008. "Live-Cell Imaging of CAMP Dynamics." *Nature Methods* 5 (1): 29–36. <https://doi.org/10.1038/nmeth1135>.
- Wootten, Denise, Arthur Christopoulos, Maria Marti-Solano, M. Madan Babu, and Patrick M. Sexton. 2018. "Mechanisms of Signalling and Biased Agonism in G Protein-Coupled Receptors." *Nature Reviews Molecular Cell Biology* 19 (10): 638–53. <https://doi.org/10.1038/s41580-018-0049-3>.
- Yang, Panzao, Joanne O. Davidson, Tania M. Fowke, Robert Galinsky, Guido Wassink, Rashika N. Karunasinghe, Jaya D. Prasad, et al. 2020. "Connexin Hemichannel Mimetic Peptide Attenuates Cortical Interneuron Loss and Perineuronal Net Disruption Following Cerebral Ischemia in Near-Term Fetal Sheep." *International Journal of Molecular Sciences* 21 (18): 6475. <https://doi.org/10.3390/ijms21186475>.
- Yang, Qi, J. Jeremiah Bell, and Avinash Bhandoola. 2010. "T-Cell Lineage Determination." *Immunological Reviews* 238 (1): 12–22. <https://doi.org/10.1111/j.1600-065X.2010.00956.x>.
- Zaccolo, Manuela, Francesca De Giorgi, Charles Y. Cho, Luxin Feng, Tom Knapp, Paul A. Negulescu, Susan S. Taylor, Roger Y. Tsien, and Tullio Pozzan. 2000. "A Genetically Encoded, Fluorescent Indicator for Cyclic AMP in Living Cells." *Nature Cell Biology* 2 (1): 25–29. <https://doi.org/10.1038/71345>.

## Bibliography

Zaccolo, Manuela, and Matthew A. Movsesian. 2007. "CAMP and CGMP Signaling Cross-Talk: Role of Phosphodiesterases and Implications for Cardiac Pathophysiology." *Circulation Research* 100 (11): 1569–78. <https://doi.org/10.1161/CIRCRESAHA.106.144501>.

Zhang, J., Y. Ma, S.S. Taylor, and R.Y. Tsien. 2001. "Genetically Encoded Reporters of Protein Kinase A Activity Reveal Impact of Substrate Tethering." *Proceedings of the National Academy of Sciences of the United States of America* 98 (26): 14997–2. <https://doi.org/10.1073/pnas.211566798>.

Zheng, Ye, Steven Z. Josefowicz, Arnold Kas, Tin-Tin Chu, Marc A. Gavin, and Alexander Y. Rudensky. 2007. "Genome-Wide Analysis of Foxp3 Target Genes in Developing and Mature Regulatory T Cells." *Nature* 445 (7130): 936–40. <https://doi.org/10.1038/nature05563>.

Zhu, Jinfang, and William E. Paul. 2008. "CD4 T Cells: Fates, Functions, and Faults." *Blood* 112 (5): 1557–69. <https://doi.org/10.1182/blood-2008-05-078154>.

## Appendix

### 6 Appendix

**Table 14. 1.** List of hazardous substances according to Globally Harmonized System (GHS) of classification and labeling of chemicals.

Chemical, Kit	H Statement	P Statement	GHS Pictogram
Ammonium chloride (NH <sub>4</sub> Cl)	H302, H319	P264, P264+P265, P270, P280, P301+P317, P305+P351+P338, P330, P337+P317, P501	07
Ammonium persulfate (APS)	H272, H302, H315, H317, H319, H334, H335	P210, P280, P301 + P012 + P030, P302+P352, P305 + P351 + P338	03, 07, 08
Ampicillin sodium salts	H317, H334	P261, P280, P342+P311	08
Calcium chloride (CaCl <sub>2</sub> )	H319	P305 + P351 + P338	07
cAMP Enzyme Immunoassay Kit, Direct	H226, H290, H302, H311, H314, H330, H335	P210, P280, P301+P312, P303+P361+P353, P304+P340+P310, P305+P351+P338	02, 05, 06
DAPI	H315, H317, H335	P261, P264, P271, P272, P280, P302+P352	07
Diethyl pyrocarbonate (DEPC)	H302	P264, P270, P301+P312, P501	07
Ethanol, Rotipuran, >99,8% p.a.	H225, H319	P210, P233, P305 + P351 + P338	02, 07
Ethanol, 70%	H225, H319	P210, P233, P305 + P351 + P338	02, 07
Ethylenediaminetetraacetic acid (EDTA) disodium salt 2- hydrate	H332, H373	P260, P271, P304 + P340, P312, P314, P501	07, 08
Forskolin	H312	P280	07
Gel Loading Dye Purple, 6x			

## Appendix

Halt protease inhibitor cocktail, 100x	H315, H319	P280, P264, P305+P351+P338	07
Hydrochloric acid (HCl), 37%	H290, H314, H335	P280, P303 + P361 + P353, P304 + P340, P305 + P351 + P338, P310	05, 07
iScript cDNA Synthesis Kit	H319	P280, P264, P305 + P351 + P338, P337 + P313	07
Isoflurane (Forane)	H336	P261, P271, P303 + P340, P312, P403 + P233, P405, P501	07, 08
Methanol, 99%			
Midori Geen Advance N,N,N',N'- Tetramethylethylenediamine (TEMED)	H225, H302 + H332, H314	P261, P280 P210, P280, P301 + P330 + P331, P303 + P361 + P353, P304 + P340 + P312, P305 + P351 + P338	02, 05, 07
Potassium hydrogencarbonate (KHCO <sub>3</sub> )	H319, H335	P261, P264+P265, P271, P280, P304+P340, P305+P351+P338, P319, P337+P317, P403+P233, P405, P501	07
QIAprep Spin Miniprep Kit	H290, H314	P280, P305+P351+P338+P310	05
QIAGEN Plasmid Plus Midi Kit	H290, H314	P280, P305+P351+P338+P310	05
RNeasy Plus Micro Kit	H226, H302, H314, H318, H412	P210, P264, P280, P305 + P351 + P338 + P30	02, 05, 07
Rolipram	H302, H315, H319, H335	P261, P264, P264+P265, P270, P271, P280, P301+P317,	07

## Appendix










		P302+P352, P304+P340, P305+P351+P338, P319, P321, P330, P332+P317, P337+P317, P362+P364, P403+P233, P405, P501	
Rotiphorese Gel 30 (37,5:1; Acrylamide)	H302, H315, H317, H319, H340, H350, H361f, H372	P201, P280, P301+P312, P302+P352, P305+P351+P338, P308+P313	07, 08
Sodium azide (NaN <sub>3</sub> )	H300 + H310 + H330, H373, H410	P262, P273, P280, P301 + P310 + P330, P302 + P352 + P310, P304 + P340 + P310	06, 08, 09
Sodium deoxycholate (SOD)	H302, H412	P273, P301 + P312 + P330	07
Sodium dodecyl sulfate (SDS)	H315, H318, H335	P261, P280, P302 + P352, P304 + P340 + P312, P305 + P351 + P338 + P310	05, 07
SDS-Solution, 20%	H315, H318	P305 + P351 + P338	05
Sodium hydroxide (NaOH)	H290, H314	P233, P280, P303 + P361 + P353, P305 + P351 + P338, P310	05
Syber Green (Perfecta) for IQ	H315, H319, H411		
Tris-acetate-EDTA (TAE) buffer, 50x	H316, H319	P264, P280, P305+351+P338, P332+P313, P337+P313	07
Triton X-100 Solution, 10%	H318	P280, P305 + P351 + P338, P313	05
Trypan blue	H350, H361	P201, P280, P202	08



## Appendix

Trypsin/EDTA, 0,25%/0,02% in PBS	H334	P261, P284, P304+P340, P342+P311	08
Type F Immersion liquid	H315, H412	P273, P280, P302 + P352	07
β-Mercaptoethanol	H301 + H331, H310, H315, H317, H318, H361fd, H373, H410	P201, P262, P280, P301 + P310 + P330, P302 + P352 + P310, P305 + P351 + P338 + P310	05, 06, 08, 09
(-)-Isoproterenol hydrochloride	H315, H319, H335	P261, P264, P271, P280, P302+P352, P305+P351+P338	07
2-Mercaptoethanol, 50 mM	H317	P280, P261, P272, P273, P320+P352, P333+P313	07
2-Propanol	H225, H319, H336	P210, P280, P305 + P351 + P338, P337 + P313	02, 07
3-Isobutyl-1-Methylxanthine (IBMX)	H302	P313, P301 + P330 + P331	07

## Appendix

Flame	Flame over circle	Exploding bomb
		
Corrosion	Gas cylinder	Skull and crossbones
		
Exclamation mark	Environment	Health hazard
		

**Figure 26. GHS hazard pictograms.** Adopted (Boelhouwer et al. 2013). Flame (GHS02), Flame over circle (GHS03), Exploding bomb (GHS01), Corrosion (GHS05), Gas cylinder (GHS04), Skull and crossbones (GHS06), Exclamation mark (GHS07), Environment (GHS09), Health hazard (GHS08).

# 7 Acknowledgments

I would like to express my deepest appreciation to Prof. Dr. Viacheslav O. Nikolaev for his excellent supervision, greatest support, and helpful suggestion during my PhD thesis research. I am grateful for being given the opportunity to work on exciting projects as well as being a member of his research group.

I would like to express my gratitude to Prof. Dr. Manuel A. Frieze for his great co-supervision, helpful Jour fixe discussions, and valuable guidance through the work on the collaborative CRC1328 project.

I would like to specially thank committee members Prof. Dr. Christian Lohr, Prof. Dr. Chris Meier, and Prof. Dr. Elke Oetjen.

I would like to extend my sincere thanks to my dear colleagues Dr. Nadja I. Bork, Ms. Paula F. Krieg, Dr. Jana K. Sonner, and Dr. Hariharan Subramanian for the vivid discussions, useful advice, and wonderful cooperation through PhD thesis.

I would like to thank the Nikolaev research group for the nice work atmosphere.

Special thanks to Ms. Victoria Hänel, Ms. Nina Kursawe, and Ms. Elisabeth Krämer for their excellent technical assistance.

I am also grateful for the CRC1328 consortium and the opportunity to expand my research knowledge, as well as for great networking during my PhD thesis work.

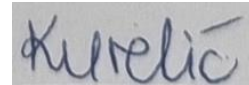
To my beloved family... Najveća hvala mojim najdražim roditeljima na bezuvjetnoj ljubavi i podršci tijekom cijeloživotnog obrazovanja, vjetru u leđa tijekom ovog putovanja koje je doprinjelo mom osobnom rastu i napretku. Veliko hvala mojem bratu, baki i teti na svoj ljubavi i potpori.

My dearest thanks also go to my closest friends (Babe Ri, Amige, Gradijent), for their absolute support, love, positivity, and compass in crucial moments during this amazing journey.

## Affidavit

Hiermit versichere ich an Eides statt, die vorliegende Dissertation selbst verfasst und keine anderen als die angegebenen Hilfsmittel benutzt zu haben.“

Hamburg, October 2022



---

Signature